UNIVERSIDAD DE CANTABRIA

PROGRAMA DE DOCTORADO EN

BIOLOGÍA MOLECULAR Y BIOMEDICINA

TESIS DOCTORAL

Aplicación De Secretoma Con Efecto Osteogénico Procedente De Células Madre Mesenquimales Para El Tratamiento De La Osteoporosis

PHD THESIS

Application Of Osteogenic-Effect Secretome derived from Mesenchymal Stem Cells For the Treatment Of Osteoporosis

Realizada por: Alberto González González

Dirigida por: José Carlos Rodríguez Rey y Flor María Pérez Campo

Escuela de Doctorado de la Universidad de Cantabria

SANTANDER 2024

UNIVERSIDAD DE CANTABRIA

El **Dr. José Carlos Rodríguez Rey**, Catedrático de Bioquímica y Biología Molecular de la Facultad de Medicina de la Universidad de Cantabria.

CERTIFICA:

Que el Graduado Alberto González González, ha realizado bajo mi dirección el presente trabajo de Tesis Doctoral titulado “Aplicación De Secretoma Con Efecto Osteogénico Procedente De Células Madre Mesenquimales para el Tratamiento de la Osteoporosis” (“Application Of Osteogenic Secretome from Mesenchymal Stem Cells for Treatment of Osteoporosis”)

Considero que este trabajo reúne los requisitos de originalidad y calidad científica necesarios para su defensa como Memoria de Doctorado por el interesado, al objeto de poder optar al grado de Doctor en Biología Molecular y Biomedicina de la Universidad de Cantabria.

Y para que conste y surta los efectos oportunos, firmo el presente certificado.

En Santander a 3 de Octubre de 2024,

Fdo. José Carlos Rodríguez Rey

UNIVERSIDAD DE CANTABRIA

La **Dra. Flor María Pérez Campo**, Profesora Contratada Doctora en el Departamento de Biología Molecular de la Facultad de Medicina de la Universidad de Cantabria.

CERTIFICA:

Que el Graduado Alberto González González, ha realizado bajo mi dirección y tutela el presente trabajo de Tesis Doctoral titulado “Aplicación De Secretoma Con Efecto Osteogénico Procedente De Células Madre Mesenquimales para el Tratamiento de la Osteoporosis” (“Application Of Osteogenic Secretome from Mesenchymal Stem Cells for Treatment of Osteoporosis”)

Considero que este trabajo reúne los requisitos de originalidad y calidad científica necesarios para su defensa como Memoria de Doctorado por el interesado, al objeto de poder optar al grado de Doctor en Biología Molecular y Biomedicina de la Universidad de Cantabria.

Y para que conste y surta los efectos oportunos, firmo el presente certificado.

En Santander a 4 de Octubre de 2024,

Fdo. Flor María Pérez Campo

Esta Tesis ha sido realizada en el Grupo de Ingeniería de Tejidos (GITC) del Departamento de Biología Molecular de la Facultad de Medicina de la Universidad de Cantabria (UC), dentro de la unidad de Enfermedades Esqueléticas, Metabólicas y Ambientales (iESQUEMA) de la Fundación Instituto de Investigación Sanitaria Marqués de Valdecilla (IDIVAL).

El autor de esta Tesis ha disfrutado de un contrato predoctoral (PREVAL20/01) dentro del Programa de Personal Investigador en Formación Predoctoral en el Área de Biomedicina, Biotecnología y Ciencias de la Salud (Referencia en el Boletín Oficial de Cantabria CVE-2020- 2049), financiado por la UC, IDIVAL, la Conserjería de Universidades, Igualdad, Cultura y Deporte y la Conserjería de Sanidad del Gobierno de Cantabria. Además, durante el desarrollo de la tesis, recibió una beca de movilidad nacional de la Fundación Española de Investigación Ósea y el Metabolismo Mineral (FEIOMM) para realizar una estancia en la Universidade de Santiago de Compostela (USC) y una beca de movilidad internacional de la Fundación Boehringer Ingelheim Fonds (BIF) para realizar una estancia en la University of Arkansas for Medical Sciences (UAMS).

Agradecimientos

Echar la vista atrás y sentarse a escribir los agradecimientos después de estos cuatro años de intenso trabajo no es tarea fácil, aunque seguro que me resulta más sencillo que escribir la tesis, así que vamos al lío.

Quiero empezar agradeciendo, por su puesto, a mis directores José y Flor. La tarea de director no debe ser fácil, pero ya veis que vuestras directrices, consejos y ánimos han dado sus frutos. Gracias por abrirme vuestras puertas. Quiero agradecer, en particular, a Flor por confiar en mí como candidato para solicitar un contrato predoctoral. Desde luego, que hace unos años ni yo mismo me veía defendiendo una tesis, pero supongo que a ti te funcionan mejor las luces largas esas de las que tanto hablas. A base de apretar un poquito cada día y tirar cuando ha sido necesario has conseguido que esto salga adelante. Sin ti habría sido imposible.

No puedo dejar de agradecer a todas las personas que han pasado por el laboratorio en estos años, Monica Dotta, Marina, Celia, Mónica (la Darling), Matilde e Itziar. Aunque sobre el papel os he enseñado yo, lo cierto es que he aprendido con cada una de vosotras a ser mejor científico y profe, y os llevo a todas a nivel personal también como amigas. Obviamente no me dejo a Dani atrás. Gracias por enseñarme (y re-enseñarme) cuando no sabía ni donde tenía la nariz, por estar ahí para suplirnos el uno al otro y por abrirme camino con tus pasos. Si ya fue una locura preparar todo el papeleo de la estancia en Estados Unidos, ni me quiero imaginar lo que habría sido sin tu ayuda. Y a los compañeros de laboratorio (de otro laboratorio), Carol, Álvaro y Tere, gracias por echar un cable para todo siempre que aparecía en vuestra puerta con “cara de pedir”. Me habéis salvado el día más de una vez y me habéis alegrado más de una mañana con la charla del café.

Quiero agradecer también a la profesora Patricia Díaz por acogerme en su laboratorio. A mis compañeros de laboratorio (temporales) de la USC, Rebeca, Patri, Luis, Lara y María Pita por recibirme y tratarme como uno más y por darme un techo cuando no tuve (literal) porque había que apurar los días. La ciencia es lo que tiene, supongo. Graciñas.

También quería agradecer por la acogida en Little Rock a Jesús. Me has ayudado mucho con los últimos experimentos de la tesis, inculcado muchas cosas importantes sobre cómo se hace ciencia y me has abierto las puertas de tu casa (y de tu coche). Qué más podía pedir. Thanks to the whole group of Jesus, Aric, Japneet, Manish, Hayley and Sharmin for helping me whenever I needed. Gostaria também de agradecer à

Adriana por ter disponibilizado o seu tempo para me ajudar tanto quanto possível nas experiências com osteoclastos. Y a Olivia por su paciencia, ya que sin ella aún seguiría intentando averiguar cómo hacer funcionar el micro-CT.

Obviously, I have a place for those who made me feel like one more in Little Rock, because being personally comfortable in a place is important and you made it easier: Mia (thank you), Shegufta (Dhanyabaad), Saúl (gracias), Vy (Cảm ơn), Silvia and Nina (grazie), Mahtab (Mam'noon) and Dani (aquí también, gracias). I specially want to thank Mahtab for helping me to survive during the tornado watching, for the talks, the walks and for being available at 2 am having glue at hand to fix my messes (shhh).

Desde luego que tengo que agradecer a todo el mundo que me ha hecho sentir que podía haber un sitio para mí aquí en Santander cuando llegué con una mano delante y otra detrás y sin saber la (de lluvia) que se me venía encima.

Paloma, Sofía, Belén, Raquel, David, Sanju, Aura y María gracias por acogerme en la ESN como falso erasmus para poder tener un sitio desde el que conocer Cantabria cuando acaba de llegar.

A Ana, gracias por confiar en que era un hombre decente desde el primer momento en que me viste y seguir aguantando a día de hoy. Lo que en un principio era simplemente una chica de Navarra muy simpática con la que tomar algo de vez en cuando, ha acabado siendo una gran amistad. Brindo por que podamos seguir despotricando de nuestros trabajos, hablando de precariedad, de política, de economía, de amor y de todo. Ah, y gracias, por supuesto, por abrirme las puertas del casoplón del Sangüesa. Gracias por la familia que hemos montado aquí en Santander, Aitana, Laura, Elena, Adriana y Sócrates. A Aitana por estar siempre dispuesta a oír una queja del laboratorio y a salir de fiesta para que se me olvide, por su preocupación en todo momento por esta cabeza que no sale volando porque la llevo pegada y por apoyarme en todo. A Laura por tener un corazón que no le cabe en el pecho, por su valentía, tenacidad y por hacerme reír a base de chistes malos. A Elena por su fuerza y su locura, por saber tratar cualquier tema como adultos, pero también saber comportarnos como niños cuando se necesita. Gracias por ser la mejor compi de escritura durante esta tesis. A Adriana por estar en todo, por sus puntos de humor, por su atención cuando he caído enfermo y por los huevos (de tu padre), claro. Qué hermosa casualidad haber conectado. A Sócrates por su pragmatismo, las bromas del fantasy, sus ánimos y los ratillos de basket para desconectar.

A Marta y Ana Marcos por su cercanía, su preocupación por mí durante los meses de escritura y los reels que animaron las tardes frente al ordenador. Señoritas, con permiso: Gracias.

A toda mi familia y amigos que han tenido que vivir esto desde lejos, gracias. Gracias a mi familia por apoyarme en todas las decisiones que tomé, por confiar en que sería capaz y por darme un sitio al que llamo hogar cada vez que vuelvo a casa necesitando descanso. Gracias a mis abuelos, que me apoyan aun sin comprender cómo su nieto “el que tanto ha estudiao’” está tan lejos del pueblo. En particular, a mi abuelo Bartolo que siempre presumía de que su nieto era “más que médico”. Mira abuelo, aquí estamos a punto de defender la tesis doctoral. Aunque no estés aquí, sé que estás viendo desde algún sitio cómo escribo estas palabras, gracias. A todos mis amigos, Miguel, Raúl, Álvaro, Yon, Jesús, Salvi, Marcos, López, Jose, Julio, Tato, Juanje, Franci, María, Eva, Lusine y Elsa, por estar ahí desde siempre y tratarme como si me hubieseis visto ayer, aunque hiciera 3 meses. Gracias por estar dispuestos para echarnos unas risas donde sea y de cualquier cosa, y por las noches en Café Teatro hablando de física, del universo, de la vida, de gamusinos…

A toda la gente que estuvo ahí y me echó un cable mientras me formaba para llegar a donde estoy ahora. Sergio, Blanca, Anda, Alicia, Edu, Gema, Tamara, Andrés, Semari, Pepillo, Ana Voltes, Olimpia, Carmen, Clàudia, Elisa, Alberto, Aiora. Gracias por la compañía en las horas de trabajos y de cervezas, os tengo presentes, aunque no nos veamos mucho.

No me olvido de quien me ayudó al principio, pero no pudo resistir todo el camino. Ana, gracias por apoyarme cuando decidí lanzarme a hacer el doctorado, a pesar de que no te gustaba que me fuese al norte, por aguantar todas las quejas, que no fueron pocas, y por ayudarme a desconectar cuando lo necesitaba. Hoy sé cuánto te costaba que estuviésemos lejos y te agradezco todo el esfuerzo que pusiste para continuar hasta que ya no se pudo más. Gracias.

En definitiva, gracias, de corazón, a todos los que han estado ahí de alguna forma durante estos años y os habéis preocupado por cómo me iba. Como dice el refrán: “Muchos pocos hacen un mucho”, y eso es lo que ha pasado aquí. Yo, como hilo conductor de esta tesis, no podría haberla sacado adelante sin esas pequeñas y grandes ayudas que muchos de vosotros me habéis dado. Por eso, esta tesis va por vosotros. ¡Que aproveche!

“Si las palabras se atraen,
Que se unan entre ellas.
Y a brillar,
¡Que son dos sílabas!”

Joan Manuel Serrat en ‘El poeta Halley’ (2016)

“Nuestra cabeza es redonda para permitir al pensamiento cambiar de dirección”

Francis Picabia

Index

Abbreviations

ActR	Activin Receptor
AEMPS	Agencia Española de Medicamentos y Productos Sanitarios
ALK	Activin-like Kinase
ALP	Alkaline phosphatase
AMP	2-amino-2-methyl-1-propanol
ASC	Adult Stem Cells
ATCC	American Type Culture Collection
ATMP	Advanced Therapy Medical Product
BCA	Bicinchoninic Acid
BM	Bone Marrow
BM-MSCs	Bone Marrow Mesenchymal Stem Cells
BMU	Basic Multicellular Units
BMD	Bone Mineral Density
BMP	Bone Morphogenetic Protein
BMP-R	Bone Morphogenetic Protein Receptor
BMU	Bone Multicellular Unit
BMP	Bone Morphogenetic Protein
BRAM	Bone Morphogenetic Protein-receptor-Associated Molecule
BRC	Bone Remodelling Compartment
BSA	Bovine Serum Albumin
BTM	Bone Turnover Markers
C3	Complement component 3
CCN2	Cellular Communication Network Factor 2
CCR	Chemokine Receptor
CD	Cluster of Differentiation
CM	Conditioned Medium
CTHRC1	Collagen Triple Helix Repeat Containing 1
CXCR	Chemokine Receptor
DCs	Dendritic Cells
DKK1	Dickkopf1

DMEM	Dulbecco's Modified Eagle's Medium
E11/PDPN/GP38	Podoplanin
EDTA	Ethylenediaminetetra-acetic acid
EFNB2	Ephrin B2
EMA	European Medicines Agency
EPHB4	Ephrin B4
ERK	Extracellular signal-Regulated Kinase
ESC	Embryonic Stem Cell
EVs	Extracellular Vesicles
FGF23	Fibroblast growth factor 23
FMOD	Fibromodulin
GADPH	Glyceraldehyde-3-phosphate dehydrogenase
GelMA	Methacrylated Gelatin
GO	Gene Ontology
GMP	Good Manufacturing Practice
HLA	Human Leukocyte Antigen
HSC	Haematopoietic Stem Cell
IBMX	3-isobutyl-1-methylxanthine
IGF-1	Insulin-Like Growth Factor Type 1
IL	Interleukin
ISCT	International Society for Cell and Gene Therapy
ISEV	International Society for Extracellular Vesicles
JNK	C-Jun N-terminal kinase
LAP	Lithium phenyl-2,4,6-trimethylbenzoylphosphinate
LRP	Low density lipoprotein receptor
M-CSF	Macrophage Colony-Stimulating Factor 1
MMP	Metalloproteinase
NFκβ	Nuclear Factor κβ
NK	Natural Killer Cells
MCP	Monocyte Chemotactic Protein
microCT	Micro-computed tomography
miRNA	Micro Ribonucleic acid

M-CSF	Macrophage Colony-Stimulating Factor
MSC	Mesenchymal Stem Cell
NaCl	Sodium chloride
NCPs	Non-Collagenous Proteins
OPG	Osteoprotegerin, Tumor necrosis factor receptor superfamily member 11B
OCN	Osteocalcin
OVX	Ovariectomized
PdI	Polydispersity Index
PLGA	poly(lactic-co-glycolic-acid)
pNPP	*p*-Nitro-Phenyl Phosphate
pNF	*p*-Nitro-Phenol
PREPL	Prolyl Endopeptidase Like
PTH	Parathyroid hormone
PTHR	Parathyroid hormone type 1 receptor
PTHrP	Parathyroid Hormone-related Peptide
PVA	Polyvinyl Alcohol
qPCR	Quantitative Polymerase Chain Reaction
RANK	Receptor activator of nuclear factor-κB
RANKL	Tumor necrosis factor ligand superfamily member 11
RNA	Ribonucleic acid
RT	Room Temperature
RUNX2	Runt-related transcription factor 2
S1P	Sphingosine 1 phosphate
SF	Soluble Fraction
SEMA3A	Semaphorin 3A
SFRP	Secreted Frizzled Related Protein
Smad proteins	Small mothers against decapentaplegic proteins
SMURF	SMAD ubiquitination regulatory factor
SOST	Sclerostin
SPARC	Secreted Protein Acidic And Cysteine Rich
TAB	TAK binding protein
TAK	TGF-β activated kinase

TBS	Tris buffered saline
TBS-T	Tris buffered saline with Tween
TEM	Transmission Electron Microscopy
TIMP	Tissue Inhibitor of Metalloproteinases
TNFRSF6B/FASL/CD95L	Tumor necrosis factor ligand superfamily member 6
TGF-β	Transforming Growth Factor β
TRAP	Tartrate-resistant acid phosphatase
VF	Vesicular Fraction
WNT10B	Protein Wnt-10B
WNT16	Protein Wnt-16
XIAP	X-linked inhibitor of apoptosis protein

List of Figures

List of Tables

RESUMEN

Resumen

El hueso es un tejido dinámico que se renueva constantemente para garantizar el correcto desempeño de sus funciones. Este proceso de renovación continua es lo que se conoce como remodelado óseo, y es llevado a cabo por un complejo sistema de comunicación intercelular en el que los osteoclastos degradan matriz ósea que posteriormente es reemplazada por nueva matriz producida por los osteoblastos. La correcta ejecución y coordinación del remodelado óseo es fundamental para el mantenimiento de la homeostasis del hueso, y la alteración en este proceso conlleva cambios en la arquitectura ósea.

En la osteoporosis, este balance se ve alterado, en parte debido a una disminución de la diferenciación de las células madre mesenquimales (MSCs) hacia osteoblastos, lo que conduce a una disminución en la formación de nueva matriz ósea. Cuando este desequilibrio persiste en el tiempo, provoca el adelgazamiento o la pérdida de las estructuras trabeculares dentro del hueso trabecular, así como una disminución del grosor y un aumento de la porosidad en el hueso cortical, lo que desemboca en fracturas osteoporóticas que afectan a la calidad y a la esperanza de vida de las personas afectadas.

Existen tratamientos para la osteoporosis, que pueden clasificarse según sus mecanismos de acción en agentes antirresortivos que inhiben la actividad osteoclástica, osteoformadores, que estimulan los osteoblastos, y agentes que poseen acción dual, antirresortiva y osteoformadora. Sin embargo, la implementación de estos tratamientos requiere una intrincada toma de decisiones por parte de los médicos, además de la combinación de agentes farmacológicos o estrategias terapéuticas secuenciales, todo ello dirigido a maximizar los beneficios terapéuticos y reducir los efectos secundarios que pueden derivar que, aunque infrecuentes, pueden ser muy graves. De esta manera, existe una búsqueda de nuevas terapias alternativas que faciliten la práctica clínica, mejoren la adherencia al tratamiento y sean más costo-efectivas.

En este contexto, el uso de MSCs empezó a investigarse con resultados muy prometedores. Las buenas características de estas células como su fácil recolección, su capacidad de diferenciación a varios tejidos y su baja

inmunogenicidad, han hecho que se usen para el tratamiento de patologías de diversa índole. En concreto, el uso para patologías óseas es de los más extendidos debido a la conocida capacidad de las MSCs de la medula ósea para formar osteoblastos de manera fisiológica. Sin embargo, el empleo de estas MSCs como terapia también presenta algunos inconvenientes como las bajas tasas de implantación, los problemas de supervivencia o el potencial tumorígeno.

Simultáneamente, en los últimos años se ha producido un cambio de paradigma que afirma que el principal determinante de la eficacia terapéutica de las MSCs es la producción de factores en el microambiente, por encima de la implantación y diferenciación directas de estas células. En consecuencia, se han iniciado estudios sobre este conjunto de factores generados por las MSCs y secretados al medio extracelular, denominado secretoma. El empleo del secretoma de MSCs como terapia supone ventajas en muchos aspectos respecto al uso directo de las MSCs. Estas ventajas incluyen evitar los problemas de supervivencia celular tras la implantación, reducir aún más el riesgo inmunogénico, facilitar la producción y la aprobación legal como medicamento, simplificar la logística de almacenamiento, y la posibilidad de crear un producto adaptado a patologías específicas, atribuible a su alta plasticidad inherente.

En trabajos previos, nuestro grupo de investigación determinó que el silenciamiento del gen *Smurf1*, que actúa como un inhibidor de la vía de señalización de las proteínas morfogenéticas óseas (BMPs), una vía esencial que rige la diferenciación de las MSCs hacia osteoblastos, hacía que las MSCs mostraran un mayor potencial osteogénico. Dado que el secretoma de las MSCs constituye un reflejo de las propias células, la hipótesis que plantea este trabajo es que el silenciamiento del gen *Smurf1* en MSCs conduce a estas células a producir un secretoma que, de manera similar, posee un mayor potencial osteogénico, y que podría ser usado como terapia en trastornos del déficit óseo como la osteoporosis.

Así, el objetivo último de este proyecto es sentar las bases de un sistema terapéutico para el tratamiento de la osteoporosis, basado en el uso de secretoma de MSCs en las que se ha inhibido el gen *Smurf1*.

Inicialmente, se determinó que el silenciamiento de este gen en las MSCs sanas podía lograrse mediante la aplicación un tipo particular de oligonucleótidos antisentido conocidos como GapmeRs, así como la posterior producción del secretoma o medio condicionado (CM)[1].

Estudiamos el efecto del CM *in vitro* sobre MSCs de rata (rMSCs) y en la línea celular de MSCs de tejido adiposo humano ASC52telo. Los resultados demostraron que el CM de MSCs en las que el gen *Smurf1/SMURF1*[2] está silenciado (CM-*Smurf1/SMURF1*) promueve la diferenciación osteogénica *in vitro*, como así se verificó mediante el estudio de marcadores osteogénicos, actividad fosfatasa alcalina y de mineralización usando la tinción rojo alizarin. Los resultados obtenidos *in vivo* en el modelo ectópico reforzaron las conclusiones iniciales extraídas de los modelos *in vitro*, corroborando que ese incremento de la capacidad osteogénica de las MSC tratadas con CM-*Smurf1* se conservaba en un organismo vivo.

Sin embargo, estos modelos distaban considerablemente del contexto clínico que pretendíamos abordar, ya que el CM se administró a MSCs sanas. Por ello, se llevó a cabo un experimento para analizar el efecto sobre el potencial osteogénico de MSCs procedentes de pacientes con osteoporosis (hOP-MSCs). Las hOP-MSCs tratadas con el CM-*SMURF1* mostraron incrementos significativos en la actividad fosfatasa alcalina y en la mineralización, con resultados similares a los obtenidos cuando estas células se estimulaban con la molécula pro-osteogénica BMP2. El siguiente paso consistió en el modelo *in vivo* de osteoporosis en ratones, diseñado para emular la osteoporosis asociada a la menopausia. El CM-*Smurf1* mostró una atenuación significativa de la pérdida ósea trabecular como consecuencia de la ovariectomía, lo que indica un efecto protector óseo pronunciado.

Se examinó el efecto de CM-*SMURF1* sobre funciones biológicas básicas de las MSCs, como la capacidad proliferativa, de migración y de quimiotaxis. Los

[1] Si bien, en general, en la literatura científica, estos términos se utilizan con frecuencia indistintamente, hay que señalar que se entiende estrictamente como secretoma al conjunto de factores liberados por la célula. Sin embargo, a nivel experimental no es posible aislar el secretoma sin un medio de cultivo que lo contenga. En consecuencia, el término secretoma sería un concepto más teórico, mientras que, en la práctica, se trabaja con medio condicionado.

[2] *Smurf1* para células murinas. *SMURF1* para células humanas.

datos indicaron que inducía un incremento de la migración y de la atracción quimiotáctica sobre MSCs, lo cual podría contribuir a la actividad regeneradora del CM.

Para dilucidar mejor los mecanismos que sustentan la actividad del CM-*SMURF1* se separó la fracción soluble (SF) de la fracción vesicular (VF) y el potencial osteogénico de cada fracción se evaluó de forma independiente. Las evaluaciones revelaron que ambas fracciones estimulaban un mayor potencial osteogénico en las MSCs, concluyendo en que el desarrollo de una terapia en base al CM-*SMURF1* debía estar constituida el CM completo dado que las dos fracciones ejercen colectivamente un efecto sinérgico que optimiza la aplicación de cualquiera de las fracciones de forma aislada. En busca de una mejor comprensión del contenido del CM-*SMURF1*, se llevó a cabo un análisis de espectrometría de masas de la SF y la VF. De acuerdo con los hallazgos del estudio de inducción osteogénica de las fracciones, se identificaron proteínas estrechamente relacionadas con la actividad osteogénica en ambas fracciones del CM-*SMURF1*, como PREPL (Prolyl Endopeptidase Like), FMOD (Fibromodulin), SPARC (Secreted Protein Acidic and Cysteine Rich) y CCN2 (Cellular Communication Network Factor 2), lo que reforzó la idea de una acción sinérgica de la SF y VF.

Finalmente, dado que se prevé que la administración de CM-*SMURF1* en el tejido óseo de pacientes afecte no solo a las MSCs, sino también a otras células del microambiente óseo, realizamos un análisis del efecto de CM-*Smurf1/SMURF1 ex vivo* sobre fragmentos óseos de pacientes e *in vitro* sobre osteocitos y osteoclastos. Todos estos estudios apuntaron hacia una inducción de un perfil pro-osteogénico del CM-*Smurf1/SMURF1* sobre el microambiente óseo mediante reducción de resorción ósea.

En general, nuestros resultados indican que el medio condicionado de MSCs en las que se ha silenciado el gen *Smurf1/SMURF1,* representa una base prometedora para el desarrollo de un sistema terapéutico destinado a la prevención o el tratamiento de los síntomas asociados a la osteoporosis.

SUMMARY

Summary

Bone constitutes a dynamic tissue that undergoes continuous renewal to ensure the appropriate performance of its functions. This process of continuous renewal is known as bone remodelling and is carried out by a complex system of intercellular communication in which osteoclasts resorb bone matrix which is subsequently replaced by new matrix produced by osteoblasts. The correct execution and coordination of bone remodelling is fundamental for the maintenance of bone homeostasis, and alterations in this process lead to changes in bone architecture.

In osteoporosis, this balance is disturbed, partially attributable to a reduction in the differentiation of mesenchymal stem cells (MSCs) into osteoblasts, then leading to a decrease in the formation of new bone matrix. When this imbalance persists over time, it leads to thinning or loss of trabecular structures within the trabecular bone, as well as decreased thickness and increased porosity within the cortical bone, resulting in osteoporotic fractures that affect the quality of life and life expectancy of the affected individuals.

There are treatments for osteoporosis, which can be classified according to their mechanisms of action into antiresorptive agents that inhibit osteoclastic activity, osteoforming agents that stimulate osteoblasts, and agents that have dual antiresorptive and osteoforming actions. However, the application of these treatments requires intricate decision-making by clinicians, in addition to the combination of pharmacological agents or sequential therapeutic strategies, all aimed at maximising therapeutic benefits and reducing the side effects that can result, which, although infrequent, can be severe. Thus, there is a search for new alternative therapies that facilitate clinical practice, improve adherence to treatment and offer greater cost-effectiveness.

In this context, the investigation into the use of MSCs began, yielding promising outcomes. The advantageous characteristics of these cells, including their ease of harvesting, their capacity to differentiate into various tissues, and their low immunogenicity, have facilitated their application in the treatment of diverse pathologies. Specifically, the use in bone pathologies is one of the most

widespread due to the known capacity of bone marrow MSCs to form osteoblasts physiologically. However, the use of MSCs as therapy also has some drawbacks such as low implantation rates, survival problems or tumorigenic potential.

At the same time, a paradigm shift has occurred in recent years, with the assertion that the main determinant of the therapeutic efficacy of MSCs is the production of factors in the microenvironment, rather than the direct implantation and differentiation of these cells. Consequently, studies have been initiated on this array of factors generated by MSCs and secreted into the extracellular environment, which is called the secretome. The use of the MSC secretome as a therapy has many advantages over the direct use of MSCs. These advantages include avoiding cell survival issues after implantation, further reducing immunogenic risk, facilitating production and legal approval as a drug, simplifying storage logistics, and the possibility of designing a product tailored to specific pathologies, attributable to its inherent high plasticity.

In previous work, our research group found that silencing the *Smurf1* gene, which acts as an inhibitor of the bone morphogenetic proteins (BMPs) signalling pathway, an essential pathway in the differentiation of MSCs into osteoblasts, resulted in an augmented osteogenic capability of MSCs. Considering that the secretome of MSCs mirrors the cells, the hypothesis posited in this study is that silencing the *Smurf1* gene in MSCs leads these cells to produce a secretome that similarly possesses greater osteogenic potential, which could be used as a therapy in bone deficit disorders such as osteoporosis.

Thus, the main objective of this project is to establish the basis of a therapeutic system for the treatment of osteoporosis, based on the use of MSCs secretome in which the *Smurf1* gene has been silenced.

Initially, it was determined that silencing of this gene in healthy MSCs could be achieved by the application of a particular type of antisense oligonucleotides known as GapmeRs, as well as the subsequent production of the secretome or conditioned medium (CM)[3].

[3] While these terms are frequently used interchangeably in the scientific literature, it is worth noting that the term secretome is strictly understood as the set of factors released by the cell. However, at experimental level, it is not possible to isolate the secretome without a culture medium containing

We investigated the effect of CM *in vitro* on rat MSCs (rMSCs) and on the human adipose tissue MSC cell line ASC52telo. The results revealed that CM of MSCs in which the *Smurf1*/*SMURF1*[4] gene is silenced (CM-*Smurf1*/*SMURF1*) promotes osteogenic differentiation *in vitro*, as verified by the analysis of osteogenic markers, alkaline phosphatase activity and mineralisation using alizarin red staining. The results obtained in the *in vivo* ectopic model reinforced the initial conclusions drawn from the *in vitro* models, corroborating that this increase in the osteogenic capacity of MSCs treated with CM-*Smurf1* was maintained in a living organism.

Nonetheless, these models were considerably distant from the clinical scenario we sought to address, as CM was administered to healthy MSCs. Thus, an experiment was conducted to evaluate the impact on the osteogenic potential of MSCs derived from patients suffering from osteoporosis (hOP-MSCs). The hOP-MSCs treated with CM-*SMURF1* exhibited substantial increases in alkaline phosphatase activity and mineralization with similar results to those obtained when these cells were stimulated with the pro-osteogenic molecule BMP2. The next step was an *in vivo* model of osteoporosis in mice, designed to closely simulate menopause-associated osteoporosis. CM-*Smurf1* showed a significant attenuation of trabecular bone loss following ovariectomy, indicating a pronounced protective effect on bone.

The influence of CM-*SMURF1* on basic biological functions of MSCs, such as proliferation, migration and chemotaxis capacity, was examined. The data indicated that it induced increased migration and chemotactic attraction on MSCs, which could contribute to the regenerative efficacy of CM.

To further elucidate the mechanisms underlying CM-*SMURF1* activity, the soluble fraction (SF) was separated from the vesicular fraction (VF) and the osteogenic potential of each fraction was assessed independently. The evaluations indicated that both fractions elicited an enhanced osteogenic potential in MSCs, leading to the conclusion that the development of a CM-*SMURF1*-based therapy should consist of the entire CM, as the two fractions

it. Consequently, the term secretome would be a more theoretical concept, whereas in practice, we work with conditioned medium.

[4] *Smurf1* for murine cells. *SMURF1* for human cells.

collectively exert a synergistic effect that optimises the application of either fraction independently. To gain a comprehensive understanding of the composition of CM-*SMURF1*, a mass spectrometry analysis was performed on the SF and the VF. In accordance with the findings of the osteogenic induction study of the fractions, proteins closely related to osteogenic activity were identified in both fractions of CM-*SMURF1*, such as PREPL (Prolyl Endopeptidase Like), FMOD (Fibromodulin), SPARC (Secreted Protein Acidic and Cysteine Rich) and CCN2 (Cellular Communication Network Factor 2), then reinforcing the idea of a synergistic action of SF and VF.

Lastly, since CM-*SMURF1* administration in patient bone tissue is expected to influence not only MSCs but also other cells in the bone microenvironment, we performed an analysis of the effect of CM-*Smurf1*/*SMURF1* on *ex vivo* cultures of bone fragments from patients and *in vitro* on osteocytes and osteoclasts. Collectively, these studies pointed towards an induction of a pro-osteogenic profile of CM-*Smurf1*/*SMURF1* on the bone microenvironment through reduction of bone resorption.

Overall, our findings suggest that the conditioned medium of MSCs in which the *Smurf1*/*SMURF1* gene has been silenced represents a promising basis for the development of a therapeutic system aimed at the prevention or treatment of symptoms associated with osteoporosis.

INTRODUCTION

1. INTRODUCTION

1.1. The Skeletal System

1.1.1. Composition of the Skeletal System

The human skeletal system comprises 206 bones that constitute the framework for the rest of the body tissues. The skeleton has two main parts: The axial skeleton, which is the axis of the body, including the skull, vertebral, column and ribcage; and the appendicular skeleton, which is formed by appendages, such as the upper and lower limbs, pelvic girdle and shoulder girdle. In the whole skeletal system, a variety of bone shapes can be observed, each indicative of their specific primary function. Bones of the axial skeleton, for instance, serve as protective components for vital organs like the brain, spinal cord and lungs. Meanwhile, the tubular and short structure of the fingers facilitates gripping functions, and the long bones enable locomotion (1-3).

Bones are a special form of connective tissue composed of 70% of mineral content, 22% of organic phase (also called osteoid) and 8% water (Figure 1) (4).

Calcium, phosphate and magnesium comprise the primary constituents of the mineral part of the bone. The predominant part of this mineral component is held by nanostructured plate-like crystals of hydroxyapatite, $Ca_5(PO_4)_3(OH)$, measuring approximately 20-50 nm in length and 12-20 nm in width, depending on age. Overall, the skeletal structure hosts between 1-1.5 kg of calcium in the form of hydroxyapatite (3, 5).

The osteoid, the unmineralized, organic component of the bone matrix is primarily composed of type I collagen (90%) and non-collagenous proteins (NCPs) (10%). Type I collagen is a structural protein that consists of two α_1 chains and a single α_2 chain that assemble into a triple helix. While collagen encompasses nearly all amino acids, it is specially abundant in glycine, proline, and hydroxyproline, which are crucial for the structure and rigidity of the triple helix. On the other hand, NCPs play vital roles in the organization of the extracellular matrix, coordination of mineral-matrix and cell-matrix interactions

and regulation of bone mineralization. These highly specialized proteins can be broadly categorized into distinct classes (6, 7):

- Proteoglycans: Heparin sulfate, hyaluronan, small leucine-rich proteoglycans (SLRPs), and versican.
- Glycoproteins. Alkaline phosphatase (ALP), fibronectin, thrombospondin (TSP1 and 2) and vitronectin.
- Proteins of the small integrin-binding ligand N-linked glycoprotein (SIBLING) family. Dentin matrix acidic phosphoprotein 1 (DMP-1), matrix extracellular phosphoglycoprotein (MEPE), osteopontin, sialoproteins.
- Osteocalcin. The main γ-carboxyglutamic acid (Gla)-containing protein in the bone.
- Osteonectin. Also known as secreted protein acidic and rich in cysteine (SPARC).

Water is also present in the bone, both in association with the collagen-mineral composite and in free motion through canalicular and vascular conduits. The unbound water undergoes redistribution in response to skeletal stresses and plays a role in the detection of loading and the subsequent cellular response within bone tissue (6, 7).

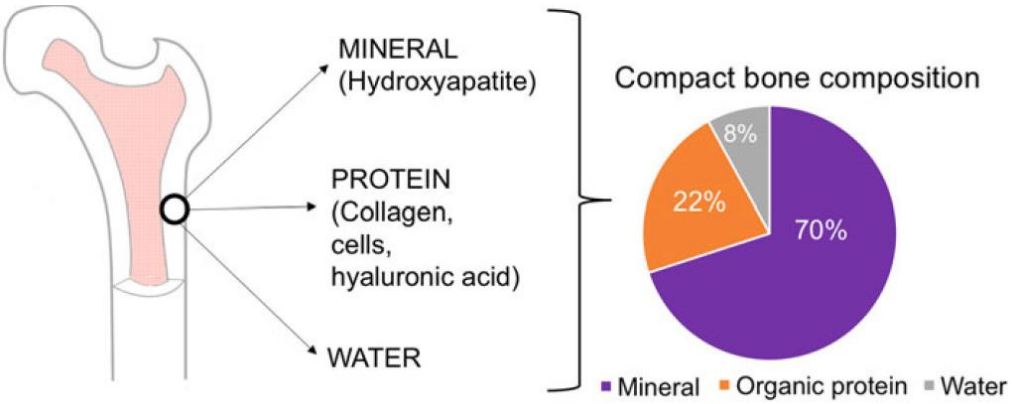

Figure 1. Schematic showing bone composition. Bone tissue is composed of 70% of mineral content, 22% of organic phase (also called osteoid) and 8% water. Image taken from Brett et *al.* 2017, in BioResearch Open Access (4).

Ensuring a healthy skeletal system lies on achieving a proper balance of the three former elements (Figure 1), referring to quantitative and qualitative

aspects. This involves attaining appropriate levels of minerals, osteoid and water along with proper organization of the mineral, crystallite size, collagen morphology and microarchitecture of the bone. Any imbalance in these parameters has the potential to impair the functions of the skeletal system (7).

1.1.2. Functions of the Skeletal System

The skeletal system contributes to several main functions in the body (2, 5-7):

- Protection. The robust and organized architecture of the bone offers protection to vital soft internal organs including the brain, heart, lungs and spinal cord. The balance that bone tissue maintains between rigidity and flexibility grants the capability to withstand reversible deformation caused by an impact, absorbing or dissipating the energy without cracking.
- Support and movement. As the rigid structures of the body, they give form and support, and in conjunction with muscles, tendons, and ligaments, bones facilitate bodily movement.
- Mineral homeostasis. Bones serve as the primary reservoir for minerals within the body, encompassing around 99% of the body's calcium, 85% of its phosphate, and 50% of its magnesium. These minerals play a crucial role in numerous physiological processes and are mobilized into the bloodstream in accordance with the body's requirements.
- Blood cell formation (haematopoiesis). Certain areas of bone, primarily consisting of trabecular bone, such as the iliac crest, vertebrae, and proximal femur, contain red bone marrow, a highly specialised tissue responsible for producing most of the body's blood cells.
- Endocrine regulation. Recently, bone has emerged as an endocrine organ due to its ability to secret hormones such as fibroblast growth factor 23 (FGF23) and osteocalcin. These hormones allow bone to regulate absorption and reabsorption processes in the kidneys and intestines. Furthermore, the influence of bone as an endocrine organ also comprises altering insulin secretion in the pancreas and impacting

skeletal muscle and adipocytes outside the bone, thus implicating bone in the regulation of energy within the entire organism.

1.1.3. Structural Organisation of the Skeleton

Bones are arranged as a multiscale and hierarchical structure. Each level of organization is precisely constructed to enable the bone to operate as a whole organ with the capability to carry out the aforementioned functions.

1.1.3.1. Nanoscopic structure

As previously mentioned, at the nanostructural level, bones are composed of type I collagen. Collagen molecules are composed of two identical α_1 helices and one α_2 helix, then forming triplets. Collagen triple helices self-assemble in line with one another into microfibrils. Then, in parallel, microfibrils are arranged in a quarter-staggered pattern to form collagen fibrils, which eventually reach 80-100nm in diameter and 10µm in length (Figure 2). This distinctive packaging results in the formation of spaces between the ends of the collagen molecules, termed "holes"; and between the laterally contiguous microfibrils, known as "pores". These spaces produce an oscillating surface topography of axially repeating bands along the fibril length called D-spacing which exists as a distribution of values near the theoretical 67 nm. These gap regions serve as a template for the deposition of bone mineral plates (6-8).

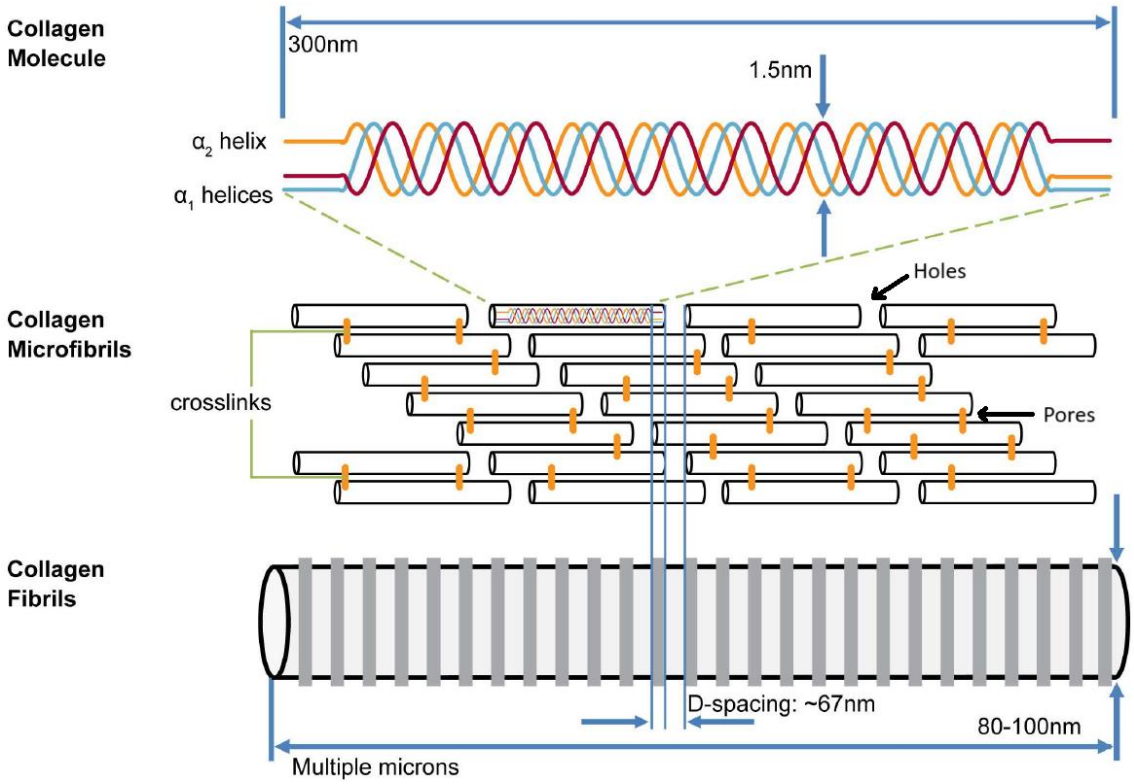

Figure 2. Collagen Structure and organisation. Characteristic organisation of collagen molecules, which self-assemble in a quarter-staggered array to form microfibrils and fibrils. This structure provides distinctive properties. Image taken from Canelón et *al.* 2016, in PLOS ONE (8).

The elemental organization of the collagen is crucial for bone function as the collagen-mineral composite provides unique material characteristics that combine from the rigidity of mineral and the pliability of collagen. Lateral and longitudinal aggregation of collagen molecules is essential to extend from the nanoscale to the microscale level (6).

1.1.3.2. Microscopic structure

At the microstructural level, the collagen-mineral composite exhibits an arrangement characterized by distinct parallel sheets referred to as lamellae. This laminar bone organize itself in circumferential concentric bands, creating lacunae spaces between these bands. It is within these lacunae that osteocytes, the primary bone structural cells, are located. These osteocytes communicate with one another through a physical connection that link the lacunae, called canaliculi (1, 2).

1.1.3.3. Macroscopic structure

The primary difference in bone composition at the macroscopic scale is between cortical (compact) bone and cancellous (spongy or trabecular) bone. Microscopically, both types are composed of lamellar bone, making them biochemically identical. However, they exhibit distinct structural characteristics, leading to different arrangements and functions that complement each other (1).

In the cortical bone, the arrangement of lamellae is highly compact, composing the predominant portion of bone mass in the skeletal system. This thick, mineralized tissue acts as a barrier, hindering the diffusion of oxygen and nutrients while impeding the removal of cellular waste products. To ensure proper nourishment of the tissue, the cortical bone is organised into osteons or Harvesian systems (Figure 3), which consist of multiple concentric layers of lamellae surrounding a central channel housing blood vessels, nerves and lymphatics. These central channels, called Harvesian canals, are typically aligned parallel to the bone's axis and branch out transversally into Volkmann's canals, facilitating physical communication through vessels and nerves within osteons and between the inner and outer surfaces of the cortical bone (2, 7).

Cancellous bone is comprised of plate- and rod-like structures, with a thickness of approximately 200 µm in humans. The arrangement of the bone laminae exhibits a relatively parallel orientation in relation to the trabecular surface. Due to their diminished thickness, these laminae do not require the presence of a canal structure, as observed in cortical bone, in order to facilitate proper irrigation. Instead, being located within the medullary cavity of the bone, these laminae are nourished by the diffusion of nutrients and oxygen through the vessels present in this space (Figure 3) (6, 7).

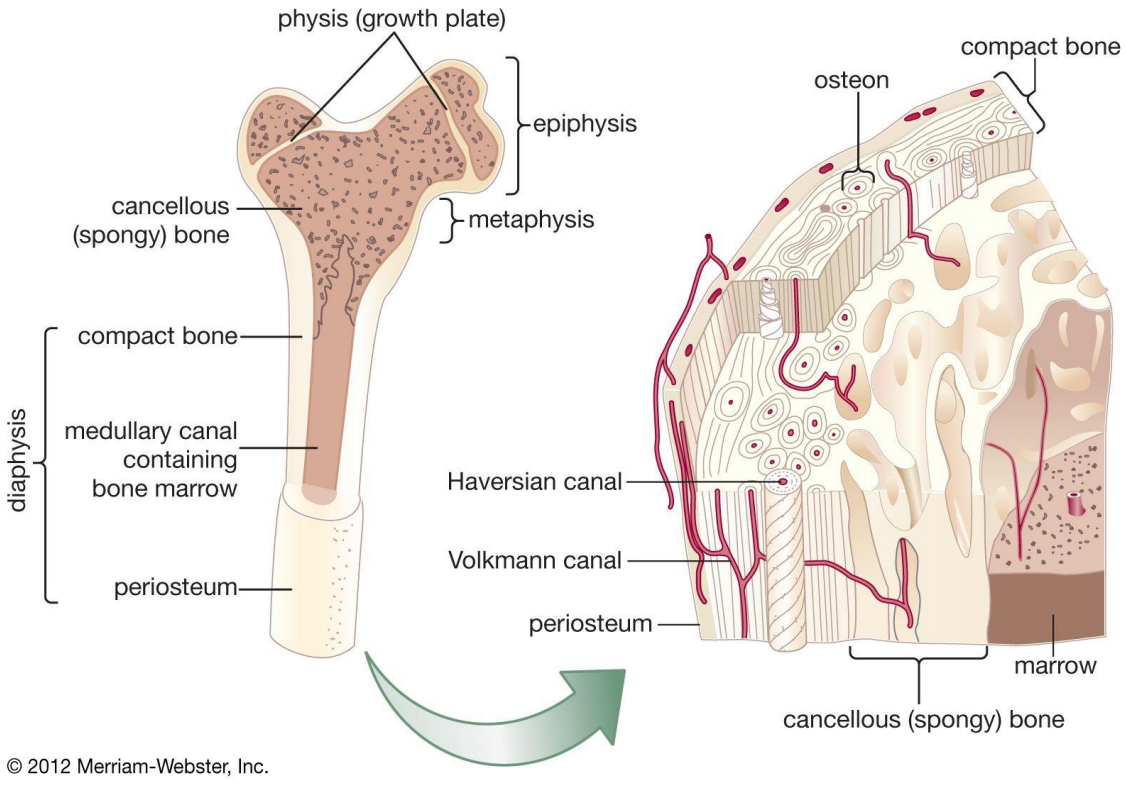

Figure 3. Bone is macroscopic structure, where dense cortical bone forms the outer shell and cancellous (trabecular) bone is present within the marrow cavity. Cortical bone at the macroscopic scale consists of numerous osteons, which feature a central canal housing blood vessels, nerves, and lymphatics surrounded by concentric lamellae, the Harversian canals. Trabecular bone, though also lamellar in nature, exhibits a structure characterized by a mix of lamellae running parallel to the trabecular surface alongside remnants of older bone that have been remodelled and may resemble osteons in certain regions. Image taken from Enciclopedia Médica Ferato (Hueso - Enciclopedia Médica Ferato).

Cancellous bone is found is typically found in the interior of bones, such as the ends of long bones (epiphyses), within the vertebrae, the ribs, the skull, and the pelvic bones. This type of bone offers structural reinforcement to the bone but avoiding substantial additional weight. Cortical bone is the predominant component of the long and short bones in the axial skeleton and is found around the cancellous bone of the vertebral body, at the ends of the long bones, in the iliac crest and in the skull. Cortical bone serves as a protective shield thanks to its load-bearing capabilities (Figure 3) (6).

1.1.3.4. Organ-level organization

As an organ, bone is composed not only of osseous tissue but also of other associated structures essential for its function. These structures include the periosteum, endosteum and bone marrow.

The periosteum is a thin fibro-cellular envelop that covers the outer surface of the bone (Figure 3). It consists of two layers: an outer fibrous layer containing dense connective tissue and an inner cambium layer populated with highly osteogenic cells. While the outer layer primarily provides support and protection to the bone, the inner cambium layer is responsible for bone formation in situations such as growth, development, modeling/remodeling and fracture repair. On the other hand, the endosteum is a fenestrated layer of flattened osteoprogenitor cells, also known as lining cells, that covers the entire inner surface of the bone. This includes the cortical wall of the medullary space, the surface of the trabecular bone and the inner walls of the osteons. These lining cells are associated with capillaries near the bone surface and sinusoids in the marrow. Therefore, in addition to their role in bone formation, lining cells also play a crucial role in regulating the flow of hydrophilic ions, like calcium, between the bone and blood (6, 9).

Bone marrow is a soft, spongy tissue found in the hollow interior of bones, responsible for the production of blood cells, including red blood cells, white blood cells, and platelets, through the process of haematopoiesis, starting from hematopoietic stem cells (HSCs). Bone marrow is located within the medullary cavity of long bones, vertebrae, ribs, sternum, skull, shoulder girdle and the pelvis. Bones provide protection to this vital tissue. For effective haematopoiesis, mesenchymal stem cells within the bone marrow (BM-MSCs) provide support and regulation to HSCs and to their more specialised progenitors. As a result of its rich vascular supply and the presence of haemoglobin in erythroid cells, the bone marrow displays a red coloration, hence it is called as red bone marrow. However, from the early postnatal period onwards, BM-MSCs, predominantly from long bones, begin to accumulate lipid droplets and lose their capacity for haematopoietic support, giving rise to what is referred to as yellow bone marrow. This transformation occurs due to the presence of adipocytes derived from BM-MSCs. Although it has been demonstrated that, under conditions of necessity, MSCs in yellow bone marrow can regain their haematopoietic supportive characteristics, their primary function is to serve as an energy reserve (2, 10, 11).

1.2. Bone Biology

Bone is a dynamic tissue that undergoes continuous adaptation throughout adulthood to maintain body structure and mineral homeostasis. The primary mechanism behind this phenomenon is bone remodelling, involving the simultaneous processes of bone formation and bone removal (resorption). These processes must be carefully coordinated to ensure the preservation of bone mass. Osteoclasts, osteoblasts and osteocytes are the cell types responsible for ensuring that these two opposite activities are tightly coupled in time and space (12).

1.2.1. Bone Cells

Osteoclasts, cells with a monocyte-macrophage origin, possess a high degree of specialization. These cells exhibit several unique characteristics, including the ability to degrade mineralized bone matrix. The main morphologic characteristic of osteoclasts is their large size and multinucleated nature, which is a result of the fusion of mononuclear precursor cells during the maturation process. After fusion takes place, the cytoskeleton of the osteoclast starts to reorganize, resulting in the cells becoming polarized. This polarization leads to the formation of an apical membrane domain that encounters the bone surface, as well as a basolateral membrane domain on the opposite side of the cell. Within the apical membrane domain, the osteoclasts are anchored to the bone through integrin receptors to Arg-Gly-Asp (RGD)-containing matrix proteins (osteopontin and bone sialoprotein). This attachment defines the sealing zone, which is the region where a strong union cell-bone occurs. Once attached, osteoclasts initiate the secretion of protons (H+) towards the bone, causing the acidification of the entire area. The production of protons is facilitated by the carbonic anhydrase enzyme. Protons are then released by the proton pump. To prevent intracellular polarization, the secretion of protons is balanced by the release of chloride ions (Cl-) through the chloride channel H+/Cl- exchange transporter 7 (CIC-7). HCl dissolves the hydroxyapatite component of the bone and exposes the osteoid, which is subsequently digested by enzymes that are also released by the osteoclast itself. These enzymes include Cathepsin K, Tartrate-resistant acid phosphatase (TRAP), and metalloproteinases such as Metalloproteinase 9

(MMP9) and Metalloproteinase 14 (MMP14). The region of the bone that undergoes degradation is referred to as the resorption Howship lacuna, while the portion of the osteoclast membrane involved in this process is known as the ruffled border. Once the bone has been degraded, the resorption products are internalized and eliminated within lysosomes (Figure 4) (12).

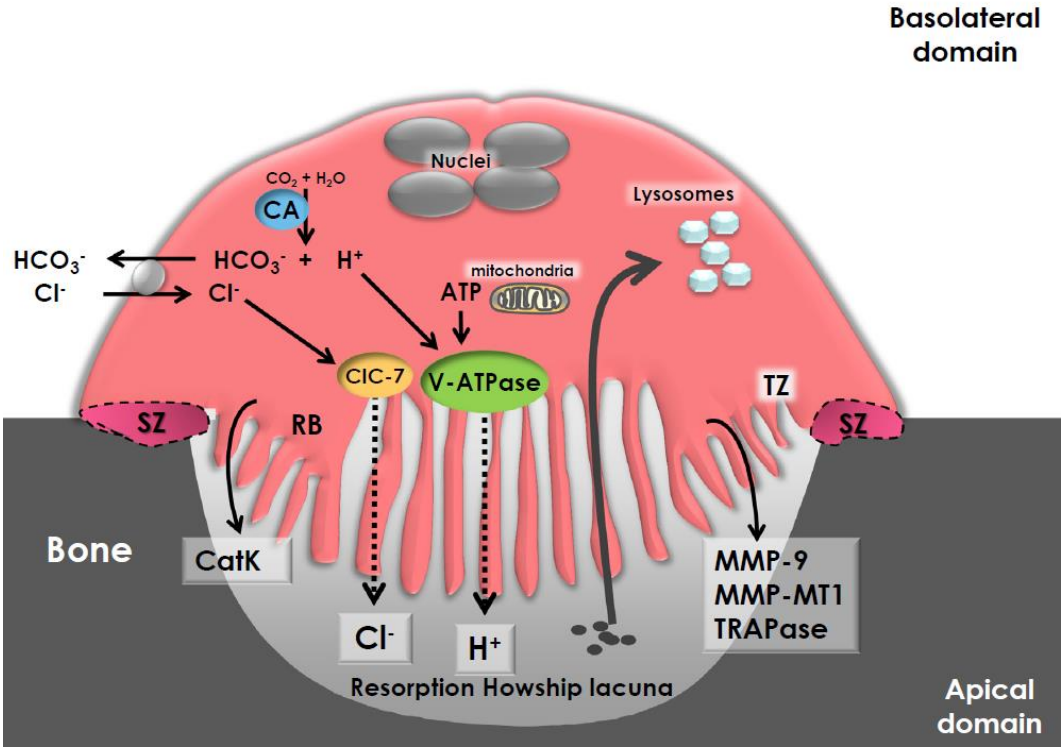

Figure 4. The morphology and functionality of osteoclasts are depicted schematically, illustrating key components such as the sealing zone (SZ), ruffled border (RB), transition zone (TZ), nuclei, and resorption lacuna. Osteoclasts in their mature state exhibit polarization, with the apical domain oriented towards the bone surface. Carbonic anhydrase-mediated proton production is essential, as these protons are conveyed to the RB membrane via the V-ATPase for secretion. The process of acidifying the resorption lacuna entails chloride ions (Cl−) being secreted through chloride channel 7. To maintain electroneutrality and prevent alterations in pH and/or membrane polarization, a basolateral bicarbonate/chloride exchanger operates. ATP production is facilitated by mitochondria. Cathepsin K, matrix metalloproteases (MMPs), and tartrate-resistant acid phosphatase (TRAP) collectively contribute to bone dissolution. Degradation products from bone are discharged into the bone microenvironment, taken up by the cell, and broken down within the lysosomes. Imagen taken from Bellido et *al.* 2019, in Basic and Applied Bone biology (12).

Osteoblasts, on the other hand, are responsible for bone formation. These cells are derived from mesenchymal stem cells (MSCs), which also have the potential to differentiate into various other types of cells including chondrocytes, muscle cells and adipocytes. The determination of the cellular lineage originating from the MSCs depends on the expression of specific transcription factors. For the osteoblastic lineage, the differentiation of MSCs into osteoblasts is regulated

by the master transcription factor runt-related transcription factor 2 (RUNX2). The primary role of osteoblasts is to produce osteoid. Consequently, they exhibit the characteristic morphology of cells that secrete high levels of proteins. These cells are cuboidal in shape, with large nuclei positioned close to the basal membrane of the cell. They have an enlarged Golgi apparatus on the apical surface of the nuclei, along with an extensive endoplasmic reticulum. Alkaline phosphatase (ALP) and osteocalcin are highly expressed in these cells (12, 13).

As the osteoblasts generate osteoid, they become trapped within this organic phase. A proportion of these cells ranging from 5% to 20% are engulfed by the matrix they produce, which subsequently undergoes mineralization. The rest of osteoblasts (60-80%) endure apoptosis or remain quiescent on the bone surface. These quiescent osteoblasts exhibit a flattened morphology, which is indicative of decreased protein production, and are referred to as bone lining cells. Bone lining cells serve as a reservoir of osteogenic precursors and are also believed to participate in calcium exchange, given their presence at the interface between bone and the extracellular bone marrow compartment (12).

Osteoblast that become trapped within the osteoid and do not undergo apoptosis, will form cytoplasmic projections to establish contact with each other, enabling their differentiation into osteocytes. As the bone matrix around them mineralises, lacunae (space around the cell body) and canaliculi (space around the dentritic processes) are formed. The expression of the membrane-associated proteins podoplanin (E11/PDPN/GP38) and MMP-14 is essential for this progression.

Osteocytes represent 90 to 95% of all bone cells and are uniformly dispersed throughout the bone structure. They possess a lengthy half-life, which distinguishes them from osteoclasts and osteoblasts which are only transiently present in bone, in limited numbers, and at variable locations. Osteocytes are not merely structural cells; their dendritic processes form connections with each other, and with the bone lining cells on the surface, creating the core of the functional syncytium that defines the bone as an organ. Within the lacunae, osteocytes can detect changes in mechanical signals (such as strain or fluid flow), and levels of circulating factors (ions or hormones). This ability permits signal amplification, resulting in adaptive responses of the skeleton to environmental

cues. Consequently, osteocytes play a pivotal role in bone metabolism, regulating the functions of osteoclasts and osteoblasts in response to various stimuli (12).

1.2.2. Bone Cells Intercellular Communication

Although the entire communication network that exists in bone is more complex, involving immune, endocrine, muscle and nervous system cells, here we will focus on a general overview of interactions occurring exclusively among bone cells. Within the bone microenvironment, osteocytes, osteoblasts and osteoclasts engage in continuous communication and coordinate responses to both internal and external stimuli (14).

Osteocytes, as the predominant cells in bone tissue, possess a significant relevance in bone communication, orchestrating the activity of osteoclasts and osteoblasts. The secretion of macrophage colony-stimulating factor 1 (MCS-F) by osteocytes promotes proliferation of osteoclast precursors. Osteocytes are also the primary source of tumour necrosis factor ligand superfamily member 11 (RANKL) in bone tissue. This protein facilitates the differentiation and fusion of precursor cells into multinucleated osteoclasts by targeting its receptor (receptor activator of nuclear factor-κB, RANK) on these cells. Additionally, osteocytes synthesize tumor necrosis factor receptor superfamily member 11B (osteoprotegerin, OPG), which acts as a decoy receptor for RANKL, thereby modulating its impact on osteoclasts. In terms of their interaction with osteoblasts, osteocytes are a major source of Wnt signaling inhibitors, such as Dickkopf1 (DKK1) and sclerostin (SOST). The Wnt pathway is crucial for the differentiation and function of osteoblasts, and the actions of SOST and DKK1 inhibit the binding of Wnt ligands to the Wnt receptors low-density lipoprotein receptor-related proteins (LRPs) 5 and 6 and Frizzled receptors, ultimately preventing the translocation of β-catenin to the nucleus (Figure 5) (15, 16).

In addition to the intrinsic regulatory role of osteocytes over osteoclasts and osteoblasts, these two cellular types engage in reciprocal communication, involving several known factors and receptors.

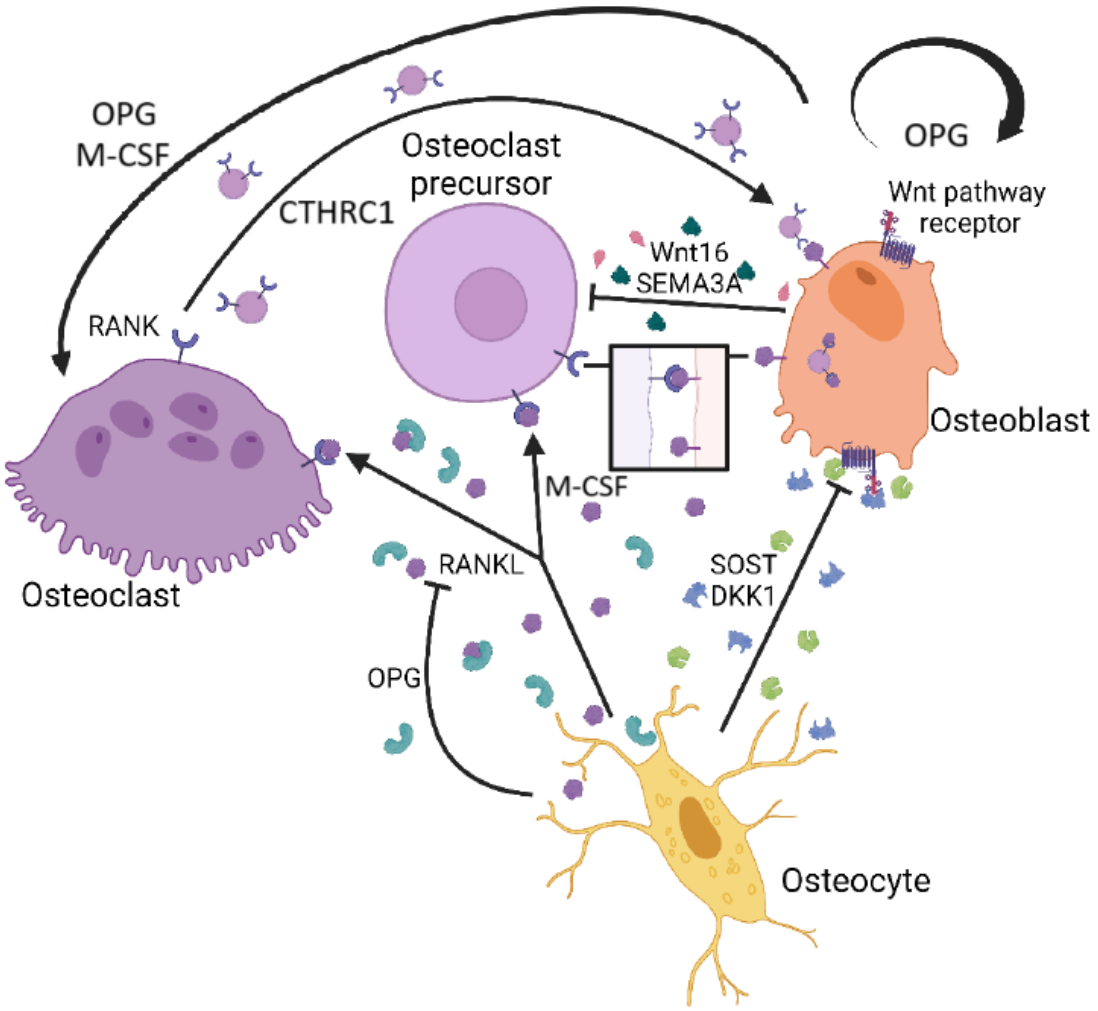

Figure 5. Crosstalk between bone cells. A schematic and simplified representation depicting the interplay between bone cells. Osteocytes display a pivotal role on bone regulation, modulating the action of osteoclasts through RANKL, MCS-F and OPG, while influencing osteoblasts by producing antagonists of the Wnt signalling pathway SOST and DKK1. Concurrently, osteoclasts activate osteoblasts by releasing RANK-loaded EVs and producing other factors such as CTHRC1. Furthermore, osteoblasts impact osteoclasts and their progenitors via MCS-F, RANKL, OPG, Wnt16, SEMA3A, and additional signalling molecules. Image taken from Daniel García Sánchez PhD thesis, 2023, in Universidad de Cantabria (14).

While RANK acts as a receptor for RANKL on the osteoclasts surface, osteoclasts can release extracellular vesicles (EVs) containing high concentrations of RANK factor, which in turn promotes the early stages of osteoblast differentiation upon binding to osteoblast membrane-bound RANKL. Several other factors secreted by osteoclasts have effects on osteoblasts functions, including Sphingosine 1 phosphate (S1P), which promotes osteoblasts migration and survival, Collagen Triple Helix Repeat Containing 1 (CTHRC1), which support the recruitment of osteoblast precursor cells and osteoblastogenesis and Complement component 3 (C3), Protein Wnt-10B

(WNT10B), and Ephrin B2 (EFNB2), which also stimulates osteoblastogenesis. Additionally, osteoclasts produce mediators that block osteoblast differentiation, such as semaphorin 4D (17, 18).

As osteoblasts belong to the same cell lineage as osteocytes, they produce MCS-F and, as just discussed, membrane-bound RANKL, which are pro-osteoclastogenic factors. They also produce factors that negatively affect osteoclasts, including surface receptors like Ephrin B4 and Semaphorin 3A (SEMA3A), which impedes osteoclastogenesis and Tumor necrosis factor ligand superfamily member 6 (TNFRSF6B/FASL/CD95L), which induces osteoclasts apoptosis. Osteoblasts likewise secretes factors like OPG and Protein Wnt-16 (WNT16), which also block osteoclastogenesis (18).

This communication between bone cells is crucial for the proper functioning of bone metabolism and, therefore, for bone remodelling.

1.2.3. Bone Remodelling

Bone remodelling is the primary process in the adult organism that facilitates the maintenance of bone health and functionality. Within the bone structure, remodelling takes place in discrete spatial units known as Bone Remodelling Compartments (BRCs), which allow the concentration of local factors facilitating the coupling of bone resorption and formation (Figure 6). Continuous bone remodelling involves the constant distribution of BRCs throughout the bone anatomy at various stages. This intricate process entails the collaboration of multiple cell types collectively referred to as the Bone Multicellular Unit (BMU), ensuring the successful progression of the five phases of remodelling, which may take, in humans, 4-6 months to be completed (12, 19). The characteristics of those phases are given in the following text:

1. Activation. Bone remodelling is instigated by physiological requirements and is typically triggered by specific stimuli. Although it can be initiated by mineral homeostasis needs, a significant portion of bone remodelling occurs in response to damage, where the initiation event involves osteocytes apoptosis. Microdamage is often the primary cause of osteocytes apoptosis due to the physical breakdown of their cytoplasmic

connections. Additionally, osteocyte death and network rupture can occur in the absence of microdamage, induced by factors such as oestrogen, mechanical inactivity, or excessive glucocorticoids. Prior to apoptosis, osteocytes actively communicate with bone lining cells to initiate the formation of the BRC, and with osteoclast precursors to stimulate recruitment and differentiation into mature osteoclasts. These osteocytes release RANKL and M-CSF, which, as previously mentioned, have a critical role in osteoclastogenesis. Conversely, healthy osteocytes produce anti-osteoclastic agents such as OPG, allowing a signalling pattern to be established to locate the start of the process (12, 19).

2. Resorption. The establishment of the BRC includes the retracting of bone lining cells from the bone surface, leading to the exposure of the mineralized matrix to the action of osteoclasts. These mature osteoclasts can then begin mineral degradation using proteinases, as previously described, a process that typically spans 3-6 weeks (12, 19).
3. Reversal. The resorption phase concludes when the degradation of bone by osteoclasts ceases. This cessation signal is initiated by the osteoclasts themselves, acting as a mechanism of negative feedback. The degradative activity of osteoclasts leads to the secretion of previously latent factors within the bone matrix, including Transforming Growth Factor β1 (TGF-β1) and Insulin-Like Growth Factor Type 1 (IGF-1), which promote the proliferation and differentiation of preosteoblasts into mature osteoblasts. Subsequently, these mature osteoblasts induce the cessation of resorption and the eventual apoptosis of osteoclasts through interactions involving surface receptors like EPHB4, FASL, SEMA3A; and secreted factors such as OPG and WNT16 (18).
4. Formation. The communication between osteoblasts and osteoclasts is a two-way process. Just as it inhibits osteoclast activity, these signals also stimulate bone formation in osteoblasts. Surface proteins on osteoclasts like EFNB2 or secreted such as S1P, CTHRC1, C3 and WNT10B support the survival and function of mature osteoblasts, facilitating the deposition of osteoid in regions resorbed by osteoclasts (18, 19).
5. Quiescence. Once the osteoid has been formed, covering the same amount of bone matrix that had been eroded away, the bone returns to the

resting state, with bone lining cells covering the bone surface. The osteoid will continue to mineralise for a period that may extend for a year or more, but this time is not considered part of the duration of the bone remodelling cycle (19).

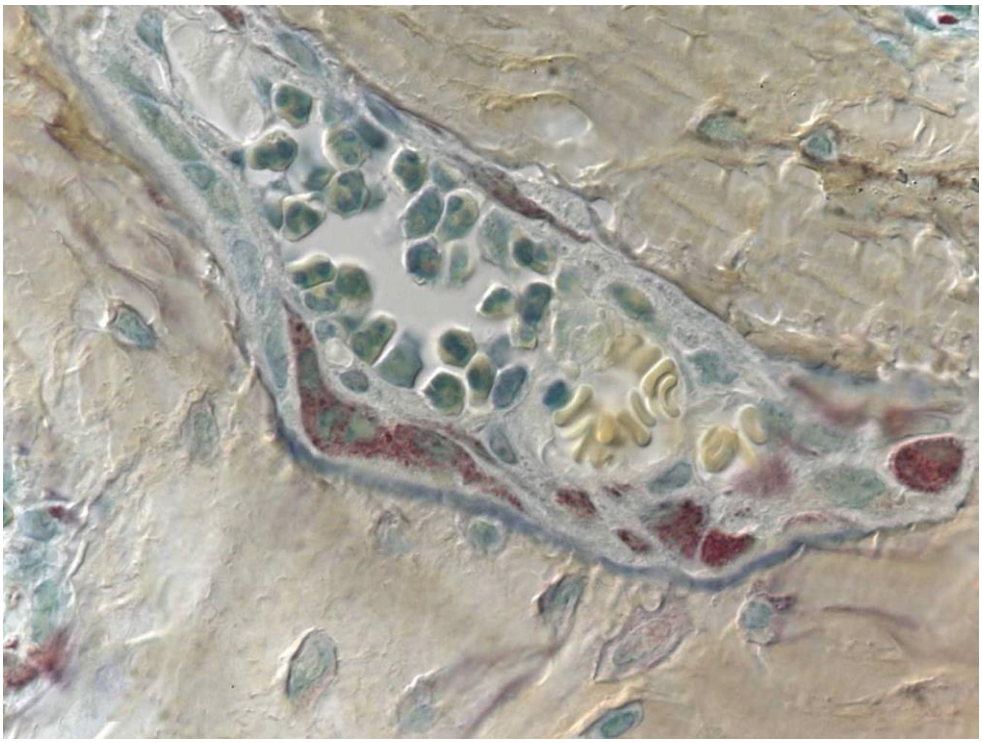

Figure 6. **Whole bone remodelling compartment observed in murine vertebral trabecular bone.** Visualization of DNA-specific stain methyl green and TRAP staining obtained using a Nomarski differential interference contrast microscopy. A cluster of osteoclasts displaying TRAP-positive red granules is observed as they erode through at the lower side of the panel. Osteoblasts are observed at the upper left side of the panel, actively engaged in the formation of new bone. The depositing osteoid line can be seen to the left of the bunch of osteoblasts. Osteocytes can be recognized embedded in the bone matrix. 630X. Image courtesy of Prof. Dr Robert S. Weinstein, University of Arkansas for Medical Sciences, USA.

1.3. Mesenchymal Stem Cells

1.3.1. Characteristics and Properties of Mesenchymal Stem Cells

The term "stem cells" refers to cells that exhibit two essential features: the ability to undergo self-renewal and the capacity to differentiate into different cell lineages. Stem cells can be categorized into two main groups based on their origin: Embryonic Stem Cells (ESCs) and Adult Stem Cells (ASCs).

ESCs are derived from the inner cell mass of the blastocyst and possess pluripotency, enabling them to generate all cell types within an organism. However, the use of human ESCs in therapy remains disputed due to their significant tumorigenic potential, as well as the ethical and legal issues associated with them. On the other hand, ASCs are extracted from adult tissues and exhibit multipotency, allowing them to differentiate into a wide array of cell lineages without facing the problems linked to ESCs (14, 20).

The concept Mesenchymal Stem Cells (MSCs) was first used by Caplan in 1991 (21) to described cells with tissue differentiation capabilities similar to ESCs, yet found forming reservoirs in adult individuals, contributing to the maintenance of adult cell turnover. Caplan successfully extracted MSCs from bone marrow (BM) and periosteum and demonstrated their potential to differentiate into bone (osteoblasts) and cartilage (chondrocytes). Moreover, he postulated that these cells could potentially pave the way for “self-cell therapy”, wherein patients would receive treatment using their own MSCs.

Since then, MSCs have been collected from various tissue sources, including umbilical cord, adipose tissue and dental pulp, among others. More recently, MSCs have been harvested from menstrual blood and endometrium (20). As a result of their distribution across multiple tissue types, with tissue-specific properties, the definition of MSCs has become less distinct. Thus, the International Society for Cell and Gene Therapy (ISCT) introduced specific criteria that must be met for cells to be identified as MSCs to standardize their characterization for research purposes. The criteria, outlined in Figure 7, encompasses growing in adherent culture under standard conditions, exhibiting CD105, CD73, and CD90 markers and absence of CD45, CD34, CD14 or CD11b, CD79a or CD19, and HLA-DR markers. MSCs should also display the capacity to differentiate into osteoblasts, adipocytes, and chondroblasts *in vitro* when exposed to specific stimuli.

1 Adherence to plastic in standard culture conditions

2 Phenotype	Positive (≥ 95% +)	Negative (≤ 2% +)
	CD105	CD45
	CD73	CD34
	CD90	CD14 or CD11b
		CD79α or CD19
		HLA-DR

3 *In vitro* differentiation: osteoblasts, adipocytes, chondroblasts (demonstrated by staining of *in vitro* cell culture)

Figure 7. Minimum ISCT criteria to classify MSCs. Summary of criteria established by International Society for Cell and Gene Therapy (ISCT) that cells must fulfilled to be identify as mesenchymal stem cells (22). CD: Cluster of Differentiation, HLA: Human Leukocyte Antigen. Image taken from Dominici et *al.* 2006, in Cytotherapy (22).

These conditions were delineated in a publication by Dominici et *al*. in 2006 (22) and persist today, serving as the established protocols that all researchers must adhere to in order to verify MSCs.

1.3.2. Use of Mesenchymal Stem Cells in Regenerative Medicine

MSCs have several characteristics that make them appealing for application in regenerative medicine:

- Obtainable from a wide range of tissue sources. While bone marrow MSCs (BM-MSCs) are considered the paragon type, MSCs have been sourced from nearly all tissues, including adipose tissue, dental pulp, synovial tissues, lungs, nasal olfactory mucosa, muscle, skin, scalp tissue, endometrium and menstrual blood, periosteum, cornea, peripheral blood, umbilical cord, amniotic fluid and placenta. This makes MSCs easily accessible (14).
- Easy to collect. Established methodologies exist for isolating MSCs from various tissue sources. Typically, these protocols are uncomplicated, often involving a digestion process and elimination of non-adherent cells (23).
- Notable proliferation capacity. While differences exist among MSCs from different sources, these cells generally exhibit robust proliferation and self-renewal abilities due to their stem cell nature (24).
- High potential for differentiation into several tissues. Beyond their ability to differentiate into mesodermal tissues like bone, fat, and cartilage, MSCs

display a broader differentiation capacity, including trans-differentiation into ectodermal tissues such as skin or neurons, and endodermal tissues like the liver or respiratory tract, given appropriate stimuli (14, 23).

- Low immunogenicity. Research indicates that MSCs lack expression of HLA-class II molecules and various costimulatory molecules like CD40, CD80, CD83, CD86, and CD154. Consequently, a degree of immunoprivilege is achieved when administrated into an organism. Moreover, these cells can induce immunosuppression *in vivo*, particularly in inflammatory environments, inhibiting a wide range of immune cells such as T cells, B cells and Natural Killer cells, as well as influencing the function of monocytes, dendritic cells and macrophages. This capability is valuable not only for regenerative purposes but also for diseases with a significant inflammatory component in their pathogenesis (24, 25).
- Homing and migration capabilities. MSCs have a wide set of adhesion molecules (e.g., CD44, Integrin α1), chemokine receptors (CCR2, CXCR4), metalloproteinases (MMP-1, MMP-9), and protease inhibitors (TIMP-1, TIMP-2), endowing them with unique homing and migration properties. These cells can move within blood vessels, cross the endothelial barrier, and home to their natural niches or migrate to sites of tissue damage where their functions are required to aid in tissue restoration (24).

Hence, as Caplan previously suggested, the use of MSCs holds enormous potential for the future. Recent publications in this year, 2024, accessible through PubMed (26), highlight therapeutic strategies utilizing MSCs for conditions ranging from glioma (27), glaucomatous optic nerve (28), rheumatoid arthritis (29), craniofacial reconstruction (30), polycystic ovary syndrome (31), ferroptosis (32), neuroinflammation (33), COVID-19 (34), thymic involution (35), hair regeneration (36), to ischemic stroke (37), just to mention some of them.

Furthermore, the focus is not solely on original articles. Global clinical trials in progress can be examined by utilizing the clinicaltrials.gov platform (38). Over 1600 ongoing clinical trials results from filtering with the term 'Mesenchymal Stem Cell', where MSCs from various sources are used to treat a wide range of

conditions (Figure 8). The exponential growth in the number of trials in recent years signifies that MSCs have transitioned from a mere promising tool to an established clinical reality.

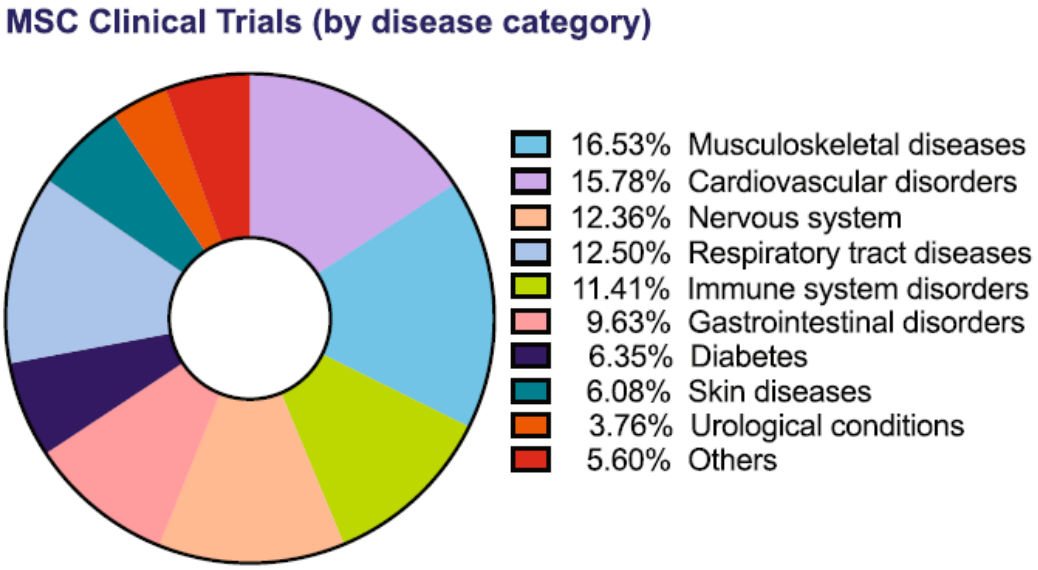

Figure 8. MSCs clinical trials by disease category. A diagrammatic illustration depicting documented clinical trials involving mesenchymal stem cells across diverse organ systems and associated disorders is presented. A pie chart was generated utilizing data on MSC clinical trials retrieved from clinical trials.gov (March 2023), facilitating the calculation of the proportional distribution of MSC trials among different disease categories. Image taken from Maldonado et *al.* 2023, in Journal of Biological Engineering (39).

1.3.3. Osteogenic Potential of Mesenchymal Stem Cells

Among all the therapeutic possibilities that can be achieved using MSCs, bone regeneration stands out as a prominent area of interest and research. One of the primary factors for this focus is the fact that BM was one of the initial sources from which MSCs were isolated (40). This led to Owen et al. in 1988 (41) to postulate that, similar to the haematopoietic system being supported by HSCs, there must be stem cells within the stromal system, identifying MSCs as strong candidates for this role. This pivotal insight laid the groundwork for the current knowledge: BM-MSCs function as precursors for osteogenesis, supporting the formation of osteoblasts, crucial for cell turnover in adult individuals, and the maintenance of the balance between bone formation and resorption (12).

The differentiation of MSCs into the osteoblastic lineage depends on the activation of specific transcription factors. Various signalling pathways are implicated in the osteogenic differentiation of MSCs, encompassing Bone

Morphogenetic Proteins (BMPs), Hedgehog, Notch, Neural Epidermal Growth Factor-like Protein 1, and the Wnt/β-catenin signalling pathways. In this section we will focus on BMPs signalling pathway (12, 14).

BMPs are growth factors that belong to the TGF-β superfamily of proteins. BMPs are involved in many vital physiological processes including cell proliferation, differentiation, inhibition of growth and maturation in different cell types, depending on their cellular microenvironment. There are at least 20 BMPs, but only 5 of them are known to induce bone formation: BMP2, BMP4, BMP5, BMP6, and BMP7. BMPs are synthesized as precursor proteins that are subsequently glycosylated, dimerized via a disulfide bond and secreted to the extracellular space. The dimerization process is key to this pathway, as they can form homodimers (e.g., BMP-2/BMP-2) or heterodimers (BMP-2/BMP-7) triggering a wide range of signals that would result in various cellular effects. BMPs act by binding to bound-membrane serine/threonine kinase receptors present on MSCs. These receptors consist of a dimer composed of a BMP receptor I (BMPR-I) and a BMP receptor II (BMPR-II). BMPs have four different BMPR-I types: activin A receptor-like type I (ACVRL1, also known as activin-like kinase I, ALK1), ActRI (activin receptor I also known as Activin Receptor-Like Kinase2, ALK2), BMPR-IA (Bone Morphogenetic Protein Receptor Type IA, also known as Activin Receptor-Like Kinase 3, ALK3) and BMPR-IB (Bone Morphogenetic Protein Receptor Type IB, also known as Activin Receptor-Like Kinase 6, ALK6); and three type II receptors: BMPR-2 (Bone Morphogenetic Protein Receptor Type II), ActRIIA (Activin Receptor Type IIA), and ActRIIB (Activin Receptor Type IIB). When the BMP molecule binds, an oligomeric complex is formed, and BMPR-II is phosphorylated intracellularly, which in turn transphophorylates BMPR-I. Here, the BMP pathway can follow two pathways: the canonical and the non-canonical BMP pathway (42).

In the canonical BMP pathway, small mothers against decapentaplegic (SMAD) proteins play a central role (Figure 9). There are three classes of SMAD proteins based on their functions: the receptor-regulated SMADs (R-SMADs), the common-mediator SMADs (Co-SMADs) and the inhibitory SMADs (I-SMADs). SMAD1, SMAD5 and SMAD8 are R-SMAD proteins that form a complex that is directly activated by BMP receptors, then the intracellular cascade of this pathway

starts. SMAD1/5/8 oligomerize with SMAD4, CoSMAD, and this complex translocates to the nucleus. Once in the nucleus, it interacts with transcription factors such as RUNX2 co-activator, targeting genes encoding important proteins for osteoblasts differentiation and function like osteocalcin, collagen α_1 chain and alkaline phosphatase (16, 42).

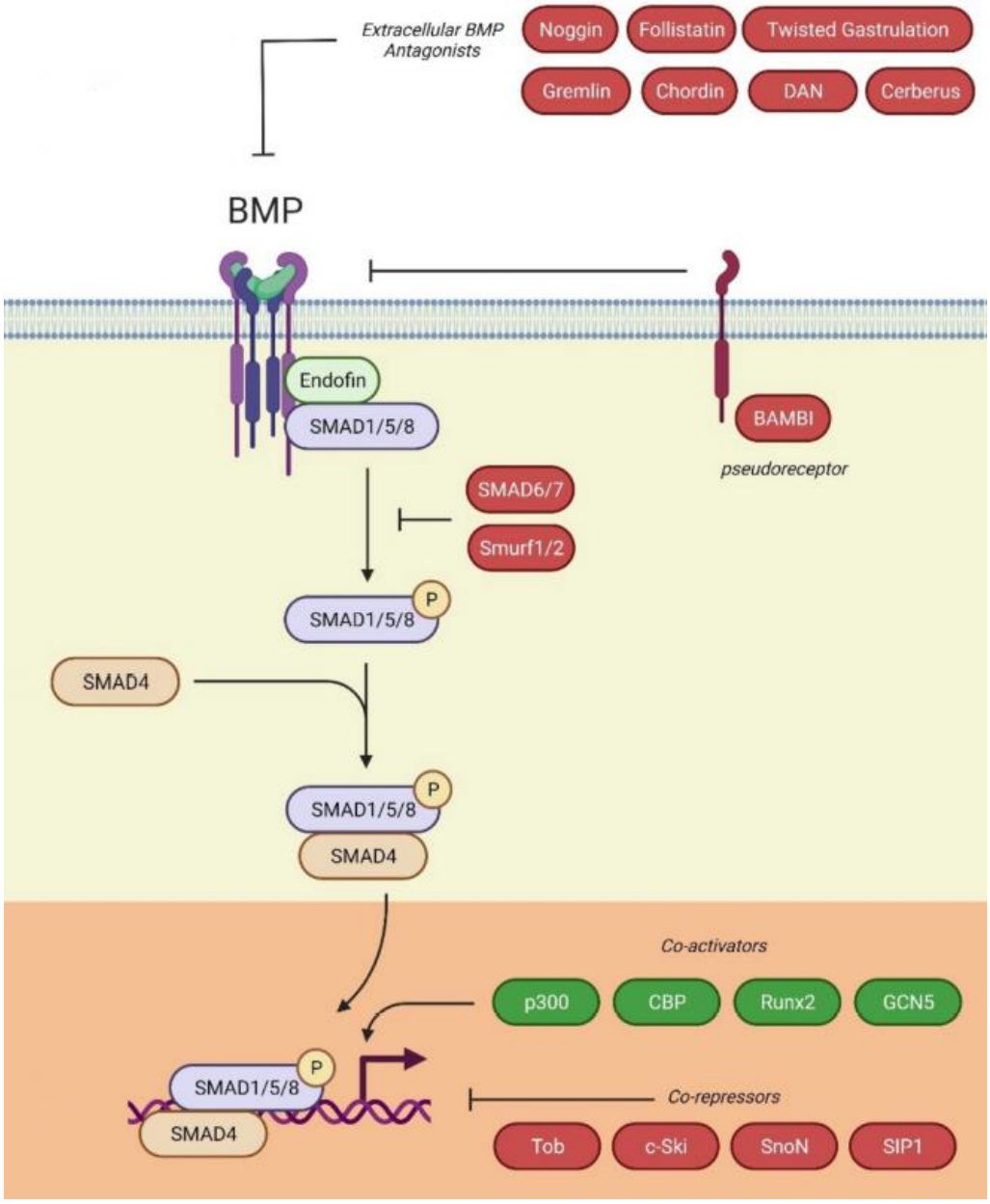

Figure 9. Diagram of the canonical BMP pathway. Schematic showing the main factors involved in the BMP pathway. BMPs bind to BMP receptors, which activate R-Smads (Smad1, Smad5 and Smad8). This complex associates with the Co-Smad Smad4 to subsequently translocate to the nucleus and allow the expression of osteogenic genes. Antagonists like Noggin, Gremlin, Smurf proteins or Tob1 constitute of checkpoints at different levels of the pathway. Image taken from Shu et *al.* 2021, in Cells (42).

The non-canonical BMP pathway is SMAD-independent. In this case, BMP receptors interact with bone morphogenetic protein-receptor-associated molecule 1 (BRAM1) and X-linked inhibitor of apoptosis protein (XIAP), and downstream molecules such as TGF-β activated kinase 1 (TAK1) and TAK1 binding protein (TAB1), that form the TAB1-TAK1 complex. The downstream signal continues with this complex activating pathways led by kinases such as extracellular signal-regulated kinase (ERK), map kinase p38, C-Jun N-terminal kinase (JNK), the nuclear factor κβ (NFκβ) and PI3K/Akt pathways signalling pathways, which finally activate RUNX2, as in the canonical pathway, or other coactivator factor such as CREB-binding protein (CBP), and trigger osteoblast genetic program (14, 42, 43).

Antagonists of the BMP pathway have been described at multiple levels. There are extracellular inhibitors, that sequester BMPs proteins preventing them to interacting with their receptors and initiating the BMP cascade; examples include noggin, chordin, gremlin, and follistatin, among other secreted proteins (Figure 9). Additionally, the BMP and activin membrane bound membrane inhibitor (BAMBI) receptor, serves as a pseudo-BMP receptor type I lacking serine/threonine-kinase segment, then impeding the progression of the signalling cascade. There are also intracellular modulators such as I-SMADs (SMAD6 and SMAD7), which compete with R-SMADs and block the downstream signal when they bind to the BMP receptor. At cytoplasmatic level, SMAD ubiquitination regulatory factors (SMURF) 1 and 2 can ubiquitinate R-SMADs leading to their degradation by the proteasome system and blocking the pathway. In the nucleus, transcriptional corepressors like Transducer Of ErbB-2 1 (TOB1) or Smad interacting protein-1 (SIP1) hinder the binding of the R-SMAD complex to DNA preventing transcription of the target genes (14, 42).

This current knowledge about MSCs and their osteogenic commitment provides the required background for developing MSCs-based therapies for bone regeneration (23). This topic will be addressed in depth in the next sections.

1.4. Osteoporosis

1.4.1. Osteoporosis Landscape

Osteoporosis is the most prevalent chronic metabolic bone disorder, according to the World Health Organization (WHO). This pathology is characterized by low bone mass, microarchitectural deterioration of bone tissue and decreased bone strength, which leads to an augmented risk of fractures (44) Clinically, osteoporosis is diagnosed when patients show low bone mineral density (BMD), as this parameter indicates low bone quantity and quality. However, bone damage usually develops progressively with no apparent manifestation until fragility fracture occurs. Therefore, fracture commonly precedes diagnose if no proper BMD screening is conducted. Vertebral, humeral, distal radius, and hip fracture are the most common type of osteoporotic fractures, and they are coupled with secondary health problems, which affect not only life quality but also life expectancy (45, 46).

Osteoporosis affects around 6.3% of men and 21.2% of women over the age of 50, translating to a global impact of approximately 500 million individuals. Each year, there are up to 37 million fragility fractures, equivalent to 70 fractures per minute, as reported by the International Osteoporosis Society (47). Due to its prevalence among the elderly and the increasing life expectancy, a substantial exponential rise in cases is anticipated in the coming years. Projections suggest a two-fold increase in osteoporosis cases over the next two decades, with 50% of females and 20% of males over 50 expected to experience osteoporotic fractures (44).

Fractures have significant social repercussions, including pain, infection risks, body image alterations, and reduced mobility, thereby diminishing the overall quality of life. Psychological distress, social isolation, or loss of autonomy are estimated to affect 66% of women who have suffered an osteoporotic fracture (14). In severe cases, such as hip fractures, up to 20% of patients may die within the first year, primarily due to pre-existing medical conditions. Moreover, fewer than half of those surviving a hip fracture regain their prior level of functionality

(47). Economically, osteoporosis imposed a financial burden of €39 billion on the healthcare system of the European Union in 2010 (44).

Based on 2017 data, in Spain alone, around 2.8 million individuals over 50 are affected by this condition, with 330,000 new fragility fractures occurring that year, a figure expected to rise to 420,000 by 2030 due to demographic ageing. The Spanish healthcare system allocated €4.2 billion, with forecasts indicating a required increase of over 30% in 15 years, and this amounts do no considering the indirect costs such as associated sick leaves and the impact on caregivers due to the reduced mobility and limitations in daily activities suffered by these patients (47)

1.4.2. Osteoporosis Pathophysiology

As discussed in the “Bone Biology” section, bone tissue is a dynamic and integrative organ. Osteoblasts, osteocytes and osteoclasts along with their interaction with endothelial cells, adipocytes, immune cells, hematopoietic stem cells, among others, are regulated at various levels by direct cell-cell contact, soluble factors and Extracellular Vesicles (EVs) (48). This intricate communication leads to constant bone remodelling, which involves the continuous formation and resorption of bone tissue to renew and repair the skeleton (49).

The proper execution of bone remodelling action is essential for maintaining bone tissue homeostasis and any alteration of this process results in changes to bone architecture (50). In women, osteoporosis is typically caused by oestrogen deficiency that appears during menopause. In men, age-related bone loss is thought to be the primary cause, probably due to sex hormone levels reduction (51). Initially, the bone mass loss linked to osteoporosis was solely attributed to the increased osteoclasts activity. However, it is now known to also involve the differentiation of MSCs into either osteoblasts or adipocytes (52). In osteoporosis, this balance between osteoblast and adipocyte commitment is disrupted leading to an increase in adipocyte production and a decrease in osteoblasts generation. As a result, marrow fat accumulation increases while bone formation is reduced (53).

Over time, this imbalance in bone remodelling results in trabecular thinning and loss of trabeculae in cancellous bone, as well as reduced cortical thickness and increased cortical porosity in cortical bone. These changes contribute to a decrease in BMD and osteoporosis disease progression (Figure 11) (53, 54).

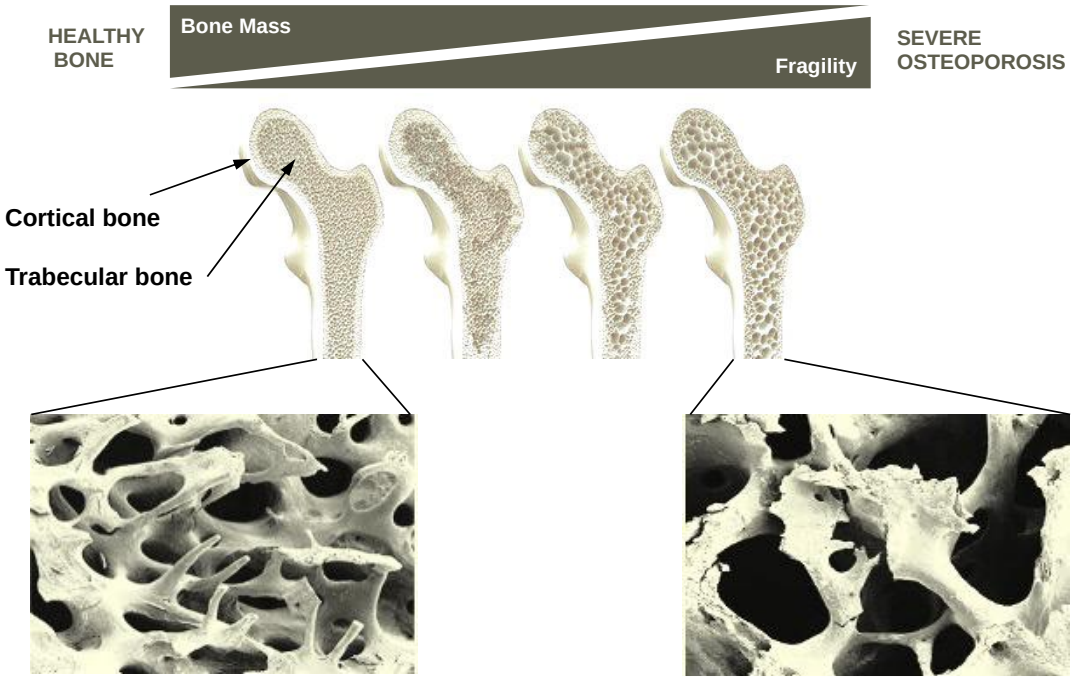

Figure 10. Bone microarchitecture shows inverse correlation between bone mass and fragility. Cortical and trabecular bone of are indicated using femur bone as a model. Image taken from Daniel García Sánchez PhD thesis, 2023, in Universidad de Cantabria (14).

1.4.2. Current Treatments

Currently, osteoporosis treatments can be classified into three different categories: anti-resorptive treatments, inhibiting osteoclast activity; bone-forming or osteoanabolic treatments, which activate osteoblasts; and treatments with a dual anti-resorptive and osteoanabolic action (49).

Various types of anti-resorptive therapies are available, each exerting their effects through distinct mechanisms of action (Figure 11):

- Biphosphonates such as alendronate, risedronate, ibandronate, and zoledronate are commonly used. Their chemical resemblance to pyrophosphate enables them to bind to hydroxyapatite in bone tissue. By disrupting the mevalonate metabolic pathway, these agents alter the osteoclast's ruffled border, ultimately inducing apoptosis.

Bisphosphonates have demonstrated efficacy in reducing bone resorption by up to 70%, thereby enhancing BMD and lowering fracture risk. However, prolonged bisphosphonate use may increase the risk of atypical femoral fractures and osteonecrosis of the jaw, which are severe adverse effects restricting their administration beyond a period of no more than 5 years (46, 49).

- Denosumab, a human monoclonal IgG2 antibody, acts by binding with high affinity to RANKL, thereby neutralising it and preventing its interaction with its receptor (RANK) on osteoclast precursors and mature osteoclasts. Inhibiting the RANKL/RANK pathway hinders osteoclast formation, function, and survival, leading to reduced bone resorption. Denosumab has been shown to lower bone turnover and significantly increase BMD over a longer duration compared to biphosphonates. However, since RANKL is expressed beyond osteoclasts, treatment with denosumab may elevate the risk of cutaneous infections (such as cellulitis, including erysipelas) and internal organ infections (pneumonia, diverticulitis, urinary tract infections). Other complications include atypical femoral fractures, osteonecrosis of the jaw, and hypocalcemia, limiting treatment to approximately 8 years (46).
- Selective oestrogen receptor modulators (SERMs) interact with oestrogen receptors on osteoblasts, modulating osteoblast-derived factors that promote osteoclast activity, thus reducing bone resorption. These agents are commonly used for postmenopausal bone loss and osteoporosis prevention and management. Raloxifene, an approved SERM therapy, mimics oestrogen by inhibiting osteoclast recruitment and activation, primarily suppressing RANKL release. While raloxifene reduces bone turnover, increases bone mass, and lower fracture risk, its efficacy is somewhat lower compared to bisphosphonates and denosumab. Adverse effects associated with SERMs include hot flushes, restless legs, peripheral oedema, gallstones, infrequent venous thromboembolism, and in rare cases, fatal strokes in women with ischemic heart disease. Although lasofoxifene and bazedoxifene have demonstrated anti-fracture benefits, only bazedoxifene in combination with oestrogen is currently approved for clinical use (46, 49).

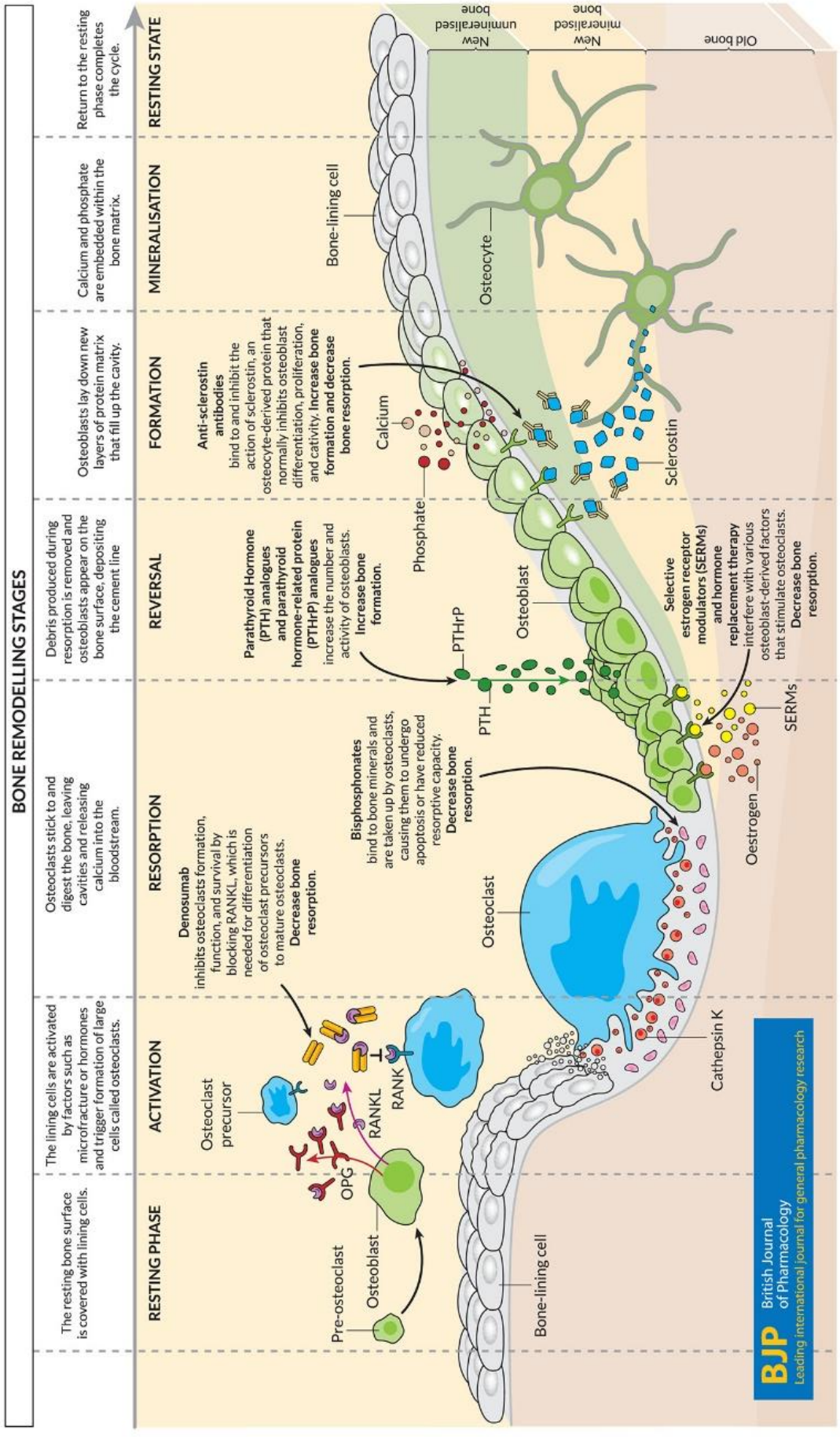

Figure 11. **Bone remodeling and the impact of several current treatments**. Visual representation outlining the distinct stages of bone remodeling and the way different treatments influence this process. Image taken from Langdahl 2020, in British Journal of Pharmacology.

Osteo-anabolic therapies:

- Parathyroid hormone analogues act through the parathyroid hormone type 1 receptor (PTHR) located on osteoblasts, thereby enhancing osteoblast number, differentiation, activity, and inhibiting apoptosis, ultimately improving bone quantity, quality, and strength. Teriparatide and abaloparatide are the current drugs targeting the PTH1 receptor. Teriparatide, a recombinant human PTH analogue, consists of the first 34 amino acids of the N-terminal end of PTH, while abaloparatide is a 34-amino acid synthetic analogue of PTHrP. Both drugs significantly reduce fracture risk, despite mild side effects such as nausea, headache, dizziness, leg cramps, and slight hypercalcaemia. Since preclinical studies in rats suggest an elevated risk of osteosarcoma, these treatments are restricted to a duration of 24 months, with abaloparatide not being endorsed by the European Medicines Agency (EMA), thus making it unavailable outside the United States (46, 49).

Dual-acting therapies:

- Anti-sclerostin antibodies target sclerostin, an osteocyte-derived glycoprotein regulated by the SOST gene. It has been found to regulate bone turnover arresting osteoblastogenesis and bone formation through the inhibition of the Wnt signalling pathway in osteoblasts, which play a crucial role in bone formation (55). Romosozumab, by binding to sclerostin, prevents its inhibitory effect, allowing Wnt ligand to bind to LRP-5 or LRP-6 Wnt receptors, activating the signalling pathway and promoting bone formation. Studies on bone turnover markers reveal that the unique mechanism of action of Romosozumab, increases bone formation and decreases bone resorption. The reduction in bone resorption is suggested to be linked to increased expression of OPG (osteoprotegerin), which acts as a decoy receptor to RANKL, thereby diminishing RANKL-RANK binding, and reducing osteoclastogenesis and bone resorption (56). Romosozumab has shown improved BMD and reduced fracture risk compared to Denosumab and Alendronate, making it a promising therapy. Nevertheless, the use of Romosozumab in clinical practice has some

drawbacks, such as the fact that bone formation reaches a plateau within 6 months of continued treatment. In addition, there are reports of cardiovascular adverse effects, and its costly nature as a humanised antibody implies an economic challenge (49).

Although effective when applied correctly, current therapies require intricate decision algorithms by clinicians to tailor treatments for each patient, often involving combination or sequential therapies to mitigate potential long-term adverse effects. Therefore, the imperative to enhance and streamline therapies persists to facilitate clinical practice and treatment adherence, urging the ongoing development of cost-effective treatments (45, 54).

1.4.3. Mesenchymal Stem Cells: Problem and Solution

Considering the weakened osteogenic capacity of MSCs as a contributing factor to osteoporotic pathology, the use of healthy MSCs appears to be a viable strategy for mitigating or reversing symptoms of osteoporosis. Numerous preclinical therapeutic endeavours have been conducted recently to explore this approach.

Most experimental investigations employing MSCs as a treatment for osteoporosis have been carried out using animal models such as mice, rats, and rabbits. These studies have explored various osteoporotic models including the glucocorticoid-induced model, immune-deficient model, and the senescence accelerated mouse prone 6 (SAMP6) model, which mimics age-related osteoporosis. Among these models, the rat ovariectomy model is frequently referenced due to its ability to induce bone loss resembling postmenopausal osteoporosis in women, without hormonal or pharmacological interventions. Various sources of MSCs have been utilized, with bone marrow-derived MSCs being the most commonly employed, though adipose-derived and umbilical cord-derived MSCs have also been studied. These cells have been administered either locally or systemically. Studies have reported positive outcomes in the osteoporotic phenotype, including improvements in bone microarchitecture, strength, stiffness, the formation of ossification cores at the histological level, and increased expression of osteogenic markers (52, 57-64).

Efforts to refine this therapeutic approach have included genetic modifications to MSCs to promote engraftment and differentiation at osteoporotic sites (65, 66), targeted delivery of cells, or the use of scaffolds to facilitate implantation (67, 68). An interesting method developed by our research group involved silencing *Smurf1* gene in rat MSCs and incorporating them into scaffolds implanted in calvaria bone defects in ovariectomized Sprague-Dawley rats, resulting in augmented bone regeneration compared to control subjects (69).

In the field of clinical trials, MSCs have shown promise as a therapeutic option for various diseases, as demonstrated by their clinical efficacy (39). Approved medications like Alofisel, designed for treating complex perianal fistulas in Crohn's disease patients (70), underscore the clinical potential of MSC-based therapies. However, there is a noticeable lack of clinical trials specifically targeting osteoporosis. A search on clinicaltrials.org (38) reveals only five registered trials at present, with one ongoing (NCT04501354), one concluding with positive outcomes (NCT01532076) (71), one completed without reported results (NCT02566655), and two suspended (NCT05152381; NCT05284604).

These findings reflect the challenges associated with MSC-based therapies, such as low engraftment rates, survival issues, and potential tumorigenicity (72, 73), further compounded by the complexities of osteoporotic pathology, a systemic condition necessitating systemic treatment that may lead to complications like fibrosis (74) or pulmonary embolism (75) following venous infusion. Furthermore, the efficacy of MSC therapies is still debated due to significant variations, mainly attributed to differences in age of the donor, *in vitro* passage number, culture conditions, administration procedure, and pathological microenvironments faced by the transplanted cells (76, 77). Consequently, further research is necessary to enhance the reproducibility and safety of MSC-based therapies and to uncover the precise mechanisms behind the regenerative effect.

1.5. Mesenchymal Stem Cell Secretome

1.5.1. MSC Secretome as a Cell-free Therapy

The secretome can be defined as the set of substances produced by cells and released into the extracellular milieu. These factors comprising the autocrine and paracrine communication system of cells consist of soluble proteins (growth factors, cytokines, antioxidants...), free nucleic acids, lipids, and Extracellular Vesicles (EVs), which are further divided into apoptotic bodies, microvesicles, and exosomes, carrying proteins and nucleic acids including microRNAs (78).

In recent years, the focus on MSC-based therapies has shifted from engraftment and differentiation to paracrine signalling as the primary determinant of therapeutic effect (76). Multiple studies support this assertion (79-83), having quantified that between 50% and 80% of the effect corresponds to these released factors (84). Thus, the secretome emerges as a promising tool for cell-free regenerative therapy. Instead of transplanted MSCs, using the secretome as a treatment offers various advantages (85):

- Overcoming survival issues after MSCs transplantation. A considerable number of transplanted MSCs did not survive in the host tissue (72). A significant amount and duration of MSC engraftment are necessary for the cells to directly enhance tissue repair. Expanding MSCs *in vitro* multiple times to overcome this hurdle may induce genome instability and increase the risk of tumorigenesis in MSCs.
- Reduced immunogenic risk. Although the absence of MHC-II and other markers means that MSCs generate low immunogenicity, among the components of the secretome there are fewer cell surface proteins, further lowering this risk. This low immunogenicity implies that the cells do not need to come from the patient, making it possible to have a ready-to-use product, shortening the time between diagnosis and treatment (85).
- Ease of production. With current advances in dynamic culture, it is possible to maintain MSCs for extended periods, consistently generating secretome under controlled conditions, thus creating a scalable and

reproducible method for secretome production (86). Additionally, this contributes to a more cost-effective production.

- Tailor-made product. The secretome exhibits plasticity allowing it to alter its composition in response to specific stimuli (78), such as factors in the culture medium or exposure to inflammatory agents, among others. This process, known as preconditioning or priming enables secretome-based therapies to be adapted to fit the specific requirements of damaged tissues (87). We will revisit this topic in detail later.
- Similar to conventional medicine. MSCs secretome may be evaluated for safety, dosage and potency similarly to conventional pharmaceutical compounds (85), facilitating their approval by regulatory agencies.
- Simplified storage. The secretome can be stored safely and without loss of potency. Additionally, the use of cryoprotective agents, which are needed to freeze cells, is avoided, thereby preventing toxicity associated with these substances (78).

1.5.2. Mesenchymal Stem Cell Secretome Components for Bone Regeneration

The discovery that a significant portion of the regenerative effect of MSC-based therapies is attributable to the MSC secretome has led to extensive efforts to characterise the bioactive factors within it that are responsible for these beneficial properties in regenerative medicine. Although the composition of the secretome may vary depending on the tissue of origin, isolation methodology, age of donor, culture medium chosen and the species from which the MSCs originate (88), several factors have been recognized as consistently present.

1.5.2.1. Mesenchymal Stem Cell soluble factors

A total of 1,533 proteins have been detected in the soluble fraction secreted by MSCs, known for their roles in various beneficial functions across regenerative processes, including immune modulation, anti-apoptotic actions, antioxidant properties, and pro-angiogenic effects (77).

One of the primary functions of MSC-based therapies is their immunomodulatory capabilities. There is mounting evidence supporting the

interaction of MSC soluble factors with lymphocytes, dendritic cells (DCs), natural killer (NK) cells, and macrophages, leading to immunosuppressive and anti-inflammatory effects (Figure 12). Notably, MSCs release hepatocyte growth factor (HGF), transforming growth factor-β1 (TGF-β1), indoleamine 2,3-dioxygenase (IDO), prostaglandin E2 (PGE2), and IL-10, impacting the differentiation, proliferation, and activation of T-lymphocytes while promoting polarization towards T regulatory cells (89). The secretion of PGE2, IDO, TGF-β1, interleukin-6 (IL-6), and nitric oxide (NO) by MSCs has been shown to significantly suppress NK cell cytotoxicity and proliferation(89). Furthermore, IL-10, in particular, stands out as a key inducer of M2 macrophage polarization (90).

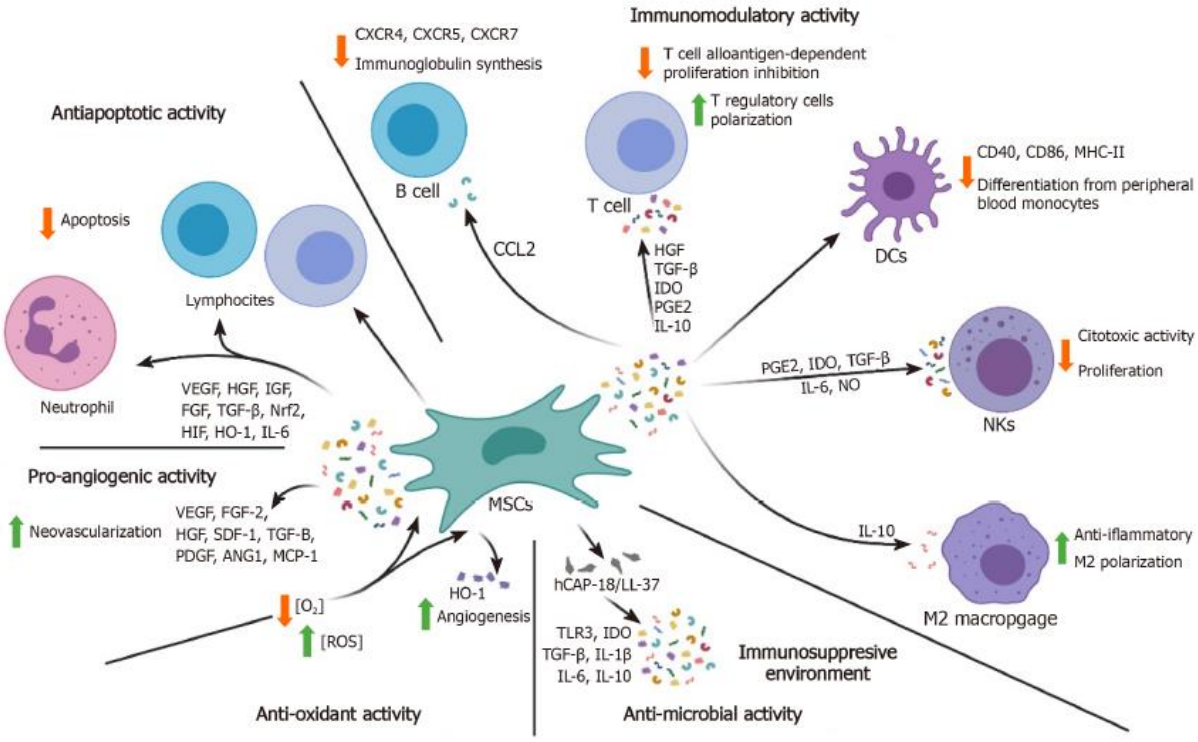

Figure 12. Summary of the plethora of soluble factors secreted by mesenchymal stem cells and their functions. HGF: Hepatocyte growth factor TGF-β: Transforming growth factor–β; IDO: Indoleamine 2,3-dioxygenase; PGE2: Prostaglandin E2; IL: Interleukin; DCs: Dendritic cells; CCL: CC-chemokine ligand; NKs: Natural killer cells; MSCs: Mesenchymal stem cells; CXCR: C-X-C chemokine receptor type; VEGF: Vascular endothelial growth factor; IGF: Insulin-like growth factor; FGF: Fibroblast growth factor; Nrf2: Nuclear factor erythroid-related factor 2; HIF: Hypoxia-inducible factor; SDF: Stromal cell-derived factor; PDGF: Plateletderived growth factor; ANG1: Angiogenesis 1; MCP-1: Monocyte chemotactic protein-1; ROS: Reactive oxygen species; hCAP: Human cathelicidin anti-microbial peptide; HO-1: Heme oxygenase; NO: Nitric oxide. Image taken from previous work of our group, published in 2020 in World Journal of Stell Cells (77).

Additional paracrine factors are secreted by MSCs, including vascular endothelial growth factor (VEGF), IL-6, HGF, insulin-like growth factor (IGF), fibroblast growth factor (FGF), TGF, nuclear factor erythroid-related factor 2

(NRF2), hypoxia-inducible factor (HIF), and heme oxygenase (HO-1). These factors play a crucial role in protecting against apoptosis in environments characterized by intense inflammation, such as those following injuries, affecting immune cells including T and B cells (91). It has been noted that HO-1 not only possesses antioxidative and anti-inflammatory properties vital for cell survival, but also leads to the up-regulation of pro-angiogenic growth factors like VEGF-A, stromal cell-derived factor-1 (SDF-1), and HGF (92). Furthermore, the secretome of MSCs contains additional pro-angiogenic factors such as FGF2, platelet-derived growth factor (PDGF), angiopoietin-1 (Ang-1), and monocyte chemotactic protein-1 (MCP-1), which have been shown to promote the differentiation of endothelial progenitor cells. Specifically regarding bone repair, the MSC secretome appears to enhance bone regeneration through the synergistic actions of IGF-1 and VEGF, as evidenced by Osugi et al. in 2012 (93), who used a rat model of bone defects. Moreover, Ogata et al. (94) successfully augmented the osteogenic differentiation, migration, and proliferation of MSCs by employing a combination of MCP-1, IGF-I, and VEGF, mimicking the concentrations present in the MSC secretome.

1.5.2.1. Mesenchymal Stem Cell Extracellular Vesicles

Besides soluble components, a significant portion of the secretome consists of Extracellular Vesicles (EVs). According to the International Society for Extracellular Vesicles (ISEV), EVs refer to the non-replicable small particles delimited by a lipid bilayer that lack a functional nucleus (95). EVs are produced by most cell types and can be categorized, depending on their size and biogenesis, into three primary classes: Exosomes, Microvesicles, and Apoptotic bodies. Exosomes, ranging from 30-150 nm in size, are generated within the endosomal network and released through the internal budding of multivesicular bodies; microvesicles, with a diameter of 50-1,000 nm, are large membranous vesicles produced by budding from the plasma membrane; lastly, apoptotic bodies, with a diameter of 800-5,000 nm, are released by cells undergoing programmed cell death (87, 96). Tetraspanins such as CD9, CD63, and/or CD81 are often used to identify EVs (Figure 13) (97).

In 2010, Lai et al. (98) conducted one of the initial studies demonstrating that the factors responsible for tissue regeneration were predominantly present in the exosomes of MSCs (MSC-Exos). Currently, it is recognized that numerous of these elements possess the ability to induce a pro-osteogenic effect (87).

According to ExoCarta (99), a repository of exosome content, a total of 938 functional proteins have been identified in MSC-Exos through various independent proteomic assessments, with studies outlining a well-established pro-osteogenic influence.

The presence of monocyte chemotactic protein-1 (MCP-1), MCP-3, and SDF-1 in MSC-EVs has been reported. MCP-1 is known to stimulate angiogenesis, whereas MCP-3 plays a role in promoting cell proliferation. Moreover, MCP-1, MCP-3, and SDF-1 have the capability to attract MSCs to the site of injury, initiating the bone regeneration process. IL-6, FGF-2, and PDGF-BB are also identified in MSC-EVs, contributing to endothelial cell proliferation, angiogenesis, and osteogenesis. Notably, PDGF serves as a crucial regulator in bone fracture healing by aiding in the formation of blood vessels and bones. The angiogenic impact of MSC-EVs reveals VEGF as a pivotal protein involved. Its role in facilitating the migration and proliferation of vascular endothelial stem cells, as well as in blood vessel formation, is well recognized. Additionally, VEGF stimulate osteoblast activity, promoting an overall pro-osteogenic effect and underscoring the significance of cellular communication between endothelial and bone cells in bone regeneration (77). Proteomics analysis by Munshi et al. (100) identified Angiopoietin-related protein 2 (ANGPTL2), neuropilin 1 (NRP1), fibronectin 1, IGF-I, and TGFβ-1 in MSC-EVs. ANGPTL2 and NRP1 are involved in angiogenesis, while fibronectin 1 and IGF-I enhance the actions of chondrocytes and osteoblasts. Furthermore, TGFβ-1 promotes the migration, proliferation, differentiation of osteoprogenitor cells, as well as cellular matrix production (Table 1) (101, 102).

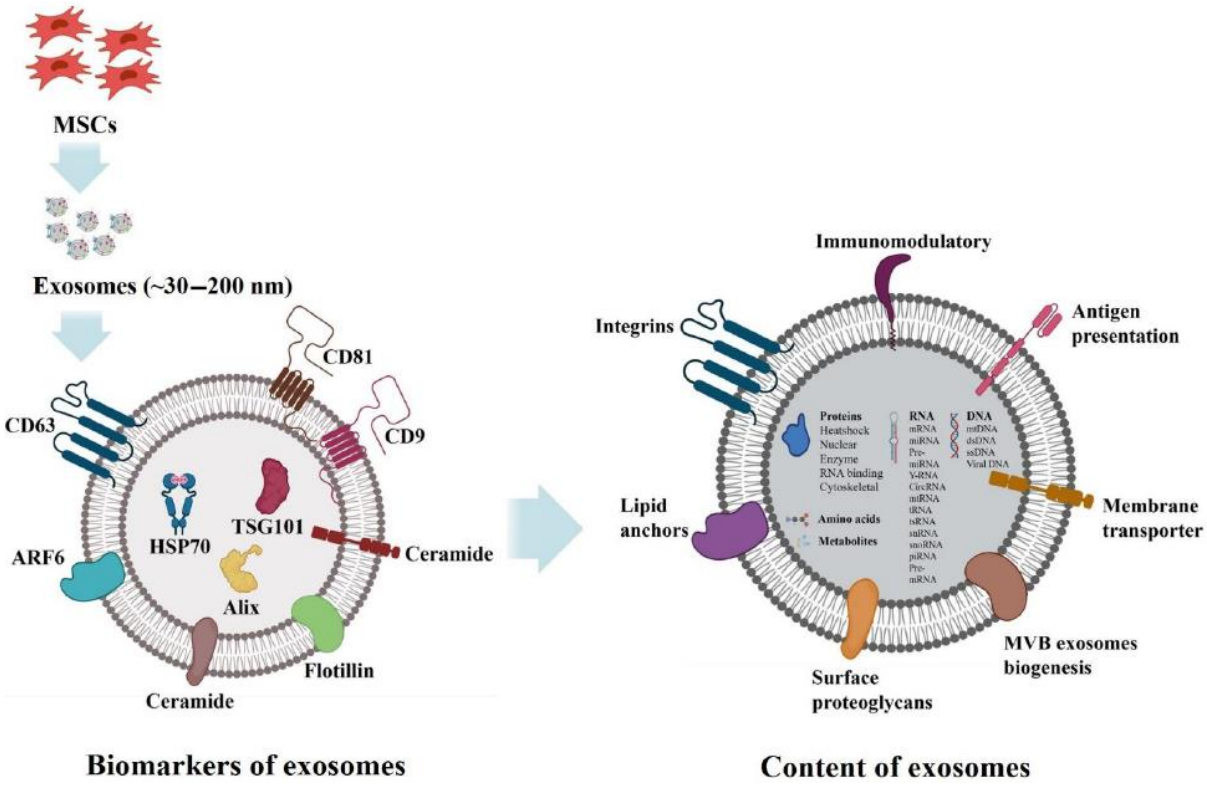

Figure 13. **Typical exosome structure**. Exosomes serve as a robust mode of communication between nearby and remote cells within the human body, exhibiting varied capabilities. These exosomes, originating from cells like MSCs, release therapeutic cargo comprising proteins, nucleic acids, lipids, enzymes, and metabolites. Image taken from Hade et *al.* 2021, in Cells (103).

In addition to proteins, MSC-EVs carry various nucleic acids, including different types of RNA and DNA, serving as crucial mediators of intercellular communication (Figure 13). Among these, microRNAs (miRNAs) have gathered significant attention in recent years. MiRNAs are short RNA molecules comprising 19-25 nucleotides that post-transcriptionally regulate gene expression. More than 150 distinct miRNAs have been identified in MSC-EVs, playing roles in the pathogenesis of numerous diseases, and emerging not only as therapeutics but also as diagnostic tools (104, 105).

Recent studies have identified several miRNAs within MSC-EVs that influence bone homeostasis. A comprehensive overview of key miRNAs found in EVs cargo and their specific roles in bone regeneration is presented in Table 1 (77).

Table 1. Main proteins and miRNAs in MSCs-EVs cargo having an effect in bone homeostasis. Their functions and references are indicated. Table taken from previous work of our group, published in 2020 in World Journal of Stell Cells (77).

MSC-EVs cargo		
Proteins	**Bone healing functions**	**References**
MCP-1	Induces angiogenesis and MSCs recruitment to injury site	(106)
MCP-3	Promotes cell proliferation and MSCs recruitment to injury site	(106)
SDF-1 α	Recruits osteoprogenitor cells to wound area	(107)
IL-6	Induces endothelial/endothelial progenitor cell proliferation angiogenesis and osteogenesis	(106)
FGF-2	Fosters proliferation, differentiation and migration of vascular cells, chondrocytes and osteoblasts	(108-110)
PDFG-B	Promotes mesenchymal proliferation, potentiates cartilage and intramembranous bone formation and stimulates angiogenic pathways	(102, 108, 111)
VEGF	Promotes revascularization, regulation of vascular endothelial cell migration, proliferation, and capillary production, and improves the cellular activity of osteoblasts	(112)
ANGPTL2	Potentiates sprouting in endothelial cells	(102)
Fibronectin	Collaborates in cell movement and migration and provides provisional fibers in cartilaginous matrices	(108)

IGF-I	Induces collagen synthesis, reduces collagen degradation, promote clonal expansion of chondrocytes and proliferation of preosteoblastic cells, and regulates migration of osteoblasts and MSCs	(108)
TGF-β1	Chemoattraction of macrophages, enhances migration, proliferation and differentiation of osteoprogenitor cells and cellular matrix production	(102, 108, 113)
NRP1	Induces endothelial cell migration and regulates other proangiogenic actions through VEGF family and PDGFR	(100)
microRNAs	**Bone healing functions**	**References**
miR-10a	Improves mesenchymal stem cell differentiation capacity of hBM-MSCs and reduces cell senescence	(114)
miR-10b	Increases in vitro migration of BM-MSCs	(115)
miR-218, miR-92a and miR-199b	Enhance osteoblast differentiation of BM-MSCs	(116, 117)
miR-217 and miR-34	Promote proliferation and osteoblast differentiation of BM-MSCs	(116, 118)
miR-375, miR-216a, let-7c and miR-22	Stimulate osteogenic differentiation of hAD-MSCs	(119-121)
miR-196a	Increases osteogenic differentiation of hAD-MSCs and osteogenic activity of osteoblasts	(122, 123)
miR-494	Induces endothelial cell migration	(124)

miR-129 and miR-136	Promote endothelial cell proliferation	(125)
miR-130a, miR-135b, let-7f and miR27b	Promote vascular tube formation	(126-128)
miR-1246	Enhances of endothelial migration and tube formation	(129)
miR-23a and miR-424	Cause migration, proliferation and tube formation of endothelial cells	(130, 131)
miR-214	Fosters prevention of cell senescence, migration and tube formation endothelial cells.	(132, 133)
miR-27a, miR-206, miR-29b, miR-181a and miR-302a	Induce osteogenic activity of osteoblasts	(122, 134-136)
miR-21	Assists osteogenic differentiation, migration and senescence prevention in BM-MSC; migration and proliferation of fibroblasts; migration, proliferation and ability to form endothelial tubes of endothelial cells.	(137-140)

MSC: Mesenchymal stem cell; EVs: Extracellular vesicles; MCP: Monocyte chemotactic protein; SDF-1: Stromal cell-derived factor-1; IL-6: Interleukine-6; FGF-2: Fibroblast growth factor-2; VEGF: Vascular endothelial growth factor; ANGPTL: Angiopoietin-related protein; IGF: Insulin-like growth factor; TGF-β: Transforming growth factor–β; NRP1: Neuropilin 1; miR: microRNA; hAD: Human adipose; BM: Bone marrow; BMM: Bone marrow monocytes; RANKL: Receptor activator of nuclear factor kappa ligand.

MiR-10a enhances MSC stemness and reduces senescence, while miR-10b boosts cell migration. MiR-218, miR-92a, miR-199b, miR-375, miR-216a, let-7c, miR-22, and miR-196a promote osteoblast differentiation in MSCs, with miR-217 and miR-34 additionally enhancing MSC proliferation. Furthermore, miR-196a, miR-27a, miR-206, miR-29b, miR-181a, and miR-302a are known to

stimulate osteoblast activity. Angiogenesis is a crucial process in various repair mechanisms, including bone formation, with several miRNAs found in MSC-EVs playing roles in this process.

MiRNAs such as miR-494, miR-129, miR-136, miR-130a, miR-135b, let-7f, miR27b, miR-1246, miR-23a, and miR-424, miR-214 contribute to different aspects of angiogenesis, including endothelial cell migration, proliferation, and tube formation (77).

MiR-21 deserves particular attention within this section. This specific miRNA was found at notably high levels in MSC-EVs during experiments conducted by Furuta et al. (141) and Nakamura et al. (124). It has been associated with anti-apoptotic effects and the prevention of cell death induced by H2O2. Additionally, research has shown that miR-21 enhance the migration and proliferation of fibroblasts, as well as induces migration, proliferation, and tube formation in endothelial cells. Recent studies by Yang et al. (140) have demonstrated that miR-21 not only stimulates osteogenic differentiation and migration of BM-MSCs *in vitro*, but also upregulates the expression of angiogenesis-related genes (HIF-1α and VEGF). Notably, enhanced new bone formation was observed in critical-size defects in rat and canine animal models following treatment with miR-21-modified MSCs seeded in β-tricalcium phosphate (β-TCP) scaffolds.

1.5.3. Mesenchymal Stem Cell Secretome for Treating Bone-related Diseases

Several experimental models have been utilized to explore the potential of the MSC secretome in treating bone-related disorders. *In vitro* studies have revealed that the MSC secretome can enhance osteogenesis in MSCs and promotes angiogenesis in endothelial cells (94, 142, 143). Moreover, the therapeutic efficacy of MSC secretome has been validated through *in vivo* models including calvaria defects, distraction osteogenesis, and osteonecrosis (101, 142-144).

The utilization of MSC-EVs has recently gained significant attention due to their regenerative potential and potential role as biocarriers (145). Numerous

studies have highlighted the pro-osteogenic effects of MSC-EVs in various experimental settings. Generally, MSC exosomes have demonstrated efficacy in promoting bone regeneration in animal models of bone defects (such as calvaria defects and fractures) and diseases like osteonecrosis and osteoporosis. These studies showed that MSC exosomes stimulate new bone formation along with vascular support, leading to enhanced morphological, biomechanical, and histological outcomes. Positive effects on cell survival, proliferation, migration, osteogenesis and angiogenesis, have also been observed (146, 147).

Among the most relevant works, Furuta et *al.* (141) reported that in a femur fracture model of $CD9^{-/-}$ mice lacking MSC-EVs production, there was a notable delay in bone union due to impaired callus formation. This study also demonstrated that secretome depleted of MSC-EVs failed to promote fracture healing, whereas the application of MSC-EVs led to a shortened healing time compared to wild-type controls, resulting in enhanced healing processes. Qi et al. (148) investigated the use of MSC-EVs in combination with β-tricalcium phosphate (β-TCP) scaffolds in critical-size calvaria defects in osteoporotic model rats. The results indicated a significant dose-dependent increase in bone microarchitecture and neovascularization parameters, as well as elevated levels of osteogenic (OCN and OPN) and vascular markers (CD31). Quayoom et al. (149) revealed in their research on osteoporosis that MSC-EVs provoked a reduction in the osteoporotic phenotype in ovariectomised rats. These findings were supported by Qiu et al. (150), who also noted an enhancement of *in vitro* osteoblast proliferation and differentiation, alongside inhibited apoptosis.

It is worth mentioning that the first clinical case report using secretome MSCs in patients was documented in 2017 (151). These patients required bone augmentation prior to dental implant placement. No systemic or local complications were reported throughout the study and radiographic evaluation revealed early bone formation in all cases. Although few clinical trials have been conducted with secretome at present, it has so far been reported to be safe feasible and practical to use as it can be efficiently stored and transported efficiently as a ready-to-use product (38, 85).

1.5.4. Mesenchymal Stem Cell secretome Preconditioning

A key benefit of utilizing MSC secretome for therapeutic purposes lies in its ability to be tailored to the specific needs of damaged tissue by adjusting both its composition and exosome cargo. This adaptability is attributed to the MSC secretome reflecting cellular cytosolic activities and MSCs' ability to respond to physiological or pathological changes, thereby maintaining homeostasis. Various strategies have been developed to precondition the MSC secretome and exosome cargo for an improved outcome in bone regeneration (Figure 14) (78, 87).

Hypoxia stands out as a prevalent method for priming MSCs to enhance the production of a secretome with greater regenerative potential. Culturing MSCs under hypoxic conditions, replicating the *in vivo* MSC niche microenvironment, allows cells to maintain their biological features, thereby amplifying regenerative, cytoprotective effects, and secretion of bioactive factors (152). Notably, increased proangiogenic, immunomodulatory, chemoattractant, anti-apoptotic, and antifibrotic activities has been demonstrated, with an elevation in factors such as VEGF, TGF-β1, angiogenin (Agn), granulocyte-macrophage colony-stimulating factor (GM-CSF), SDF-1, or MCP-1 (87, 153). Recent research indicates that hypoxic preconditioning of MSCs enhances the therapeutic efficacy of their exosomes in various injuries, including bone fractures (124). This improved bone regeneration capability of exosomes is frequently associated with raised pro-angiogenic activity (154) and increases in levels of miRNAs such as miR-126, miR-210-3p, let-7f-50, miR-4732-3p have been linked to this phenomenon (154-156).

The addition of proinflammatory stimuli into the culture medium has also received significant attention as a viable approach for manipulating the MSC secretome. An acute inflammatory phase is crucial for initiating an effective regeneration process, as it attracts immune cells and MSCs to the injury site, thereby triggering a series of reparative mechanisms (157). Commonly used factors such as IL-1β, IFN-γ, TNF-α, and lipopolysaccharide (LPS) are employed to induce this initial inflammatory response, which leads to subsequent anti-inflammatory and angiogenic effects, including inhibition of peripheral blood

mononuclear cell proliferation, promotion of the M2 macrophage phenotype, induction of T-cell anergy, and enhancement of MSCs' anti-fibrotic therapeutic potential (87, 158). These outcomes ultimately facilitate bone regeneration (159, 160). Increased release of molecules such as HGF, SDF-1, VEGF, PGE2, IDO, IL-10, TGF-β, MCP-1, and miRNAs like miR-15b, miR-19b, and miR-22 within the MSC secretome has been documented, supporting the mentioned effects (76, 161, 162).

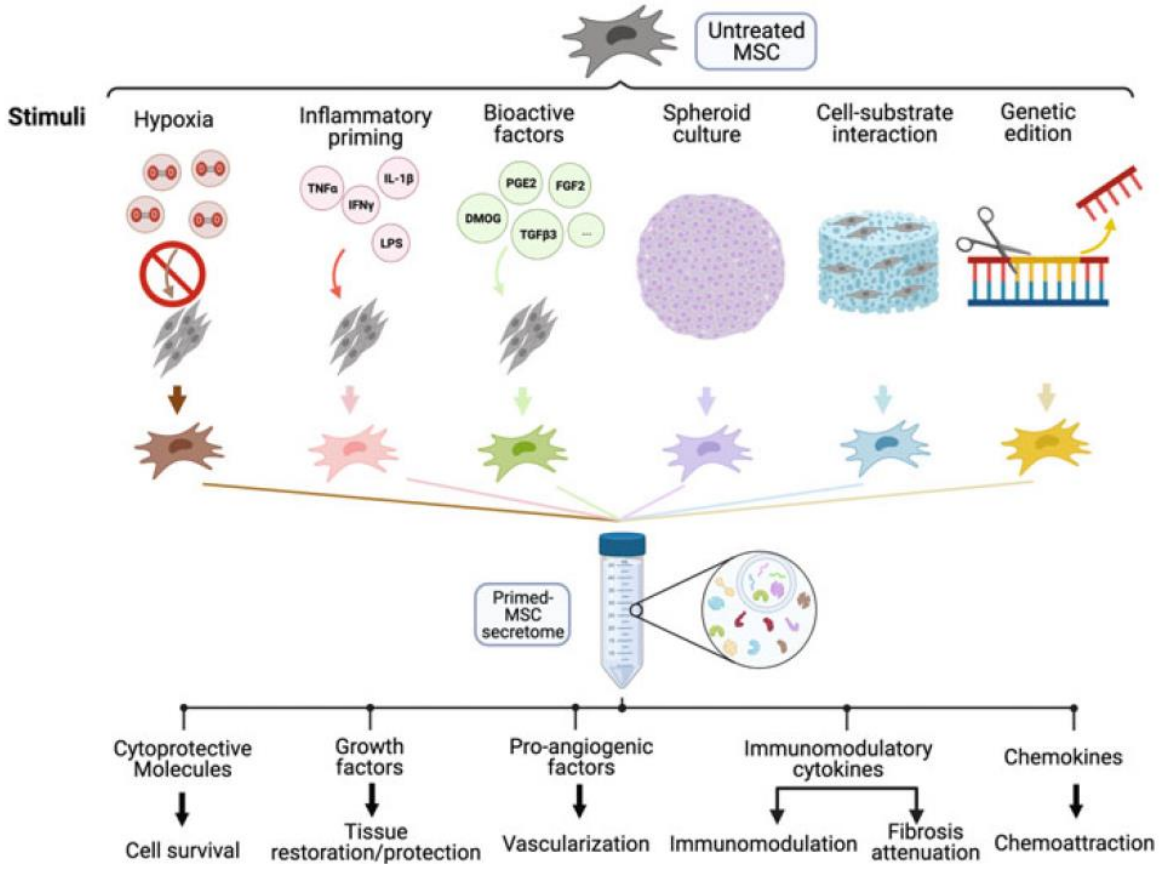

Figure 14. The commonly used MSCs' secretome modulation methods to enhance their therapeutic properties. Hypoxia, inflammatory factor priming, induction of bioactive factors, spheroid culture, cell-substrate interaction, and genetic edition are the most well-studied stimuli that have been reported to treat different pathologies using primed secretome. Image taken from previous work of our group, published in 2022 in Handbook of Stem Cell Therapy (87).

MSCs have been preconditioned by adding a diverse array of bioactive molecules to the culture medium during cell cultivation. For instance, incorporating dimethyloxaloylglycine (DMOG), a small molecule recognized for its capacity to stabilize hypoxia-inducible factor 1α (HIF-1α), or deferoxamine (DFO), an iron chelator, present a strategy to mimic hypoxic conditions without subjecting cells to actual hypoxia. This hypoxia-mimicking agent boosts the expression of angiogenic growth factors in MSCs and has exhibited significant

efficacy in promoting bone regeneration (76). The presence of growth factors like FGF-2 and BMP-2 in the MSC culture medium has shown a positive impact on MSCs by fostering in vitro osteogenesis and bone formation in critical bone defects and ectopic models, as these factors play pivotal roles in MSCs stemness and osteogenesis signalling pathways (163, 164).

Interestingly, two seemingly unrelated molecules to bone homeostasis, trichostatin A (TSA), a histone deacetylase inhibitor, and tauroursodeoxycholic acid (TUDCA), a molecule involved in lipid transport and cholesterol homeostasis, have proven to be effective preconditioning agents. MSC secretome primed with TSA exhibited elevated MSC osteogenesis *in vitro*, with secretion of MSC-EVs enriched in osteogenic miRNAs and facilitated bone formation in vivo. Similarly, MSC secretome treated with TUDCA demonstrated enhanced osteogenic capability alongside an anti-inflammatory effect (165, 166). Various other substances such as resveratrol, omentin-1, and thrombin have been extensively explored for their potential to enhance angiogenesis (167, 168), while valproic acid, melatonin, PGE2, substance P (SP), and tetrandrine have been observed to render MSCs more anti-inflammatory (76, 169, 170).

While two-dimensional (2D) culture is commonly used for MSC growth *in vitro*, it is important to note that this setting deviates from physiological conditions. The 2D culture method leads to a reduction of essential receptors, an increase in pro-inflammatory chemokines expression, and a lack of cell-cell interactions, thus diminishing MSCs stemness. In contrast, researchers have explored spheroid formation and scaffold utilization as viable alternatives. The transition to culturing MSCs as spheroids induces alterations in cell-cell and cell-matrix interactions, consequently impacting cell morphology, cytoskeletal organization, intracellular signalling pathways, and gene expression. This approach creates a microenvironment mimicking the natural niche of cells (87), fostering the enrichment of immunomodulatory, angiogenic, and anti-apoptotic factors in the MSC secretome (76, 171). Notably, the hypoxic core within MSC spheroids prompts the upregulation of proangiogenic factors via HIF-1α and HIF-2α cascades, alongside the release of IL-1, which reinforces the anti-inflammatory profile (172). Studies have highlighted the heightened expression of stemness and osteoinduction mediators in bone marrow MSC spheroids, promoting bone

regeneration *in vivo* (173). The use of scaffolds allows researchers to adjust cell-substrate interaction and customize extracellular signals critical for cell adhesion, organization, migration, and proliferation. The properties of biomaterials, including composition, stiffness, topography, and porosity, enable the manipulation of the MSC secretome composition. Various investigations have demonstrated that altering these parameters when culturing MSCs on scaffolds enhances the regenerative secretome profile, leading to increased secretion of factors such as VEGF, PGE2, iNOS, FGF2, LIF, MCP-1, and MCP-2 in the MSC secretome (174-177).

Genetic engineering of MSCs has the potential to enhance the expression of specific molecules that promote bone formation, resulting in an increased presence of these factors in the soluble factors and extracellular vesicles derived from MSCs. Augmenting the levels of proteins like RUNX2, BMP2, GATA 4, or HIF-1α has been documented to boost cell viability, angiogenesis, and bone-forming capabilities in various studies (178-182). Additionally silencing osteogenic inhibitors is a valid approach to stimulate osteogenic commitment, as demonstrated by García-Sanchez et al (183). In this work, conducted by our group, Secreted frizzled related protein 1 (Sfrp1), an antagonist of the Wnt/β-catenin signalling pathway, was transiently silenced on MSCs. This led to osteogenic effects on osteocytes and MSCs of osteoporotic patients *in vitro* and increased osteogenic profile in an *ex vivo* calvaria model, even resulting in the enrichment of proteins related to osteogenesis in MSC secretome. Due to concerns regarding the tumorigenic potential linked to genetic alterations, this preconditioning method was not extensively investigated in the past. Nonetheless, cell-free therapies presents a new array of opportunities by avoiding the direct administration of genetically modified cells into patients (87).

Alternative innovative strategies, such as mechanical forces, electromagnetic field exposure, or treatment with a combination of factors mimicking disease conditions, have also shown promise in customizing the secreted factors of MSCs for the treatment of bone disorders or injuries. Hence, MSC secretome emerges as a versatile tool with vast potential for tissue regeneration purposes (87).

HYPOTHESIS AND OBJECTIVES

2. HYPOTHESIS AND OBJECTIVES

2.1. Hypothesis

Osteoporosis is a disease characterized by a reduction in bone mass, leading to an increased susceptibility to bone fractures. At the cellular level, the aetiology arises from an imbalance between bone formation and bone resorption. This imbalance is partly attributed to a diminished efficacy of MSCs in generating osteoblasts. The use of healthy MSCs emerged as a therapeutic option to treat this disease. In recent times, there has been a paradigm shift in the approach to utilizing MSCs for regenerative purposes: The primary benefits do not result from the direct differentiation of these cells into damaged tissue, but rather from the secretion of proteins and extracellular vesicles containing factors that induce a regenerative impact on resident cells, known as the secretome.

Previous investigations by our research group have shown that silencing *Smurf1* expression, an inhibitor of the BMPs pathway, in MSCs enhances the osteogenic potential of these cells, significantly promoting bone formation *in vivo*. Since the secretome of MSCs mirrors the state of the cells themselves, we posited that the inhibition of *Smurf1* expression in MSCs would result in the generation of a more osteogenic secretome. This highly osteogenic secretome would represent an optimal candidate for an alternative therapeutic approach to manage osteoporosis. The inherent properties of the secretome would facilitate its clinical application and the recent advancements in scalable methodologies for secretome production would render it a financially viable treatment option necessary for addressing this medical condition.

2.2. Objectives

The main objective of this thesis is to produce an osteogenic secretome from MSCs to regenerate bone tissue by silencing an inhibitor of the osteogenic signalling pathway of the BMPs, *Smurf1*. This main objective is divided into several secondary objectives.

1. To effectively silence *Smurf1* expression in MSCs using a specific antisense oligonucleotide system called GapmeRs, in order to subsequently harvest the secretome of these cells.
2. To assess the *in vitro* effect of the MSC secretome on the osteogenic capacity of MSCs.
3. To examine the *in vitro* effect of the MSC secretome on proliferation and migration of MSCs.
4. To evaluate the *in vivo* effect of the MSC secretome on the osteogenic capacity of MSCs.
5. Characterisation of the secretome. Separation of the soluble and vesicular fractions to study the osteogenic capacity of each of the fractions separately, as well as a proteomic analysis of their components.
6. To evaluate the effect of the MSC secretome on other cells of the bone microenvironment: osteocytes and osteoclasts.

MATERIALS AND METHODS

3. MATERIALS AND METHODS

3.1. Primary MSCs Harvesting and Culture

Rat MSCs (rMSCs) were obtained from two month-old healthy Sprague-Dawley rats. These cells were cultured from the bone marrow of femurs, as previously described (184). The animals were sacrificed using a CO_2 chamber. The work was performed under aseptic conditions in a Class II Biosafety Cabinet. To begin the femur extraction, the skin from the back of the knee was removed using a scalpel. Holding the tibia, the muscles around the leg were removed by scraping with the scalpel. The tibia and femur were separated applying gentle but sustained force to hyperextend the knee joint, allowing the tibia to be removed without breaking the femur. Once the femur was held by its distal end, the scalpel was introduced into the acetabulum and force was applied to separate the joint and free the proximal region of the femur. Remaining soft tissues were cleaned with a gauze and femurs were sprayed with ethanol 70% and placed in a cell culture dish with 1X Phosphate saline buffer (PBS) (Cat. 12821680, Fisher Scientific, Hampton, NH, USA). Next, both ends of the femurs were carefully cut with the scalpel and MesenPRO RS Complete Medium, containing MesenPRO RS supplements (Cat.12746012, ThermoFisher Scientific, Waltham, MA, USA) and GlutaMAX supplement (Cat. 35050061, ThermoFisher Scientific, Waltham, MA, USA) was flushed through the medullary canal using a 22G needle. Cell aggregates were dissolved by gently passing the culture medium several times through the needle. Finally, rMSCs from every femur were seeded in an individual 25cm^2 flask with 5 mL of MesenPRO RS complete medium. Cells were left to form colonies and proliferate for 10-14 days at 37°C and 5% CO_2 in MesenPRO RS complete medium and were allowed to grow until confluent, performing only one cell passage after this to avoid replicative senescence.

Human MSCs (hMSCs) were isolated from femoral heads of patients suffering from osteoporotic fractures and requiring hip replacement surgery, following previously described protocols (185). Bone cylinders were extracted from the femoral head using a trephine and placed in a 50 mL Falcon tube containing 35 mL of PBS. Then, bone cylinders were vortexed for 30 seconds and PBS containing MSCs was filtered with a 0.7 µm nylon cell strainer (Cat.

431752, Corning Life Science, Glendale, Arizona, EEUU) and collected. Another 35 mL of PBS were then added to the 50 mL Falcon tube containing the bone cylinders and this step was repeat two times more. Approximately 100 mL of PBS with cells were collected in two 50 mL falcon tubes. These tubes were centrifuged 2,000 rpm for 5 min at room temperature (RT). The supernatant was discarded, and the cell pellet was resuspended in 5 mL of PBS and subsequently subjected to a Ficoll gradient (Cat. 17144002, Ficoll-Paque PLUS, Cytiva, Marborough, MA, USA) by adding very carefully the resuspended cells over the Ficoll solution in a 15 mL Falcon tube. Cells were centrifuged for 20 min at 2,000 rpm and 4°C, with acceleration at medium speed and no brakes to avoid disturbing the gradient. The interphase containing mononuclear cells was visible after centrifugation, which was collected and washed using PBS in a 50 mL tube. This tube was centrifuge for 5 min at 2,000 rpm at RT and the cell pellet was resuspended in 5 mL of MesenPRO RS complete culture media and placed into a 25cm^2 flask. Similarly to the rMSCs culture, hMSCs were left to proliferate and expand for 14-20 days at 37°C and 5% CO_2 in MesenPRO RS complete media applying just one passage to avoiding replicative senescence. Twenty-three women between 65-85 years old were studied. All of them give their consent to the experimental procedure. Patients with cancer, severe chronic disorders or under the influence of medications known to impact bone metabolism were excluded from the study.

3.2. Culture of Mesenchymal Stem Cell Lines ASC52telo and C3H10T1/2.

Human MSC line ASC52telo (Cat. SCRC4000, ATCC, Manassas, VA, USA) and mouse MSC line C3H10T1/2 (Cat. CCL-226, ATCC, Manassas, VA, USA) were cultured in Dulbecco's Modified Eagle's Medium (DMEM) with high glucose, L-glutamine, phenol red and sodium pyruvate (Cat. 31966021, Invitrogen, Waltham, MA, USA), supplemented with 10% Fetal Bovine Serum, FBS (Cat. 1020064, ThermoFisher Scientific, Waltham, MA, USA), and 1% penicillin-streptomycin (Cat. 15140122, ThermoFisher Scientific, Waltham, MA, USA). In addition, 0.2 mg/mL of geneticin, G418 Sulphate (Cat. 11811023, Corning, Manassas, VA, USA), antibiotic activity was needed to maintain immortality of ASC52telo cell line.

Cell passages were performed using TrypLE Express Enzyme (Cat. 12604021, Thermo Fisher Scientific, Waltham, MA, USA). Culture medium was discarded, and cells were washed with PBS. TrypLE solution was added and left to act for 5 min at 37°C. Then, trypLE was inactivated using a low amount of FBS. For counting cells, Trypan Blue staining 0.4% (Cat. T10282, Invitrogen, Waltham, MA, USA) was used and the number of cells was determined using a Neubauer chamber. The same passage procedure was applied for primary MSCs.

3.3. ASC52telo Cells Mesenchymal Characterization

ASC52telo characterization was accomplished by Wolbank *et al.* when establishing this cell line (186). However, culture observation, osteogenic, adipogenic and chondrogenic differentiation, and mesenchymal markers confirmation were performed to verify the identity of the cells received.

Cell culture morphology was evaluated using a Nikon inverted Phase Contrast Microscope (Nikon Instruments Inc., Melville, NY, USA).

For osteogenic differentiation capacity, 20,000 cells/cm^2 were seeded in DMEM with 10% FBS and 1% penicillin-streptomycin (complete DMEM) and were left to attach overnight at 37°C and 5% CO_2. Then, complete DMEM was replaced by DMEM supplemented with 2 mM β-glycerophosphate (Cat. G9422, Sigma-Aldrich, Burlington, MA, USA), 50 µM ascorbic acid (Cat. A4034, Sigma-Aldrich, Burlington, MA, USA) and 0,1 µM dexamethasone (Cat. D4092, Sigma-Aldrich, Burlington, MA, USA). Half of the osteogenic medium was refreshed every 2-3 days for 20 days. Mineralization is the most important mark of osteogenesis and alizarin red staining allows to show the level of mineralization dyeing calcium deposits in red. The alizarin red staining was conducted using a modified version of a previously documented procedure (187). The staining of cell monolayers was carried out by removing the culture media and adding 70% ethanol for 1 hour at RT to fix the cells. After ethanol 70% incubation, each well was washed three times with distilled water and 500 µL of Alizarin red solution at pH 4.2 (Cat. A5533, Sigma-Aldrich, Burlington, MA, USA) was left to act for 10 min. The staining was discarded, and each well was carefully washed 3 more times with distilled water. Wells were left to dry, and images were taken using the macro mode of a Samsung Galaxy A51 5G camera (Samsung Electronics, Seoul, South Korean).

The adipogenic capacity was measured using lipid-rich vesicles Oil Red staining. 15,000 cells/cm^2 were seeded and left overnight in completed DMEM at 37°C and 5% CO_2 to allow attachment. The next day, culture medium was replaced by completed DMEM supplemented with 5 mM dexamethasone, 250 mM, 3-isobutyl-1-methylxanthine (IBMX; Cat. I5879, Sigma-Aldrich, Burlington, MA, USA), 200 mM rosiglitazone (Cat. R2408, Sigma-Aldrich, Burlington, MA, USA) and 1 mg/ml insulin (Cat. I26343, Sigma-Aldrich, Burlington, MA, USA). This adipogenic medium was refreshed every 2-3 days for 12 days. Then, cells were washed twice with PBS and fixed using 10% formaldehyde (Cat. Ht501128, Sigma-Aldrich, Burlington, MA, USA) for 5 min at RT followed by a second fixing incubation again with 10% formaldehyde for 1 hour at RT. Once cells were fixed, wells were washed with 60% isopropanol (Cat. 190764, Sigma-Aldrich, Burlington, MA, USA) and were left to dry for at least 10 min. Once the wells dried out, Oil Red solution (Cat. O0325, Sigma-Aldrich, Burlington, MA, USA) was added for 10 min at RT. Next, the Oil Red solution was removed, and wells were washed three times with distilled water. Pictures were taken after the staining was dry.

The chondrogenic differentiation was done by detaching, counting and resuspending cultured ASC52telo cells in MesenPRO RS Medium with MesenPRO RS and GlutaMAX supplements to a final concentration of 80,000 cells per 5 µL. Then, the cell suspension was thoroughly homogenised, and 5 µL-drops were placed into 48-well culture plates wells. Drops were incubated for 30 min at 37°C and 5% CO_2 to form cartilage spheroids. Next, StemPro Chondrogenic differentiation kit (Cat. A1007101, ThermoFisher Scientific, Waltham, MA, USA) was used according to manufacturer guidelines: Chondrogenesis Supplement was diluted 1:10 in Chondrocyte Differentiation Basal Medium. 200 µL of the chondrogenic solution were added very carefully on the walls of each well to not disturb the drops. This solution was refreshed every 3 days. ASC52telo cartilage spheroids were collected after 18 days, fixed in 70% ethanol, and submerged in Alcian blue solution (Cat. ab145250, Abcam, Cambridge, UK) for 20 mins. Spheroids were washed with PBS and images were taken.

The mesenchymal and non-mesenchymal markers presence was assessed by multiparametric flow cytometry. Around 200,000 ASC52telo cells per tube were harvested in FACS Buffer (PBS, 5% FBS and 0.1% Sodium Azide). Antibodies used for the MSCs characterization were as follows: CD34-PE (Cat. 130-098-140, Miltenyi Biotec, Bergisch Gladbach, Germany), CD45-PerCP (Cat. 130-113-120, Miltenyi Biotec, Bergisch Gladbach, Germany), CD73-APC (Cat. 130-123-802, Miltenyi Biotec, Bergisch Gladbach, Germany), CD90-VioBlue (Cat. 130-119-890, Miltenyi Biotec, Bergisch Gladbach, Germany) and CD105-FITC (Cat. 130-098-774, Miltenyi Biotec, Bergisch Gladbach, Germany). Antibodies were added at indicated concentrations and cells were incubated 20 min at 4°C in the dark. After the incubation time, samples were washed by adding PBS and centrifuging at 2,000 rpm for 5 min to allow excess antibody removal. 200 µL of FACS Buffer were added per tube to proceed with the analysis.

Flow cytometry was carried out using a FACSCanto II flow cytometer (Becton Dickinson, New Jersey, USA) using FACSDiva Software (BD Biosciences, San Diego, USA).

3.4. MSCs Transfection Using Gapmers

For gene silencing, we used Locked Nucleic Acid Antisense Oligonucleotides (LNA-ASOs) from Exiqon (Qiagen, Vnlo, The Netherlands) whose clinical safety and high effectiveness have been well established (69). These molecules are single-stranded deoxyribonucleotides of 14-20 base pair long that can specifically bind to target mRNA creating a recognition site for the RNase H then causing its degradation. GapmeRs possess a unique structural design with a fully phosphorothioate (PS)-modified backbone, conferring enhanced efficiency due to the augmented stability and resistance to endonuclease degradation. GapmeRs were delivered to the cells via lipofection, using Dharmafect (Cat. T-2005-01, Dharmacon, Horizon Discovery, Cambridge, UK), following the manufacturer's guidelines, as described in our previous work (69). Briefly, on the preceding day, rMSCs and C3H10T1/2 were seeded at 20,000 cells/cm^2 and the ASC52telo line at 15,000 cells/cm^2. Two hours before transfection, the culture medium was replaced by serum-deprived Opti-MEM I medium (Cat. 31985047, ThermoFisher Scientific, Waltham, MA, USA). Opti-

MEM I medium and the recommended amount of Dharmafect lipofection agent (Table 2) were mixed and incubated at RT for 5 min. Separately, Opti-MEM I medium was mixed with the GapmeR before being added dropwise to the Dharmafect mix (Table 2). The resulting mixture was incubated for 20 min at RT and then added dropwise to the seeded cells, which were subsequently left at 37°C. Twenty-four hours later, an equal volume of DMEM supplemented with 10% FBS and 1% penicillin-streptomycin was added to the Opti-MEM I medium and cells were incubated for an additional 24 hours at 37°C.

To test the efficiency of GapmeR delivery, we used Antisense LNA GapmeR Negative Control A (Cat. 339516 LG00000002-DFA) labeled with fluorescein (FAM). After completing the transfection protocol, the cells were collected, washed, and resuspended in FACS buffer (PBS, 5% FBS and 0.1% Sodium Azide) for flow cytometry analysis. A FACSCanto II flow cytometer with FASCDiva Sofware (BD Bioscience, San Diego, CA, USA) was used to for this analysis.

Specific GapmeRs from Exiqon were acquired for *Smurf1/SMURF1* silencing in human (Cat. 3633952 LG00783776-DDA), rat (Cat. 3688232 LG00220909-DDA) and mouse (Cat. 339511 LG00220909-DDA) cells[5]. *Smurf1/SMURF1* GapmeRs were design to be complementary to a sequence located in exon 12 (69).

Table 2. Amounts of reagents used for Dharmafect lipofection. Volumes are referred to one well.

	Dharmafect mix		GapmeR mix		Total volume per well
Plate	**Dharmafect**	**Opti-MEM**	**GapmeR (5µM)**	**Opti-MEM**	
24-well plate	0.5 µL	39.5 µL	2 µL	38 µL	80 µL
6-well plate	2.5 µL	197.5 µL	10 µL	190 µL	400 µL
100mm plate	20 µL	1580 µL	80 µL	1520 µL	3200 µL

[5] Human: ASC52telo, rat: primary rMSCS, mouse: C3H10T1/2.

3.5. Conditioned Media Production

Once the transfection protocol was completed, cells were washed with PBS and 0.2 mL/cm^2 of MesenPRO RS Medium with GlutaMAX (without supplements) was added. After 48 hours of incubation at 37°C and 5% CO_2, the conditioned media (CM) was collected and centrifuged at 400g for 10 min at 4°C to eliminate cell debris. The supernatant was recovered and transferred to a new tube for a second centrifugation at 1000g for 10 min at 4°C. This second step is performed to ensure complete elimination of cellular debris. The CM was then filtered through 0.22 µm filters and stored at -80°C until further use.

For some experiments, the CM must be concentrated before freezing. In these cases, Vivaspin turbo 15 concentration units (Cat. VS15T02, Sartorius Stedim Lab Ltd, Gloucestershire, UK) with a 10,000 KDa molecular weight cutoff were used. The membrane tubes were pre-rinsed with water prior to use to eliminate glycerine and sodium azide traces. Ten mL of CM were added to these units, followed by centrifugation at 4,000g at RT. The time required to concentrate the CM 50-fold (50X CM) was approximately 20 min.

3.6. *In Vitro* Assessment of Conditioned Media Effect in Osteogenic Differentiation

A total of 20,000 cells/cm^2 were seeded and incubated overnight to allow attachment in 24 well-plates. The same number of cells was used for the rMSCs, hMSCs and ASC52telo experiments. Cells were washed with PBS and 0.25 mL/cm^2 of CM was added for 48 hours. Osteogenic induction was subsequently achieved by replacing the CM with osteogenic media. The osteogenic media for rMSCs and hMSCs consisted of complete DMEM supplemented with 20 mM β-glycerolphosphate, 50 µM ascorbic acid and 1 µM dexamethasone. For ASC52telo cells, complete DMEM was supplemented with 2 mM β-glycerolphosphate, 50 µM ascorbic acid and 0.1 µM dexametasone. Half of the osteogenic media was replaced with fresh osteogenic media every 2-3 days until the end point of differentiation, when gene expression, alkaline phosphatase activity and mineralization were assessed. The days for differentiation

assessment and end points varied depending on the specific characteristics of the cells evaluated.

3.7. Quantitative RT-qPCR Gene Expression Analysis

Gene expression analyses were carried out by real-time quantitative Polymerase Chain Reaction (qPCR). mRNA was isolated from the cells in culture by scraping the wells with TRIzol reagent (Cat. 15596026, Invitrogen, Waltham, MA, USA) after rinsing then twice with PBS. The RNA extraction from the TRIzol solution was performed using phenol-chloroform. In brief, 0.2 mL of chloroform per mL of TRIzol was added to each sample, shaken for 15 seconds manually and incubate for 3 min at RT. This resulted in distinct phases: an aqueous upper phase and a pinkish bottom phase. The samples were centrifuged at 13,300 rpm for 15 min at 4°C to facilitate the strong establishment of the two phases and their subsequent separation. The aqueous phase, containing the mRNA, was transferred to a new tube and an equal volume of 100% isopropanol was added. The samples were vortexed thoroughly, and mRNA precipitation was induced by incubating them at -80°C for 30 min. After incubation, the samples were centrifuged at 13,300 rpm for 10 min at 4°C. The supernatant was discarded, and the mRNA pellet should be visible at the bottom of the tube. Cold 70% ethanol diluted in Ambion DEPC-treated Nuclease-Free water (Cat. AM9906 ThermoFisher Scientific, Waltham, MA, USA) was added to the pellet, and the tube was vortexed to wash the sample. A further centrifugation at 13,300 rpm for 5 min at 4°C was performed to reform the pellet. The supernatant was carefully discarded, and the tube was heated at 55°C for 5 min to dry the pellet. Finally, the pellet was resuspended in nuclease-free water. RNA quantification was performed using spectrophotometric analysis with a DeNovix DS-11 Spectrophotometer (DeNovix, Wilmington, DE, USA).

Once the mRNA was extracted, it was reverse-transcribed into cDNA. This RNA reverse transcription was performed using the PrimeScript RT Reagent kit (Cat. RR037A, Takara Bio Inc, Shiga, Japan) following the manufacturer's instructions. An average of 500 ng of RNA per sample was brought to a final volume of 5 µL with nuclease-free water in a PCR 200 µL tube. The reagents from the PrimeScript RT Reagent Kit were mixed with the samples to a final volume of

5 µL (Table 3). The PCR protocol for reverse transcription consisted of an initial cycle of 15 min at 37°C for reverse transcription, followed by a 5-second pulse at 85°C to inactivate the PrimeScript RT Enzyme and finally cooling at 4°C. The cDNA was stored at -20°C until further use.

Table 3. **PrimeScript RT Reagent Kit mix used for reverse transcription per sample**.

Reagent	Volume
5X PrimeScript Buffer	2 µL
Random 6 mers (100 µM)	2 µL
Oligo dT Primer (50 µM)	0.5 µL
PrimeScript RT Enzyme Mix I	0.5 µL

Specific TaqMan assays probes (Applied Biosystems, Waltham, MA, USA) for each gene were used to determine changes in gene expression. For these analyses, 1 µL of cDNA and 3.5 µL of nuclease-free water were added per well to the microAmp Optical 96-well Reaction plate (Cat. I10N4Q611, Applied Biosystems, Waltham, MA, USA). Then, the probe mix was prepared using 5 µL of TaqMan Universal PCR Master Mix (Cat. 4324018, Applied Biosystems, Waltham, MA, USA) and 0.5 µL of the specific TaqMan probe (Table 4) and added to each corresponding well, reaching a total volume of 10 µL. qPCR was performed using an Applied Biosystems 7,500 fast Real-Time PCR System, following a standard run protocol: an initial hold for 10 min at 95°C, followed by 40 cycles of 15 seconds at 95°C and 1 min at 60°C.

Glyceraldehyde-3-phosphate dehydrogenase *(Gadph)* was used as a housekeeping gene. The *Smurf1* probe was employed to measure the level of *Smurf1* silencing achieved. *Runx2, Alpl* and *Bglap* probes were used to monitor changes during osteogenic differentiation. Additionally, *Tnfsf11* (*Rankl*), *Tnfrsf11b* (*Opg*), *Csf*-1 (*M-csf*), *Sost* and *Dkk1* were used to test the effects of the CM on human *ex vivo* bone and osteocytes. For qPCRs analysis, the threshold cycles (Ct) were determined by default settings, and gene expression was measure by normalizing to the housekeeping gene expression using the comparative 2^-ΔΔCt method (188).

Table 4. List of TaqMan probes used for qPCR in human, rat and mouse for gene expression analyses.

Gene	Human assay reference	Rat assay reference	Mouse assay reference
Gadph	Hs99999905_m1	Rn01775763_g1	Mm999999915_g1
Smurf	Hs00410929_m1	Rn01412801_m1	Mm00547102_m1
Runx2	Hs00231692_m1	Rn01512298_m1	----------
Alpl	Hs00758162_m1	Rn01516028_m1	----------
Bglap	Hs01587814_g1	Rn00566386_g1	----------
Tnfsf11	Hs00243522_m1	----------	Mm00441906_m1
Tnfrsf11b	Hs00900358_m1	----------	Mm00435454_m1
Csf-1	Hs00174164_m1	----------	Mm00432686_m1
Sost	----------	----------	Mm00470479_m1
Dkk1	----------	----------	Mm00438422_m1

3.8. Quantification of Alkaline Phosphatase Activity

For the quantification of Alkaline phosphatase (ALPL) activity in cultured cells, wells containing the cells were washed twice with PBS prior to sample collection in Eppendorf tubes by scrapping in 200 µL of 0.05% Triton X-100 (Cat. 9036-19-5, Merck KGaA, Darmstadt, Germany) to lyse the cells. The samples were subjected to three cycles of sonication (30 seconds of sonication followed by 30 seconds of rest) at 4°C. Afterwards, samples were stored at -80°C until further analysis.

Alkaline Phosphatase enzymatic activity was quantified as previously described (189). This enzymatic activity involves the transferring of a phosphate group from *p*-Nitro-Phenyl Phosphate (pNPP) to 2-amino-2-methyl-1-propanol (AMP), liberating *p*-Nitro Phenol (pNP) according to the following reaction:

p-Nitro-Phenyl Phosphate + AMP $\longrightarrow$ *p*-Nitro-Phenol + Phosphate

The rate of p-Nitrophenol formation, measured photometrically, is proportional to the concentration of alkaline phosphatase present in the samples (190).

First, the samples were thawed and kept on ice. All reagents used were also kept cold during the analysis. AMP buffer[6] and pNPP buffer[7] were freshly mixed in equal proportions (1:1). 100 µL of each sample were mixed with 300 µL of the AMP/pNPP mix. A total of 100 µL of that mix was added to one well in a 96-well plate. This procedure was done in triplicates to obtain three independent readings from each sample. A standard curve of known increasing quantities of pNP[8] diluted in 0.5N NaOH was prepared to translate the colorimetric results into activity values (nmol p-nitrophenol/µg protein). Once the samples and the standard curve were loaded, the plate was incubated for 60 min at 37°C in the dark with constant shaking. After incubation, 50 µL of 0.5N NaOH was added to each sample well (excluding the standard wells) to stop the reaction. Absorbance was measured using an Eon Microplate Spectrophotometer (BioTek, Winooski, VT, USA) at 405 nm. To normalize the activity to the protein content of each sample, protein quantification was also performed. A total of 100 µL of each sample extract was transferred into new Eppendorf tubes, and 300 µL of PBS was added to each sample yielding a final volume of 400 µL. Then, a total of 100 µL of each diluted sample extract was added in triplicate to a 96 well-plate in three different wells. A standard curve was also prepared using Bovine Serum Albumin (BSA, Cat. A7906, Sigma-Aldrich, Burlington, MA, USA) at 10 mg/mL as the highest concentration point and performing eight 1:2 serial dilutions in distilled water, down to a concentration of 0.039 mg/mL. The standard curve was pipetted in duplicate into the 96-well plate. The protein quantification was carried out using the Bicinchoninic Acid (BCA) protein assay. To prepare the BCA working solution we added 5 mL of Reagent A (Cat. 23228, Thermo Fisher Scientific, Waltham, MA) for each 100 µL of Reagent B (Cat. 23224; Thermo Fisher Scientific, Waltham, MA). A total of 100 µL of this final solution was added to each well containing the sample or standard. The plate was then incubated for 30 min in

[6] **AMP buffer:** Dilute 1:10 of 2-Amino-2-methyl-1-propanol (AMP, Cat. A65182, Sigma-Aldrich, Burlington, MA, USA) in distilled water, and adjust pH to 10,4. Dissolve 0,95 mg of MgCl2 (Cat. M2670, Sigma-Aldrich, Burlington, MA, USA) in 10 mL of distilled water to make a 1M solution. Add 0,8 mL of the dissolved MgCl2 1M for every 20 mL of AMP prepared.

[7] **P-NFF**: Dissolve 0,084 g of P-NFF (Cat. 71770, Sigma-Aldrich, Burlington, MA, USA) in 20 mL of distilled water.

[8] **P-NF**: 139.11 mg of P-NF (Ref. N9876, Sigma-Aldrich, Burlington, MA, USA) in 10 mL of distilled water. Dilute 1:10 in distilled water

the dark at 37°C with shaking, and absorbance was measured at 600 nm in Eon Microplate Spectrophotometer (14).

3.9. Alizarin Red Staining and Quantification

The alizarin red staining and quantification was performed using a modified version of a reported procedure (187). The staining of cell monolayers was carried out as previously mentioned in the ASC52telo cells mesenchymal characterization' section. For the quantification of the alizarin red staining, 200 µL of 10% glacial acetic acid (Cat. A6283-1L, Merck KGaA, Darmstadt, Germany) were added per well, and the plates were at RT for 30 min. The cell monolayer was then detached by scraping with the tip of a micropipette, and the content of each well were transferred to a 1.5 mL Eppendorf tube. The tubes were vortexed for 30 seconds and then sealed with parafilm before heating at 85°C for 10 min. After heating, the tubes were cooled on ice for 5 min and centrifuged 30 min at 13,300 rpm at RT to make the cellular debris precipitate. The supernatant was transferred into new Eppendorf tubes, and the pellet was discarded. Fifty-seven µL of 10% ammonium hydroxide (Cat. 142181, Panreac AppliChem, Barcelona, Spain) was added to each tube, reaching of approximately 200 µL. Each sample was then plated into two wells of a 96-well plate (100 µL per well), to have two independent readings. Absorbance was measured at 405 nm in Eon Microplate Spectrophotometer (14).

3.10. Proliferation Assessment

To test proliferation, colorimetric MTT (3-(4,5-dimethylthiazol-2-yl)-2,5-diphenyltetrazolium bromide) assay was performed. ASC52telo cells were exposed to CM for 48 hours and then plated at densities of 100, 200, 300 and 400 cell per well in 96 well plates to account for differences in analysis due to cell confluence. Four wells were seeded for each cell density and five plates were used for analysis on different days: D1, D3, D5, D7 and D9. On each of these days, the complete DMEM culture medium (DMEM with 10% FBS and 1% penicillin-streptomycin) was replaced with complete DMEM containing 0.5 mg/mL of MTT (Cat. M5655, Sigma-Aldrich, Burlington, MA, USA). After 4 hours of incubation at 37°C, the medium was discarded and 100 µL of 2-propanol were

added, followed by an additional 10 min incubation at 37°C with gentle shaking. Absorbance at 570nm was measured in an Eon Microplate Spectrophotometer.

3.11. Cell Migration Assay

A wound healing assay was executed to test the effect of the CM on the migration of ASC52telo cells. Cells were seeded in a 6-well plate at a density of 15,000 cells/cm^2 and 2 mL of CM were added for 48 hours. After incubation, the CM was discarded, and 400 µm-wide wounds were carefully performed with the tip of a 1 µL pipette. The wells were washed with PBS to remove any cellular debris and 2 mL of complete DMEM culture medium were added. The plate state was imaged at 12 hours intervals for 36 hours using a Nikon Eclipse Ti (Nikon Instruments Inc., Melville, NY, USA) live cell microscope, equipped with an incubator to maintain the cells at 37°C under normoxic conditions. Four different representative fields were captured from each well. The empty surface area in the captured images was analysed using ImageJ 1.53c software (http://imagej.nih.gov/ij).

3.12. Chemotactic Assay

The chemotactic assay was carried out on ASC52telo cell line using Transwell Permeable Support/Insert (Cat. 3464, Corning, Somerville, MA, USA). A total of 60,000 cells were seeded onto the upper side of the insert and complete DMEM medium was added in the lower side. Cells were incubated overnight at 37°C to allow cell attachment. Subsequently, complete DMEM was discarded and CM was added to the lower chamber and the cells were incubated for an additional 24 hour-incubation at 37°C. The pore size of transwell inserts was 8.0 µm, allowing for cell migration towards the lower side of the insert. Both the upper and lower sides of the insert were carefully washed twice by dipping transwell inserts into beakers with PBS. The cells were then fixed and permeabilized with 100% methanol (Cat. 34860-1L-R, Merck KGaA, Darmstadt, Germany) for 20 min at RT in a fume hood. After discarding the methanol, the cells were stained using enough crystal violet staining (Cat. C0775-25G, Merck KGaA, Darmstadt, Germany) to cover the insert for 10 min at RT on a shaker. The crystal violet stain was recovered, and the inserts were washed carefully with running water. The

upper side of the inserts were carefully cleaned with a cotton swab to remove non-migrated cells. The migrated cells were counted using Zeiss Axiovert 200 Microscope (Zeiss, Jena, Germany) and ImageJ 1.53c software.

3.13. *Ex Vivo* Human Bone Culture

Ex vivo cultures allow to study cells within their native microenvironment without the issues of *in vivo* approaches (191). To test the effects of the CM in an *ex vivo* model, we collected and cultured trabecular bone cylinders from the central part of the femoral head of osteoporotic patients using a trephine (192). These bone cylinders were cut into six smaller fragments to obtain replicates from each sample. The fragments were washed through 3 cycles of vortexing in a 50 mL Falcon tube containing PBS. The fragments were then carefully placed into a 12-well plate and fully immersed in a mixture of 50% CM and 50% α-MEM culture medium (Cat. 32571, Gibco ThermoFisher Scientific, Waltham, MA, USA) supplemented with 5% FBS, 1% penicillin-streptomycin, 0,2% normocin (Cat. NC9273499, InvivoGen, San Diego, CA, USA). On day 2, half of the culture medium was replaced with fresh media. On day 4, the bone pieces were washed twice with 1 mL of PBS, immersed in 1 mL of TRIzol, and disaggregated using T25 digital ULTRA-TURRAX (Cat. 0003725000, IKA-Werke, Staufen, Germany) dispersing instrument, with a S25N-8G (Cat. 0001024200, IKA-Werke, Staufen, Germany) dispersion tool. During tissue disaggregation, the samples were kept on ice and the disaggregation pulses were limited to a maximum of 20 seconds to prevent RNA degradation due to overheating. Once the bone fragments were reduced to a powdered appearance, the tubes were centrifuged at 2,000 rpm for 15 min at 4°C. The pellets were discarded and the TRIzol supernatant was collected into 1.5 mL Eppendorf tubes. RNA was then extracted following the RNA extraction protocol described previously. Samples were obtained from three osteoporotic women with no medications that may alter bone metabolism.

3.14. *In Vivo* Ectopic Model

All the animal experiments conducted underwent a thorough review and were approved by the Institutional Bioethics and Animal Care Committee at the University of Cantabria, as well as the relevant regulatory body (Consejería de

Agricultura y Ganadería de Cantabria, Santander, Spain). The animals were provided with unrestricted access to water and food and were subjected to a light-dark cycle of 12 hours each. All surgical procedures were conducted under aseptic conditions, with the rats and mice placed under isoflurane anaesthesia (IsoVet, Cat. 469860, B. Braun Vet Care GmbH, Tuttlingem, Germany) and positioned on a warming pad to prevent hypothermia during the operation. Post-surgery, antibiotics (Baytril 5%-Enrofloxacine, Bayer, Leverkusen, Germany) were administered via the drinking water for a minimum of 3 days.

A rat ectopic model was used to analyse the osteogenic effect of CM on MSCs *in vivo*. This model involved the use poly(lactic-co-glycolic-acid) (PLGA, ResomerRG504; Cat. 739944, Boehringer-Ingelheim, Ingelheim am Rhein, Germany) scaffolds loaded with BMP2 (Cat. Z02913-50_BMP-2, Biomedal, Sevilla, Spain), courtesy of Dr. Évora's group, from the Center for Biomedical Research of the Canary Islands (193), which served as a structure to induce ectopic bone formation in rats. These scaffolds were discoidal, with 4 mm in diameter and 1 mm of thickness, releasing BMP2 in a controlled and sustained manner.

rMSCs were harvested, cultured and counted as previously described. PLGA scaffolds were seeded with 80,000 rMSCs resuspended in 100 µL of 10X concentrated CM. The PGLA scaffolds were incubated overnight at 37°C and 5% CO_2 in MesenPRO RS medium to allow cell attachment. Water was added to the around to keep a high degree of humidity and avoid the scaffolds drying out. CM production and concentration were conducted using rMSCs as described earlier. Once prepared, the surgical procedure began, involving 2-month-old healthy Sprague-Dawley rats. The rats were anaesthetized with isoflurane as an aerosol, their backs were shaved using an electric shaving machine Air Force Ultimate (Cat. TN9300F5, Rowenta, Erbach im Odenwald, Germany) and the area was sterilized with povidone-iodine solution. Using sterile scissors and forceps, 0.5 cm incisions were made on each side of the spine, creating a space through the skin and connective tissue for the scaffolds. The scaffolds were carefully placed, and the incisions were closed by stapling the skin. A maximum of 8 scaffolds were loaded per animal.

The scaffolds remained in the recipient rats for 8 weeks. After this time, the rats were then euthanized in a CO_2 chamber, and scaffolds were collected and immersed in 10% formaldehyde solution for 6 hours to fix the cells. Subsequently, a decalcification solution consisting of 20% ethylenediaminetetra-acetic acid (EDTA; Cat. EDS-5006, Sigma-Aldrich, Burlington, MA, USA) in PBS (pH 7.4) was applied for one week at 4°C with the solution being refreshed twice during this time. Once decalcified, the scaffolds were embedded in paraffin using Cell wax Plus molds (Cat. GCA-0400-00A, CellPath, Powys, United Kingdom) to form blocks, and 5-micron sections were cut using a microtome (Cat. RM2125, Leica, Wetzlar, Germany) and a flotation bath (Cat. 3000459, J. P. Selecta, Barcelona, Spain). Sections were collected in Nunc Microscope slides (Cat.160005, ThermoFisher Scientific, Waltham, MA, USA) and were left to dry. Subsequently, scaffold sections were deparaffinized using a standard protocol consisting of heating the slides at 55°C for at least 20 min followed by rehydration through washes in xylene (Cat. 534056, Honeywell, Bracknell, UK) and consecutive washes in decreasing concentrations of ethanol.

The staining of the slides was performed at Dr. Ricardo Reyes' laboratory, at the Department of Biochemistry, Microbiology, Cellular Biology and Genetics, Institute of Biomedical Technologies, of the University of La Laguna.

Masson-Goldner Trichrome staining was used to detect collagen fibers The collagen fibers were stained blue, the nuclei black and the background red (194). Sections were re-fixed overnight with Bouin solution[9] to improve the staining quality. The samples were then washed with running water for 5 min, followed by a 1-min wash with distilled water to clean the samples from the yellow color left by the Bouin's solution. The samples were stained with Weigert's iron hematoxylin solution (Cat. HT1079-1SET, Merck KGaA, Darmstadt, Germany) for 10 min, washed for 5 min with running water and then rinsed for 1 min in distilled water. They were subsequently stained for 2 min with Biebrich Scarlet-Acid Fuscin stain (Cat. HT151-250ML, Merck KGaA, Darmstadt, Germany), followed by a 2 min staining with 1:1 mix of phosphotungstic acid-phosphomolybdic acid (PTA, Cat. 455970-10G; PMA, HT153-250ML; Merck KGaA, Darmstadt,

[9] **Bouin solution:** 400 ml Pyric acid 1.4% (Cat. RC586016, VWR International, Radnor, PA, USA), 135 ml Formaldehyde 35-40% and 27 ml glacial acetic acid.

Germany) solution and a 5-min staining in Anillin Blue (Cat. B8563-250ML, Merck KGaA, Darmstadt, Germany). The slides were then rinsed in distilled water for 1 min and incubated for 4 min in 1% glacial acetic acid. Finally, samples were dehydrated, rinsed and mounted with Nunc Thermanox coverslips (Cat. 150067, ThermoFisher Scientific, Waltham, MA, USA) for proper observation and conservation.

The indirect immunoenzymatic technique was applied to the deparaffinized and rehydrated sections in Tris buffered saline[10] (TBS) with antigen retrieval in citrate buffer at 90°C for 5 min, followed by blocking in a solution containing 2% FBS in 0.2% Tris buffered saline with Tween[11] (TBS-T). Osteogenic formation was assessed by overnight incubation at 4°C with polyclonal anti-osteocalcin (OCN) antiserum (1:100) (Cat. AB10911, Millipore, Burlington, MA, USA) and polyclonal anti-ALPL antiserum (1:100) (Cat. SAB3700631, Millipore, Burlington, MA, USA) in blocking buffer. The sections were then washed three times with TBS 10 min at RT followed by a second 10 min incubation with TBS-T. The samples were exposed to donkey anti-rabbit IgG antibody conjugated with biotin (1:500) (Cat. AP182B, Millipore, Burlington, MA, USA) for 60 min, followed by streptavidin-peroxidase (1:500) (Cat. 189733, Millipore, Burlington, MA, USA) for another 60 min. Detection of peroxidase activity was achieved using 0.005% 3,3'-diaminobenzidine (Cat. D12384, Sigma-Aldrich, Burlington, MA, USA) and 0.01% hydrogen peroxide in Tris-HCl buffer (0.05 M, pH 7.6) (Cat. T3253, Sigma-Aldrich, Burlington, MA, USA). The specificity of the immunostaining was confirmed by substituting the primary antibodies with normal serum. Peroxidase activity revealing was terminated by extensive washing with TBS. The slides were then dehydrated and mounted as described earlier.

OCN and ALPL staining were quantified using the computed-based image analysis software Leica Q-win V3 Pro Image Analysis System (Leica Microsystems, Wetzlar, Germany). Quantification of OCN and ALPL staining was performed by applying a fixed threshold to identify positive staining within the

[10] **TBS:** 24,23 g Trizma HCl, 80.06 g NaCl in 800 mL of distilled water, adjusting pH to 7,6. Add distilled water up to 1 L.
[11] **TBS-T:** Add 10 mL of Tween 20 Detergent (cat. 655204, Millipore Poole, Dorset, UK) in 990 mL of TBS.

implant region, with the positive pixel areas being standardized against those obtained from the control group and presented as relative staining intensities (193).

3.15. *In Vivo* Calvaria Model

The *in vivo* calvaria bone formation model involves creating a bone defect in the calvaria of mice that is subsequently regenerated using scaffolds that are capable of releasing CM in a sustained and controlled manner.

To achieve this, CM was produced and concentrated 50 times (50X) as previously described, using C3H10T1/2 cell line. The CM was encapsulated in microspheres applying the doble emulsion method. The protocol was optimized by Dr Díaz-Rodríguez's group, in the R+D Pharma Research Group, at Department of Pharmacology, Pharmacy and Pharmaceutical Technology of University of Santiago de Compostela (Spain). This method involved generating microparticles with an internal aqueous phase and an external lipidic phase. The inner phase contained 200 µL of 50X concentrated CM, which was mixed with 0.07% polyvinyl alcohol (PVA; Cat. 360627, Merck KGaA, Darmstadt, Germany) through vortexing. For the positive control, the CM was substituted by 1 µg/µL BMP2 (Cat. Z02913-50_BMP-2, Biomedal, Sevilla, Spain) and, for negative control, by 0.07% PVA. The lipid phase, consisting of PGLA polymer (ResomerRG504, cat. 739944, Boehringer-Ingelheim, Ingelheim am Rhein, Germany) dissolved in methylene chloride (CH_2Cl_2, Cat. 34856, Merck KGaA, Darmstadt, Germany) at 50 mg/mL, was prepared and transferred to a round-bottom Falcon polypropylene tube (Cat. 10110101, ThermoFisher Scientific, Waltham, MA, USA). To mix both phases, the lipid phase was maintained under constant vortexing for 3 min at maximum speed while aqueous phase was added dropwise using a pipette. PVA acted as a surfactant to maintain the emulsion. After 3 minutes, the emulsion was rapidly added to a 0.1% 200 mL PVA solution in a beaker and stirred with a magnetic stirrer at 500 rpm for 2 hours to allow the CH_2Cl_2 to evaporate and the microparticles to solidify. The microparticles were collected using filter paper and a Kitasato flask connected to a vacuum system. The PVA solution with the microparticles was poured onto the filter paper, which retained the microparticles containing the CM, while the excess solution

remained inside the Kitasato. Microparticles were collected in a 5 mL Eppendorf tube and incubated overnight at -80°C. The next day, microparticles were freeze-dried for 12 hours to remove excess water, resulting in a powder appearance. The protein content in the microparticles was quantify using the BCA method as described earlier. Microparticles were previously dissolved using 100% acetone (Cat. L10407.AU, ThermoFisher Scientific, Waltham, MA, USA) and the content was resuspended in distilled water to favour the protein detection. Protein quantification was also performed on the 50X CM using the same method, then allowing the determination of the success rate of the CM encapsulation process.

PhotoGel-LAP, Methacrylated Gelatin Hydrogel Kit (Cat. CC324, Sigma-Aldrich, Burlington, MA, USA) was used to resuspend microspheres and prepare the scaffolds. This kit contained purified porcine gelatine methacrylate (GelMA) and the photoinitiator lithium phenyl-2,4,6-trimethylbenzoylphosphinate (LAP). GelMA was dissolved at 10% in distilled water in an opaque container, warmed at 30°C and stirred with a magnet. Then, 0.25% of LAP and 50 microspheres/mL were added to the final solution. The GelMA-LAP-Microsphere solution was shaped into 4 mm diameter, 1 mm thickness cylindrical scaffolds using the inner space of a cut syringe and left to solidify on a cold plate. The scaffolds were then photocrosslinked by exposure to UV light for 10 minutes in a cell culture cabinet to maintain sterility (69, 193).

Once the scaffolds were prepared, the surgical procedure was initiated. Fourteen-weeks old C57BL/6 mice were anesthetized, placed on a warm pad and their heads were shaved as previously described. A longitudinal incision was made on the head, and the skin was pull aside to expose the calvaria bone. One 4 mm-diameter circular bone defect was made in the middle of the sagittal suture using a dental surgical drilling unit with a trephine constantly cooled with drops of a sterile saline. The bone was carefully removed without harming the dura mater. The scaffolds were placed into the bone defects using forceps and the incision was stapled (101). These scaffolds remained in place for 3 months. After this period, the mice were euthanized in a CO_2 chamber, and the entire heads were collected using surgical scissors and immersed in a 10% formaldehyde solution for overnight fixation. After fixation, the heads were transferred to 70% ethanol to be preserved until bone analysis.

Bone regeneration was assessed by micro-computed tomography (microCT) in the Department of Physiology and Cell Biology of the University of Arkansas for Medical Sciences. Scanco vivaCT 80 (Scanco Medical, Brüttisellen, Switzerland) was used to scan the whole heads and to obtain 3D reconstructions. The percentage of repair was evaluated using the image analysis software ImageJ 1.53c software, and the subsequent calculations were based on the following equation (69):

$$\%\ \text{bone repair} = \frac{\text{New bone area}}{\text{Original defect area}}\ x\ 100$$

3.16. *In Vivo* Osteoporotic Model

The primary aim of this project is to use secretome as a viable therapeutic approach for osteoporosis treatment; thus, the evaluation of secretome's impact in an *in vivo* model that closely mirrors the pathological features of osteoporosis is essential. To achieve this goal, we employed a commonly used experimental model for inducing osteoporosis: ovariectomized animals. This model replicates hormonal oestrogen deficiency to mimic post-menopausal osteoporosis (195).

Four-month-old female CD1 mice were used in this procedure. Mice were anesthetized, placed on a warm pad and their backs were shaved as mentioned earlier. The ovariectomy procedure was carried out following the protocol described by Souza et *al.* (195). Briefly, a single longitudinal surgical incision was performed in the lower part of the back of the mice. The musculature and other soft tissues were pushed aside to expose the ovarian fat pad, which was brought outside the incision to allow easy access to the ovary. While the ovarian fat pad was secured with forceps, the region beneath the ovary was clamped with heated forceps, allowing the ovary to be removed and the wound to be sealed at the same time, preventing excessive blood loss. The incision was stapled, and the procedure was replicated with the contralateral ovary. Four mice underwent the surgery but skipping the ovaries removal, which constituted our positive control group (Sham group, non-osteoporotic mice). The mice were observed and weighted during one week after the surgery to assured proper health status.

Once mice recovered post-surgery, CM administration was performed with the help of Dr Alfonso Fernández, specialist in traumatology from Hospital Universitario Marqués de Valdecilla. CM was produced and concentrated 50-fold (50X) as previously mentioned, using C3H10T1/2 cell line. Mice were anesthetized and the left legs were shaved and sterilized. A longitudinal incision was accomplished on the knee, and the joint was flexed to expose inner tissues. The leg was manually immobilized and a Hamilton syringe (Cat. 80500, Hamilton Company, Reno, NV, USA) loaded with 5 µL of 50X CM (or NaCl for negative control, table 5) was used to approach the medullary cavity. The content of the syringe was carefully injected in the distal end of the femur and the incision was closed by suture with a surgical thread.

Table 5. Study groups established in the *in vivo* murine osteoporotic model experiment.

Study group	Ovariectomy	Treatment	Replicates (n)
Sham	No	No	5
Negative control	Yes	0,9% NaCl	5
CM-Ctrl	Yes	5µl of Sec-Ctrl	5
CM-*Smurf1*	Yes	5µl of Sec-*Smurf1*	5

After 1 month, the mice were sacrificed in a CO_2 chamber and both femurs were extracted. The femurs were fixed for 48 hours in 10% paraformaldehyde (Cat. 047317.9L, ThermoFisher, Scientific, Waltham, MA, USA) and kept in 70% ethanol until analysis.

Bone architecture was evaluated by microCT in the Department of Physiology and Cell Biology of the University of Arkansas for Medical Sciences, as explained in the previous section. Scanco vivaCT 80 scanner and software was used to scan all femurs, measure and collect microarchitectural data from trabecular and cortical bone.

Trabecular bone analysis was carried out in the distal region of the femur. The growth plate was located as a particularly irregular-organized trabecular bone at the very beginning of the medullary cavity. A constant gap of ten slides was left between the growth plate and the first slide measured to guarantee comparison of the same region in all femurs. The area of interest was set as the

trabecular bone present into the medullary cavity (excluding the cortical bone) starting from the first slide and measuring 151 slides more in direction to the proximal end of the femur.

For cortical bone analysis, the midpoint of the femurs was found by counting the number of slides they occupied in the scan and selecting the one in the middle. For each bone, the region of interest was established measuring the mid slide, 15 slides above and 15 below, resulting in a total of 31 slides. The bone of the medullary cavity was discarded for this analysis.

3.17. Exosomes Purification, Characterization and Functionality Assays

CM was produced as mentioned in previous sections. Exosomes were isolated from CM using the ultracentrifugation method. This method consisted of a 100,000G centrifugation at 4°C for 1 hour in an Optima L90-k ultracentrifuge (Beckman Coulter, Brea, CA, USA). The supernatant constituted the soluble fraction, while the pellet was the vesicular fraction or extracellular vesicles (EVs). These two fractions were carefully separated: the soluble fraction was collected from the centrifugation tube using a serological pipette without disturbing the pellet and the pellet was then resuspended in 100 µL of PBS and recovered in an Eppendorf tube.

Once EVs were purified, characterization of CD63 and CD9 specific exosome markers was carried out using the ExoStep kit (Cat. ExoS-25-C9, ImmunoStep, Salamanca, Spain), following manufacturer's instructions. Briefly, capture beads were vortexed for 20 seconds and 50 µL were added to the 100 µL EVs suspension. This solution was gently mixed by pipetting up and down several times with a pipette and vortexing for few seconds. This mix was incubated overnight at RT without stirring. Next, 1 mL of Assay Buffer 1X was added to the sample and the tubes were placed on a magnetic rack for 5 min. After that, supernatant was removed by decanting, ensuring that no more than 100 µL remained. Then 5 µL of CD9 primary detection antibody were added to the exosome tube and to another tube with no exosomes, which was used as a negative control. The antibody was incubated 60 min at 4°C in the dark. The

samples were washed again by adding 1 mL of Assay Buffer 1X and decanting with the magnetic rack. Samples were finally resuspended in 350 µL of Assay Buffer 1X and acquired on a FACSCanto II flow cytometer with FASCDiva Software.

Average diameter of exosomes were determined by dynamic light scattering using a Zetasizer Nano (Malvern Panalytical, Malvern, UK). Morphological characterization by transmission electron microscopy (TEM) was performed using 10 µL of sample that were deposited on carbon membrane coated cooper grids (Cat. 930326, Sigma-Aldrich, Burlington, MA, USA) and stained with a 2% w/v phosphotungstic acid solution (Cat. P4006; Sigma-Aldrich, Burlington, MA, USA) for 2 min prior imaging.

To evaluate exosome functionality, their ability to internalize into MSCs was tested. CM was produced, and the soluble and vesicular fractions were separated as already explained. ASC52telo cells were seeded at 15,000 cells/cm^2 on Nunc Lab-Tek Chamber Slides (Cat. 177380, ThermoFisher Scientific, Waltham, MA, USA) and were allowed to attach overnight. Exosomes were stained with Vybrant CM-DiI Cell-Labelling Solution (Cat. V22888, ThermoFisher Scientific, Waltham, MA), slightly modifying manufacturer's indications for cell staining. A volume of 0.5 µL of Vybrant CM-DiI was added to a 500 µL-suspension of exosomes and the solution was properly mixed and incubated 1 hour at 4°C. The staining was washed by centrifuging at 1,500 rpm for 5 min at 4°C and removing the supernatant. The pellet was then resuspended in 500 µL of PBS and the wash step was repeated two times more. In the final wash, exosomes were resuspended in 2 mL of complete DMEM culture medium (DMEM with 10% FBS and 1% penicillin-streptomycin) at 37°C. ASC52telo cells seeded on the chamber slides were washed with PBS and the DMEM culture medium with exosomes was added. The cell uptake of stained exosomes was recorded using a Nikon Eclipse Ti live cell microscope, equipped with an incubator to maintain the cells at 37°C under normoxic conditions for 2 hours. After this time, DMEM culture medium was removed, and cells were washed with PBS and fixed with 3.7% paraformaldehyde for 15 min on soft stirring. Next, cells were washed twice with PBS and 0.5% Triton X-100 was added for 15 min on soft stirring to permeabilize the membranes. Cells were washed again twice with PBS. A last 3 min-wash with

0.05% Tween 20 detergent was performed, followed by two PBS washes more. Then, phalloidin cytoskeleton staining (Cat P5282, Sigma-Aldrich, Burlington, MA, USA) was diluted 1:100 in PBS and added to the cells to visualize actin fibres. Fifteen µL of phalloidin 1:100 were used for each well and the staining was incubated at RT for 30 min in the dark. The wells were washed twice with PBS and chambers were carefully disassembled. The slides were mounted with Aquashed mounting media without DAPI (Cat. HC718601, Merck KGaA, Darmstadt, Germany) and stored overnight in the dark for subsequent confocal microscopy visualization using a Nikon A1R-HD TIRF Confocal Microscope (Nikon Instruments Inc., Melville, NY, USA).

3.18. *In Vitro* Assessment of Conditioned Medium Fractions Effect in Osteogenic Differentiation

An evaluation of the *in vitro* osteogenic effect of both fractions separately was performed. CM was produced and fractions were separated as previously explained, using ASC52telo cells. The vesicular fraction was resuspended in MesenPRO RS Medium with GlutaMAX (without supplements) to match the volume of soluble fraction obtained. Then 0.25 mL/cm^2 of soluble or vesicular fraction were added to 20,000 ASC52telo cells/cm^2 for 48 hours, and the osteogenic differentiation and assessment were carried out as described in previous sections.

3.19. Mass Spectrometry

Mass spectrometry analysis was performed thanks to our collaboration with Dr Bolado-Carrancio from the Institute of Genetics and Molecular Medicine in Edinburgh. Mass spectrometry was applied to determine the protein content of the CM. Both soluble and vesicular fractions of CM-Ctrl and CM-*Smurf1* were analysed separately. For this, CM was produced and the fractions were separated as previously explained. Both fractions underwent mass spectrometry analysis following an in-solution digest protocol. Briefly, proteins were denatured with 6M guanidine hydrochloride (Cat. SRE0066, Merck KGaA, Darmstadt, Germany) reduced and alkylated with 5 mM tris(2-carboxyethyl)phosphine (Cat. C4706. Merck KGaA, Darmstadt, Germany) and 10 mM chloroacetamide (Cat. 22790,

Merck KGaA, Darmstadt, Germany), and sequentially digested with Mass Spectrometry-grade Pierce Lys-C/trypsin proteases mix (Cat. 90051, ThermoFisher Scientific, Waltham, MA, USA). Peptides were desalted and purified using 50% acetonitrile (Cat. 15661700, ThermoFisher Scientific, Waltham, MA, USA) and 0.1% trifluoroacetic acid (Cat. 302031, Merck KGaA, Darmstadt, Germany) (196). The eluted peptides were lyophilized in a Concentrator Plus (Cat. 5305000703, Eppendorf Corporate, Hamburg, Germany), resuspended in 0.1% trifluoroacetic acid and analyzed by Liquid chromatography–mass spectrometry analytical technique on a Orbitrap Fusion™ Lumos™ Tribrid™ Mass Spectrometer (Cat. IQLAAEGAAPFADBMBHQ, ThermoFisher Scientific, Waltham, MA, USA) (197). Protein identification and quantification were performed using the Data-Independent Acquisition neural networks (DIA-N/N) software and the Perseus software (197, 198) after normalizing the values by total protein in the samples. Statistical significance was determined using an adjusted t-test against CM-Ctrl, with a p-value threshold of 0.05 and a fold change of 2 or greater.

3.20. Conditioned Medium Effect on Osteocytes

To test the effect of CM on osteocytes, murine Ocy454 preosteocytes-like cells (RRID: CVCL_UW31) provided by Dr Pajevic (Boston University, MA, US) were used (199). These cells were cultured following a protocol stablished at Dr Delgado-Calle´s group. Briefly, Ocy454 cells require collagen-coated plates for proper culture; therefore, collagen type I from rat tail (Cat. A1048301, ThermoFisher Scientific, Waltham, MA, USA) was used. A 100 mL-collagen solution was prepared with 95 mL of PBS, 1 mL of glacial acetic acid and 4 mL of collagen type I. Seven mL of collagen solution were added to 75cm^2 cultures flasks followed by incubation at 37°C for 3 hours. The solution was then removed, and flasks were sterilized by 15 min-irradiation with ultraviolet light inside the culture cabinet. Collagen-coated culture flasks were kept at 4°C until use. Once culture flasks were ready, Ocy454 cells were thawed and resuspended in complete α-MEM culture medium (supplemented with 5% FBS, 1% penicillin-streptomycin and 0,2% normocin). Just before use, the collagen-coated culture flasks were washed with PBS to eliminate acetic acid residues, and the cells were

then seeded. Ocy454 cells were cultured in an incubator at 33°C and 5% CO_2 to maintain their immortality, but were transferred to 37°C for two weeks to stimulate cell maturation prior to performing the experiments. During maturation, non-coated culture flasks were used.

Matured Ocy454 cells were seeded at 30,000 cell/cm^2 in complete α-MEM culture medium and were left to attach overnight. The following day, culture medium was replaced with complete α-MEM culture medium combined with 50% of 50X CM (produced and concentrated as mentioned earlier, from C3H10T1/2 cell line) for 24 hours. After that time, RNA was extracted using TRIzol and gene expression was analysed by qPCR as explained in previous sections.

3.21. Conditioned Medium Effect on Osteoclasts

To evaluate the effect of CM on osteoclasts, the murine RAW 264.7 macrophage cell line (RRID: CVCL_0493) was used. These cells were supplied by Dr Delgado-Calle. A density of 10,000 cells/cm^2 was seeded in complete DMEM culture medium (supplemented with 10% FBS and 1% penicillin-streptomycin), incubated at 37°C and 5% CO_2 and allowed to form colonies for 48 hours. Subsequently, the culture medium was discarded and replaced with non-phenol red DMEM (Cat. 11570406, ThermoFisher Scientific, Waltham, MA, USA), supplemented with charcoal stripped FBS (Cat. A33821-01, Gibco ThermoFisher Scientific, Waltham, MA, USA) and 1% penicillin-streptomycin, in combination with 75 ng/mL of recombinant mouse RANKL protein (Cat. 50343-M01H, Sino biological, Wayne, PA, USA) and 10% of 50X CM. Half of the medium was refreshed every 2 days. Cells were stained on day 6, using the Tartrate-resistant acid phosphatase (TRACP) and alkaline phosphatase (ALP) double-stain kit (Cat. MK300, Takara Bio Inc, Shiga, Japan), following manufacturer's guidelines. Briefly, RAW 264.7 cells were washed with PBS and fixed using 200 µL of Fixation Solution for 5 min. Fixation was stopped by washing the wells twice with 2 mL of distilled water. The substrate solution was prepared by diluting the contents of the substrate for ACP vial in 10 mL of distilled water. Sodium Tartrate Solution was added at a 1:10 ratio to the Substrate Solution. The resultant solution was added to the cells, followed by an incubation at 37°C for 45 min. The reaction was stopped by removing the solution and washing the cells three times

with distilled water. Next, 5 mL of methyl green nuclear staining solution was added for 5 min at RT. The nuclear staining was washed with distilled water. Images were taken by Nikon Eclipse Ti microscope and TRAP-positive cells were counted using ImageJ 1.53c software. Cells with 3 nuclei or more were considered osteoclasts.

3.22. Statistical Analysis

Bars on graphs represent mean values of the experiments performed. The error bars on graphs represent the standard error of the mean values (SEM). Mann-Whitney U test was used for n=3 and the Students' t test for n>5.

To assay bone formation in the histological samples obtained from the rat ectopic model, statistical analysis was performed with SPSS.25 software by means of a one-way analysis of variance (ANOVA) with a Tukey multiple comparison post-test.

Three levels of significance were established: the first level at $p< 0.05$, the second level at $p< 0.01$ and the third level at $p< 0.001$.

RESULTS

4. RESULTS

4.1. Primary MSCs and C3H10T1/2 Culture

Rat and human primary MSCs were harvested from bone marrow (BM-MSCs). Despite the relatively low abundance of MSCs in the bone marrow (<1% of the total BM population) (200), their isolation was successfully achieved. Due to the limited cell yield, mesenchymal marker analysis was not performed as part of the extraction procedure. However, in line with previous studies (201, 202), the MSCs isolated is represented as the adherent cell population, and non-adherent cells were eliminated through serial passaging. Primary cell cultures of both rat and human BM-MSCs were established successfully, with cells exhibiting the characteristic spindle-shaped morphology typical of MSCs. These adherent cells formed colonies and displayed proliferative capacity (Figure 15A and 15B).

Additionally, the C3H10T1/2 cell line was cultured, as reported in previous studies (14). Phase-contrast microscopy confirmed that these cells also exhibited the spindle-shaped morphology and plastic adherence similar to primary MSCs (Figure 15C).

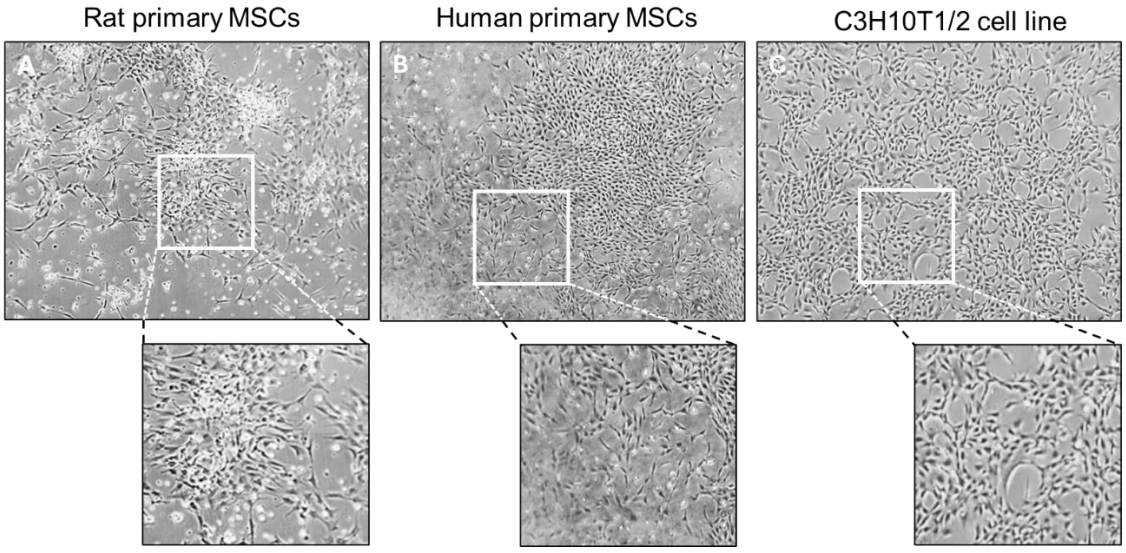

Figure 15. Primary MSCs cultures and C3H10T1/2 cell line culture. (A) Rat Mesenchymal Stem Cell (rMSCs) culture 15 days after seeding bone marrow extracted from the femur of Spargue-Dawley rats. **(B)** Human osteoporotic Mesenchymal Stem Cell (hOP-MSCs) culture 20 days after seeding bone marrow extracted from the femoral head of an osteoporotic patient. (C) Culture of the C3H10T1/2 cell line. Images taken using a phase contrast microscope. Magnification 4X.

4.2. ASC52telo Cell Line Characterization

ASC52telo cell line was purchased specifically for this project. Prior to setting up experiments with this cells line, we decided to perform an evaluation of MSCs' characteristics according to International Society for Stem Cell Research (ISTC) guidelines.

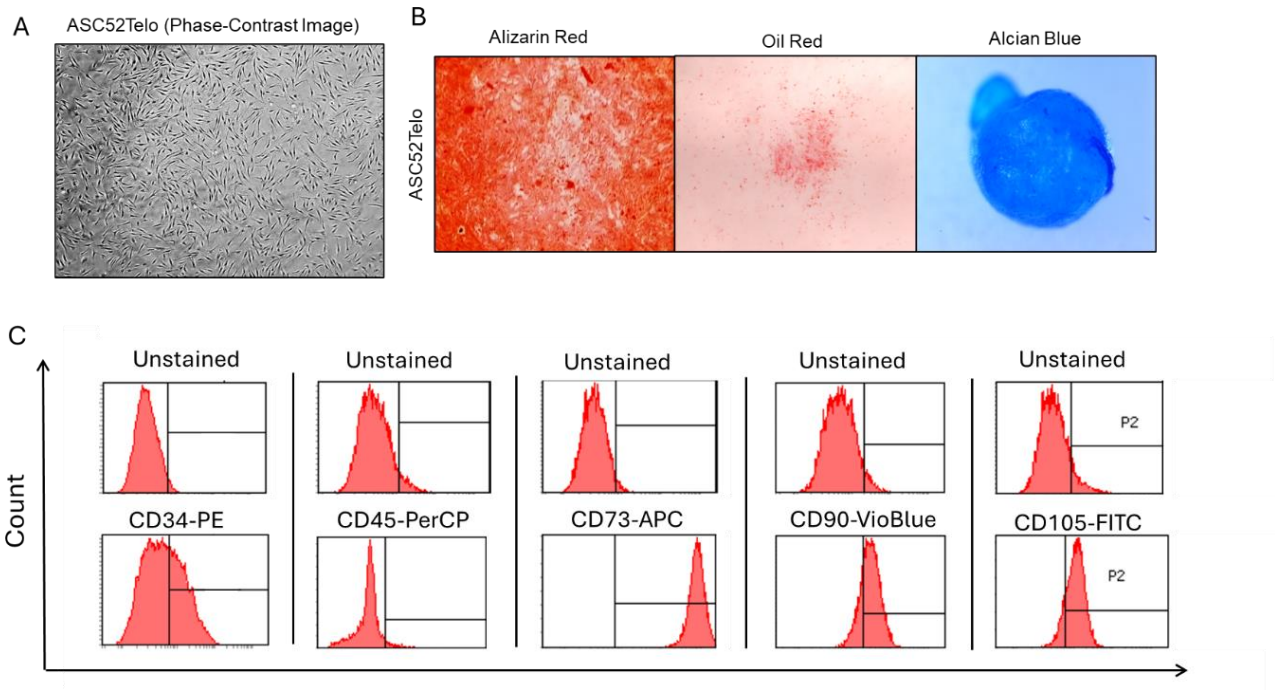

Figure 16. ASC52telo cell line characterization. (A) ASC52telo cells in standard in vitro culture show adherence to plastic and spindle shaped morphology. Phase-contrast Image. Magnification 4X. **(B)** From left to right: Alizarin Red, Oil Red and Alcian Blue staining showing osteocytic, adipocytic and chondrocytic lineage, respectively, after the correspondent differentiation. **(C)** The flow cytometry analysis displayed the cell population showed positivity for CD73, CD90 and CD105 mesenchymal markers and low presence of CD34 and CD45 non-mesenchymal markers.

First, adherence to plastic under standard culture conditions was confirmed, along with the observation of the spindle-shaped morphology (Figure 16A). Subsequent testing encompassed osteogenic, adipogenic, and chondrogenic differentiation processes. ASC52telo cells demonstrated the ability to generate fully differentiated cells from these distinct tissue subtypes as evidenced by Alizarin Red, Oil Red and Alcian blue staining, performed after specific differentiation stimuli (Figure 16B). Moreover, flow cytometry analysis of mesenchymal markers confirmed the expression of CD73, CD90, and CD105 markers. The pan-haematopoietic marker CD45 and the CD34 marker, specific of hematopoietic progenitors, were predominantly absent in the cell population.

Nevertheless, it is noteworthy that the values obtained for the latter were higher than expected (Figure 16C). Thus, verification of the mesenchymal profile of the ASC52telo cell line was achieved in accordance with ISTC guidelines. These findings corroborated the outcomes of a previous characterization study conducted by Wolbank et *al.* in 2009 (186).

4.3. Specific *Smurf1*/*SMURF1* Silencing Using Gapmers

Specific LNA-ASOs GapmeR molecules were used to silence human *SMURF1* gene in the ASC52telo cell line. Similarly, a specific GapmeR for the silencing of murine *Smurf1* gene expression in mouse (C3H10T1/2 cell line) and rat (primary rMSCS) cells was also tested. The use of GapmeRs offers several advantages such as ease of production, high cellular uptake rates, economic feasibility, clinical safety by eliminating the need for viral vectors, and enhanced efficacy attributed to their resistance to nucleases (69).

Adhering to the instructions provided by the manufacturer, we conducted the GapmeR lipofection procedure, using precise quantities to achieve a final GapmeR concentration of 20nM. Specific GapmeRs for human and rat cells were used (GpmR *SMURF1* and GpmR *Smurf1*, respectively), and a negative control GapmeR (GpmR Ctrl), with no affinity for any gene was applied as a reference.

Significant reduction in gene expression was reported in the three cell types. C3H10T1/2 cell line data is not shown as it was documented in a previous work (14), demonstrating an 80% gene silencing efficiency. Here, we present findings concerning rMSCs and ASC52telo cell line, which also exhibited approximately 80% reduction in *Smurf1/SMURF1* expression (Figure 17).

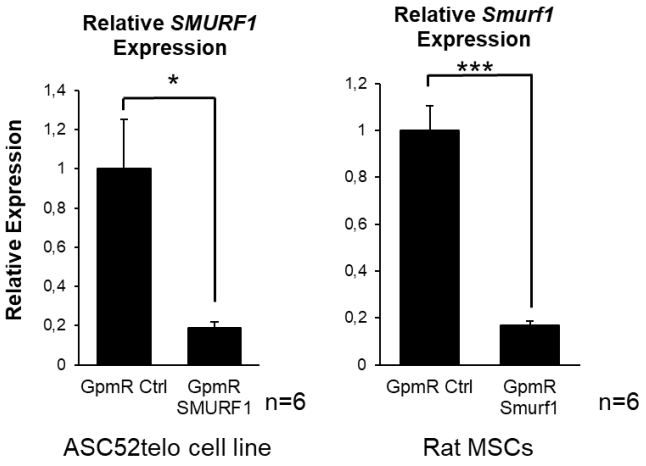

Figure 17. Relative *Smurf1/SMURF1* expression on the human cell line ASC52telo and rat primary MSCs. The graphs illustrate the expression of *Smurf1* gene through qPCR analysis in cells that were transfected with either a non-specific control GapmeR (GpmR Ctrl) or a GapmeR specifically engineered for the silencing of *Smurf1* (GpmR *SMURF1*) in ASC52telo cells and rMSCs (GpmR *Smurf1*). The graphs display the average data from six distinct experiments (n=6), with error bars indicating the standard error of the mean value. Statistical significance is indicated as follows: * for p-value <0.05 and *** for p-value <0.001.

4.4. *In Vitro* Assessment of the Effect of Conditioned Media on Osteogenic Differentiation in Rat Mesenchymal Stem Cells

Upon establishing that the silencing of *Smurf1* in MSCs enhances their osteogenic potential, as evidenced in both calvaria and ectopic models (69, 193), we proceeded to evaluate the hypothesis that the conditioned media (CM) from these *Smurf1*-silenced MSCs also exhibits increased osteogenic capabilities. Following the optimization of conditions for effective silencing of the *Smurf1* gene in rMSCs (Figure 17), CM derived from these cells (rCM-*Smurf1*) was generated. Additionally, CM samples were obtained from rMSCs treated with a control GapmeR, serving as a negative control (rCM-Ctrl) in all experiments hereafter. Primary rMSCs were exposed to rCM-Ctrl and rCM-*Smurf1* for 48 hours, after which the cells underwent osteogenic differentiation for a period of 12 days.

Important changes were observed at later time points, with no notable differences at days 0 and 4. Our findings demonstrate a significant increase in the expression of the key osteogenic transcription factor *Runx2* on day 8 of differentiation in rMSCs treated with rCM-*Smurf1* compared to those treated with rCM-Ctrl. Levels of alkaline phosphatase (*Alpl*) expression showed a significant increase in rMSCs treated with rCM-*Smurf1* at days 8 and 12. Correspondingly,

a marked elevation in ALPL activity was observed in cells preconditioned with rCM-*Smurf1* (Figure 18A). Due to the key role of ALPL in osteogenesis, this would suggest an enhanced osteogenic differentiation. This observation was further corroborated by a progressive increase in mineralization, culminating in a significant augmentation of calcium deposits in rMSCs treated with rCM-*Smurf1* on day 12 (Figure 18A), as assessed through Alizarin Red staining (Figure 18B).

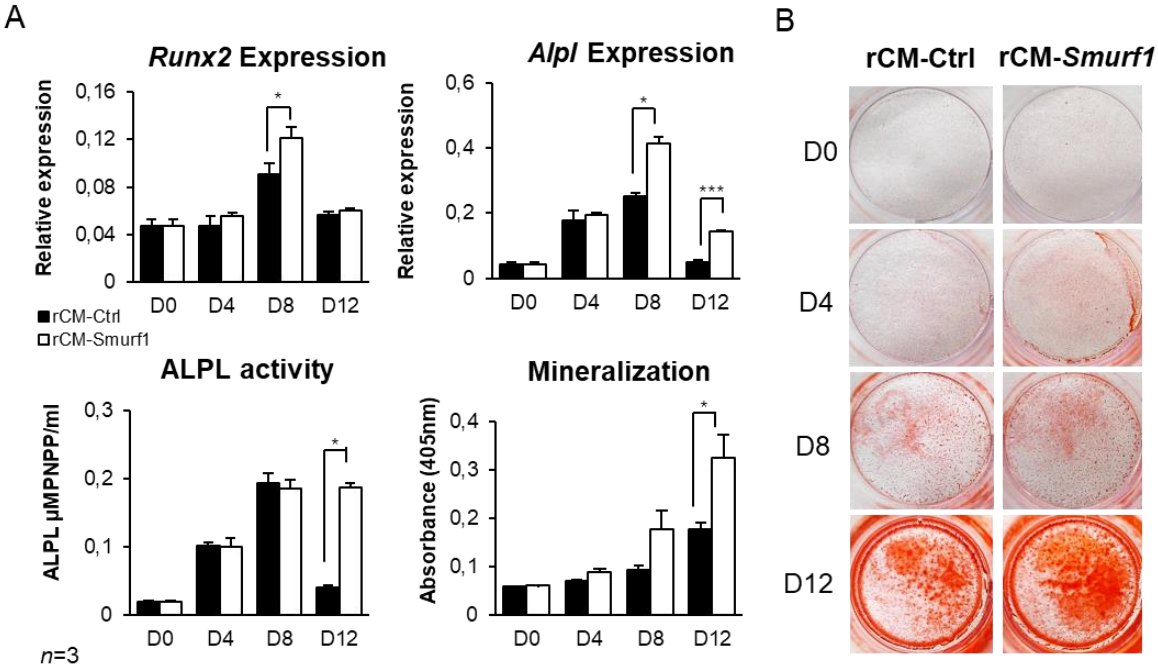

Figure 18. In vitro osteogenic potential of Conditioned Media (CM) from rat Mesenchymal Stem Cells (rMSCs). The effects of CM were measured on days 0, 4, 8 and 12 (D0, D4, D8, D12) of osteogenic differentiation after 48 hours of induction with rCM-Ctrl or rCM-*Smurf1*. **(A)** Top. Relative expression levels of *Runx2* and *Alpl* genes in rMSCs determined by quantitative PCR. Bottom. The left graph represents relative alkaline phosphatase activity in rMSCs. The right graph shows level of mineralization quantified through Alizarin Red staining. The graphs present mean values from three independent experiments (n=3). Error bars indicate the standard error of the mean value. Statistical significance is indicated as follows: * for p-value <0.05 and *** for p-value <0.001. **(B)** Alizarin Red staining during the 12 days of osteogenic differentiation showing calcium deposits in red colour.

4.5. *In Vitro* Assessment of CM-*SMURF1* Effect on the ASC52telo Cell Line

After confirming the osteogenic effect of the CM in rMSCs, we decided to replicate the experiment in human cells. This would significantly facilitate the final aim of this project, which is to transfer our findings to clinical applications. To this end, the human adipose tissue MSC cell line ASC52telo was obtained from American Type Culture Collection (ATCC). Our goal using this cell line was to

simplify cell handling, minimize the use of animals needed to produce MSCs for our experiments, enhance result reproducibility, and optimize the production process for a secretome-based medical product on a large scale. Upon confirming the efficacy of a *SMURF1*-specific GapmeR in ASC52telo cells for gene silencing (Figure 17), the CM produced by the transfected cells under study (hCM-*SMURF1*) and the control counterpart without gene inhibition (hCM-Ctrl) were assessed. ASC52telo cells underwent a stimulation period of 48 hours with hCM-*SMURF1* or hCM-Ctrl, followed by induction to differentiate for 20 days.

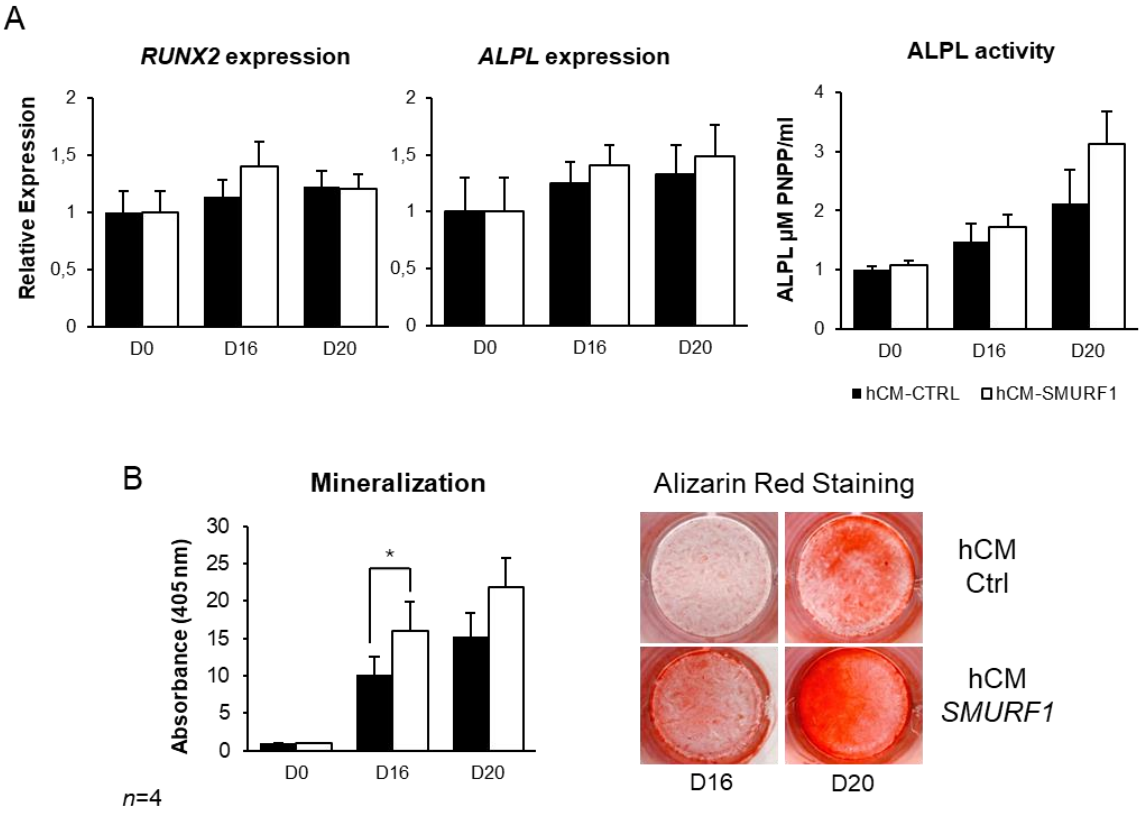

Figure 19. Analysis of the *in vitro* osteogenic potential of Conditioned Media (CM) from ASC52telo cell line. The effects of CM were measured on days 0, 16 and 20 (D0, D16 and D20) of osteogenic differentiation after 48 hours of induction with hCM-Ctrl or hCM-*SMURF1*. **(A)** From left to right. Relative expression levels of *RUNX2* and *ALPL* genes analised by quantitative PCR and alkaline phosphatase activity in ASC52telo cells. **(B)** Graph shows quantification of the Alizarin Red staining of the ASC52telo cell line. The panel displays Alizarin Red staining showing calcium deposits generated by ASC52telo during 16 and 20 days of osteogenic differentiation. The graphs present the mean values from four independent experiments (n=4). Error bars indicate the standard error of the mean value. Statistical significance is indicated as follows: * for p-value <0.05.

No substantial alterations were detected in the expression levels of *RUNX2*; however, a minor increase was observed at day 16 in ASC52telo cells exposed to hCM-*SMURF1* in comparison to hCM-Ctrl. Regarding *ALPL*, a positive trend was identified, indicating an enhancement in the expression of this

critical osteogenic marker in the hCM-*SMURF1* condition. This trend was further supported by an increase in ALPL enzymatic activity on day 20 of osteogenic differentiation, though the change remained statistically non-significant (Figure 19A). Nonetheless, marked increases were observed in mineralization assays in those cells preconditioned with hCM-*SMURF1* (Figure 19B). As shown in the Alizarin Red staining depicted in Figure 19B, we can see a significant enhancement of calcium deposits at D16 of osteogenic differentiation of ASC52telo cells when administered hCM-*SMURF1*, underscoring the biological relevance of our findings.

4.6. *In Vitro* Assessment of the Effect of CM-*SMURF1* on Human Mesenchymal Stem Cells from Osteoporotic Patients

Building upon the positive outcomes from the *in vitro* experiments involving rMSCs and ASC52telo cells, we sought to examine the influence of CM-*SMURF1* in an *in vitro* model that closely mimics the clinical context we aimed to address. Therefore, we replicated the experimental design conducted on these two cell types using MSCs from osteoporotic patients (OP-hMSCs). In our previous studies, we established that bone marrow MSCs extracted from individuals with osteoporosis show a significantly reduced osteogenic capacity compared to those sourced from healthy donors (185), thus, translating this therapeutic approach to clinical application requires confirming the osteogenic benefit of hCM-*SMURF1* on these cells. The CM employed to investigate the osteogenic response of these cells was derived from ASC52telo cells, as we required healthy human cells. Accordingly, OP-hMSCs were harvested from the femoral head of osteoporotic patients, cultured, and subjected to pre-treatment with hCM-Ctrl and hCM-*SMURF1* for a duration of 48 hours. As a positive control, we used 10 ng/mL of recombinant bone morphogenetic protein 2 (BMP2), due to its established role as an osteogenic inducer in clinical practice. Following this, osteogenic induction proceeds for 20 days. All analysis were performed at endpoint. Analyses were performed by inducing osteogenic differentiation in OP-hMSCs obtained from 23 patients individually.

The osteogenic evaluation did not reveal significant differences in the expression levels of key osteogenic genes *RUNX2* and *ALPL* between cells preconditioned with hCM-Ctrl or hCM-*SMURF1*. However, a trend towards increased *ALPL* expression was noted (Figure 20A, top). Notably, significant increases in both alkaline phosphatase activity and the level of mineralization of hMSCs-OP pre-treated with hCM-*SMURF1* were consistently observed across all experiments (Figure 20A, bottom, and Figure 20B). Furthermore, the comparison of ALPL activity and mineralization levels induced by the hCM-*SMURF1* treatment were highly similar to those observed following BMP2 treatment in the hMSCs-OP.

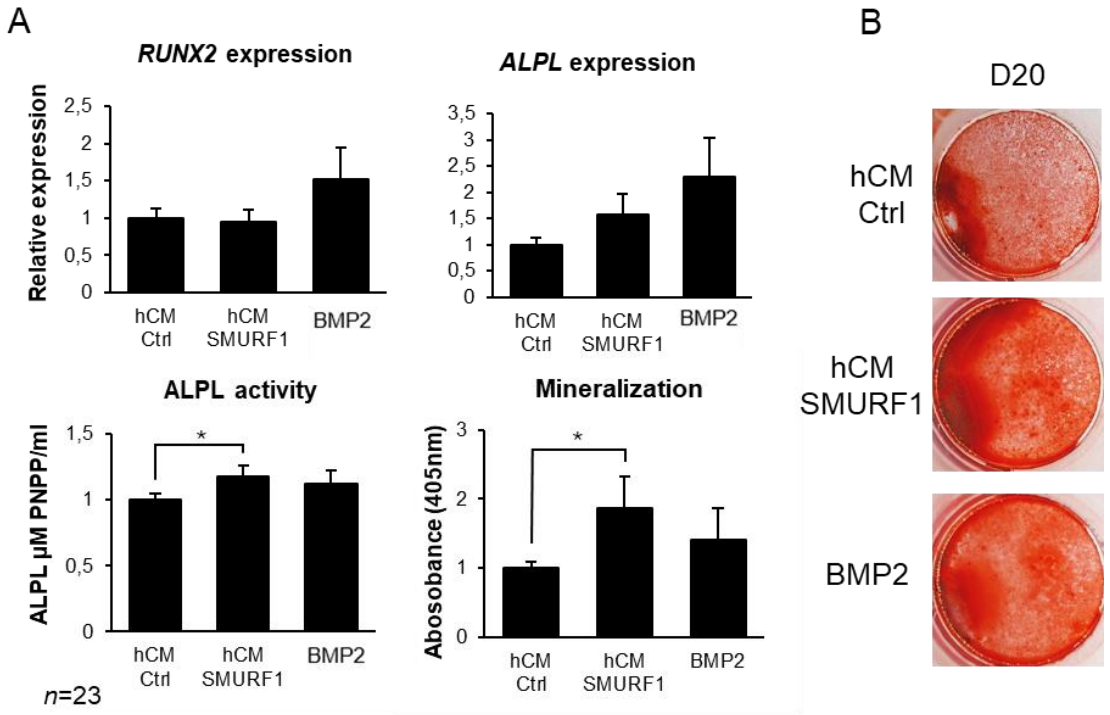

Figure 20. Analysis of *in vitro* osteogenic potential of human osteoporotic Mesenchymal Stem Cells (OP-hMSCs) treated with Conditioned Media (CM). Human MSCs derived from femoral heads from patients suffering from osteoporotic fracture were preconditioned for 48 hours with hCM-Ctrl, hCM-*SMURF1* and BMP2 before undergoing a 20 day-osteogenic differentiation. **(A)** Top. Normalized results of *RUNX2* and *ALPL* relative gene expression in hOP-MSCs by quantitative PCR after 20 days of osteogenic induction. Bottom. The left graph represents the alkaline phosphatase activity in hOP-MSCs at day 20 of osteogenic differentiation. The right graph shows quantification of the Alizarin Red staining performed at day 20 of osteogenic differentiation. The graphs present normalized values from 23 independent experiments, as cells from every patient were analysed independently (n=23). Error bars indicate the standard error of the mean value. Statistical significance is indicated as follows: * for p-value <0.05. **(B)** Representative Alizarin Red staining at day 20 of osteogenic differentiation displaying calcium deposits in red colour.

4.7. Impact of CM-*SMURF1* on Proliferation, Migration and Chemotactic Behaviour

After confirming the positive effects of rCM-*Smurf1*/hCM-*SMURF1* on osteogenesis, it is crucial to evaluate whether this CM influences other basic cellular functions of MSCs, that might either support or hinder bone regeneration. Since the production of the CM using human MSC cell lines is crucial for the industrial scalability and clinical application, we investigated the effects of the hCM-*SMURF1* on the cell proliferation, migratory behaviour, and chemotactic response.

To assess cell proliferation, ASC52telo cells were exposed to hCM-Ctrl or hCM-*SMURF1* for 48 hours. Two additional controls were included: culture medium with no CM and CM directly harvested from untransfected cells (hCM-UT). Following the 48-hour exposure, cells were cultured in standard medium for nine days, with indirect cell quantification performed every two days using MTT assays. The results showed a modest trend towards enhancement in cell proliferation among those cells treated with hCM-*SMURF1* by day 7. This effect did not persist at later time points (Figure 21A).

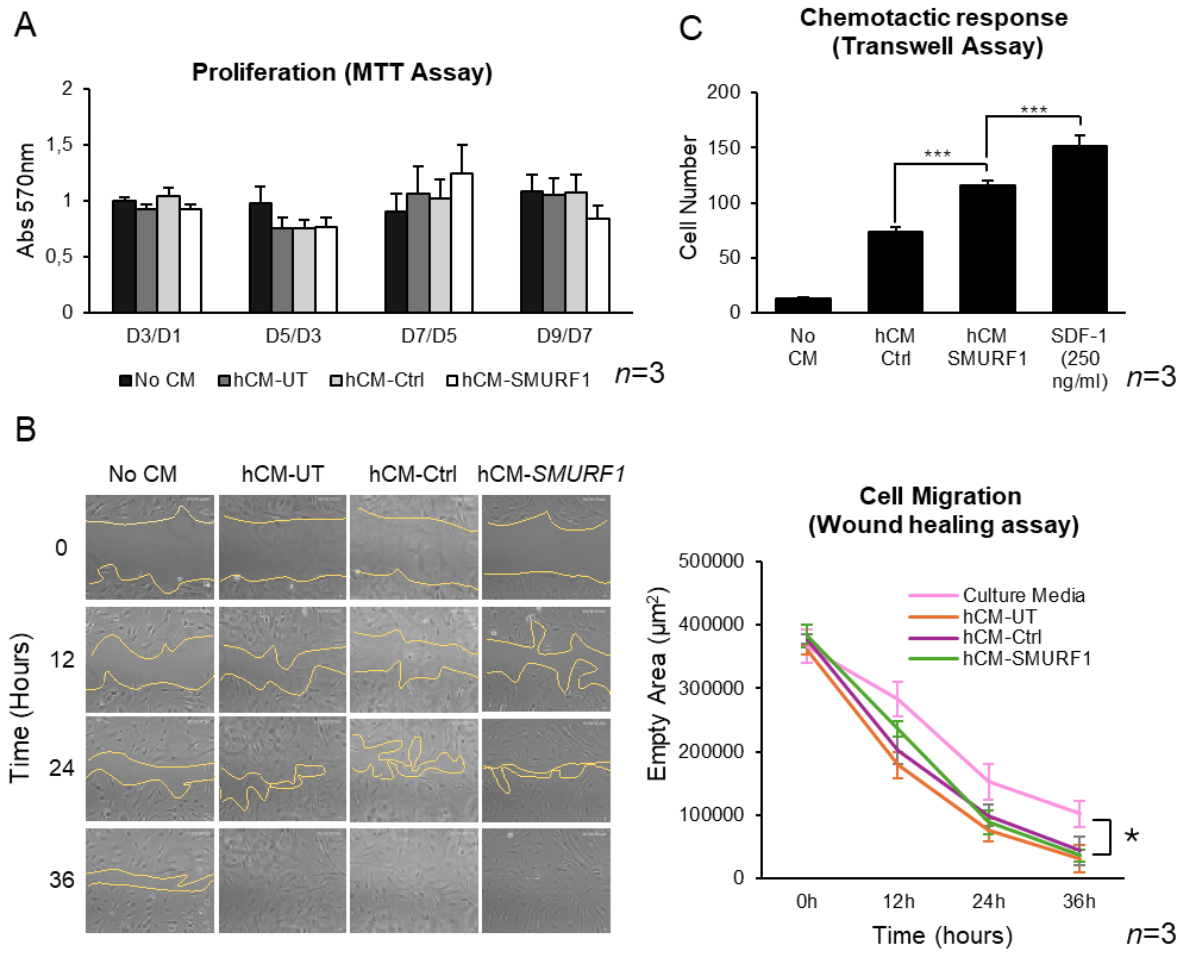

Figure 21. Analysis of the effect of Conditioned Media (CM) on basic cellular functions. (A) Results from the MTT [3-(4,5-dimethylthiazol-2-yl)-2,5-diphenyltetrazolium bromide] proliferation assay performed in ASC52telo cells for 9 days after 48 hours of pre-conditioning with culture media (no CM), CM from untransfected cells (hCM-UT), hCM-Ctrl, and hCM-*SMURF1*. The results are presented as the difference of each day relative to the previous day. (n=3) **(B)** Wound healing assay studying the influence of the culture media (no CM), CM from untransfected cells (hCM-UT), hCM-Ctrl, and hCM-*SMURF1* on cell migration to repair a mechanical damage. Graph represents the empty area in each experimental condition at different time-points (0, 12, 24 and 36 hours). **(C)** Chemotactic response of MSCs to culture media (no CM), hCM-Ctrl, and hCM-*SMURF1* was measured using transwell inserts. SDF-1α recombinant protein was used as a positive control. For all experiments, graphs represent the average values of three experiments. Error bars show standard deviation of the mean values. (*: p-value < 0.05; ***: p-value < 0.001).

To evaluate the capacity of hCM-*SMURF1* to promote cellular repair following mechanical injury, we employed a wound healing assay. Confluent ASC52telo cultures were exposed to hCM-UT, hCM-Ctrl, and hCM-*SMURF1* for 48 hours, along with a condition without CM. A defect was introduced to the cell monolayer, and the recovery process was monitored at 0, 12, 24, and 36 hours until full confluency was restored. A significant enhancement in the migratory

capacity was observed in all cells treated with CM, independently of the source of this CM (Figure 21A). While no significant differences were observed between cells pretreated with hCM-Ctrl or hCM-*SMURF1*, the wound healing process showed a considerable improvement in cells treated with hCM-*SMURF1* compared to the standard culture medium (Figure 21B).

To further explore the effects of hCM-*SMURF1* on fundamental properties of MSCs, we examined whether this CM could modulate the chemotactic response of MSCs using a Transwell assay. ASC52telo cells were in the upper chamber with different CM placed in the lower chamber. Cell migration through the membrane was used to quantify chemotactic response. Stromal cell Derived Factor 1-alpha (SDF1-α), a standard chemoattractant, served as a positive control. Both hCM-Ctrl and hCM-*SMURF1* significantly increased MSC migration compared to the control without CM. Notably, cell migration towards hCM-*SMURF1* approached levels observed with SDF1-α (Figure 21C).

4.8. Evaluation of the Effect Of CM-*SMURF1* on *Ex Vivo* Human Bone Culture.

To gain insight into how hCM-*SMURF1* affects bone formation within the context of bone's natural microenvironment, we used human *ex-vivo* bone cultures from the femoral head of osteoporotic patients. We hypothesised that this CM could be more effective in promoting osteogenesis within the bone microenvironment compared to *in vitro* models. To test this hypothesis, we investigated the effects of hCM-*SMURF1* on human bone fragments obtained from osteoporotic patients (191). The bone specimens were collected from three patients with osteoporotic fractures.

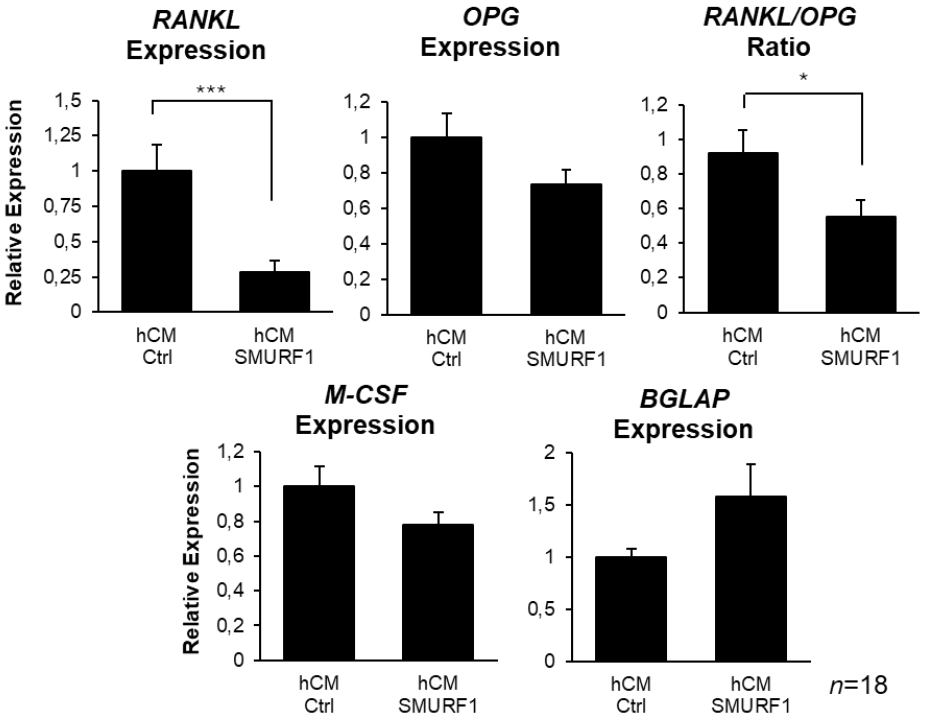

Figure 22. Pro-osteogenic effect of conditioned medium from ASC52telo on human osteoporotic bone fragments. Gene expression analysis of *RANKL*, *OPG*, *M-CSF* and *BGLAP* genes in human osteoporotic bone samples cultured *ex vivo* in 50% of hCM-Ctrl or hCM-*SMURF1* for 4 days. The graphs display the average data from eighteen distinct fragments (n=18), with error bars indicating the standard error of the mean value. Statistical significance is indicated as follows: *: p-value < 0.05; *** is p-value <0.001.

Six bone samples from each patient were cultured in appropriate medium supplemented with either 50% of hCM-Ctrl or hCM-*SMURF1* for four days. After the incubation period, the bone fragments were disaggregated, and total mRNA was extracted for gene expression analysis. hCM-*SMURF1* treatment resulted in a significant reduction in the expression of Receptor Activator of Nuclear Factor Kappa B Ligand (*RANKL*), a key regulator of osteoclast differentiation and activation, which leads to bone resorption (Figure 22). However, the expression of Osteoprotegerin (*OPG*), a decoy receptor for *RANKL*, remained unchanged, resulting in an overall reduction of the *RANKL/OPG* ratio. This ratio is a critical indicator of the balance between bone resorption and formation. No significant changes were observed in the levels of *M-CSF* (Macrophage Colony-Stimulating Factor) or *BGLAP* (Bone Gamma-Carboxyglutamate protein) (Figure 22).

4.9. Analysis of the Pro-Osteogenic Effect of the rCM-*Smurf1* in an *In Vivo* Ectopic Bone Formation Model.

The *in vitro* studies on osteogenesis, along with the evaluations of cell proliferation, migration, and chemotaxis, as well as the *ex vivo* model, suggest that CM-*SMURF1* may have a positive impact on bone regeneration. Therefore, it was essential to also evaluate this effect in *in vivo* models. For this, we first used an ectopic model where rat MSCs were seeded in alginate scaffolds and pre-treated with CM prior to their subcutaneous implantation in Sprague-Dawley rats. The ectopic location of this implants ensures that any observed osteogenic effects would be a result of the osteogenic activity over the implanted cells. As described in the materials and methods section, we evaluated the effects of rCM-Ctrl and rCM-*Smurf1*. As controls, we included an empty scaffold (No Cells) and a scaffold with untreated MSCs. Implants were surgically excised after 8 weeks and analysed for new bone formation using histological techniques. Three scaffolds per condition were subjected to this analysis.

Scaffolds seeded with rMSCs pre-treated with rCM-*Smurf1* showed extensive bone matrix formation, characterized by dark blue staining in the collagen matrix using Masson-Goldner technique (Figure 23A, top panel). Cells embedded within the bone matrix and surrounded by an empty region, resembling osteocytes within osteocytic lacunae, were observed in the rCM-*Smurf1* sample at higher magnification. Quantification of new bone formation revealed increased bone matrix presence in the rCM-*Smurf1* scaffolds, as evidenced by the more intense staining (Figure 23A, bottom).

Furthermore, immunohistochemical analysis using anti-alkaline phosphatase (ALPL) and anti-osteocalcin (OCN) antibodies indicated significant higher expression of these key osteogenic proteins in scaffolds populated with MSCs pre-treated with rCM-*Smurf1*, as evidenced by the intense staining (Figure 23B, top panel). Quantification confirmed a significant increase in ALPL and OCN levels in rCM-*Smurf1*-treated scaffolds compared with the rest of conditions (Figure 23B, bottom).

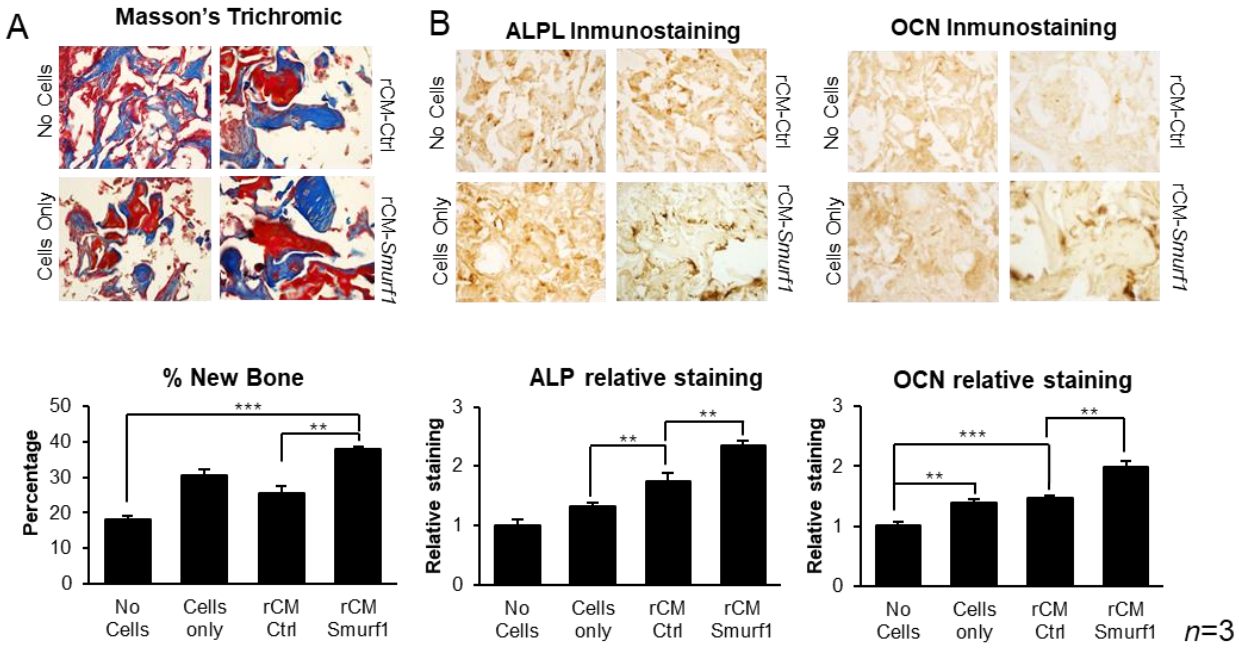

Figure 23. *In vivo* analysis of the pro-osteogenic effect of Conditioned Media (CM) in an ectopic rat model. The experiment analyse the effect of rCM-Ctrl or rCM-*Smurf1* on rMSCs seeded on scaffolds that release BMP2. Empty scaffolds (No cells) and scaffolds with cells only (no CM) were added as controls. **(A)** Masson's trichrome staining of the ectodermically implanted scaffolds. Collagen of the extracellular bone matrix stained in dark blue. Presence of osteocyte lacunae is noted in rCM-Smurf1. Quantification of new bone formation is also depicted (Bottom). **(B)** Histological sections of the scaffolds stained by immunohistochemistry with specific antibody for detection of alkaline phosphatase (ALPL) and Osteocalcin (OCN). Quantification of ALPL and OCN levels observed are obtained from the histological sections (Bottom). All histological analysis of sections were obtained from decalcified implants after 8 weeks. Representative images from all the sections quantified are shown. Graph represents the average values of four measures in three different scaffolds (n=3). Error bars show standard deviation of the mean values. (** is p-value <0.01; *** is p-value <0.001).

4.10. Analysis of the Pro-Osteogenic Effect of the mCM-*Smurf1* in an *In Vivo* Calvaria Bone Defect Mouse Model

Although the ectopic model showed promising results, it does not fully replicate a clinical context, as there is no injury to be repaired, and the implanted MSCs are healthy and preserve a fully osteogenic capacity. This could lead to outcomes different from those expected in bone regeneration therapies. To investigate whether CM-*Smurf1* can stimulate a regenerative response in endogenous MSCs, we designed an experimental protocol that entailed the generation of a calvaria bone defect in healthy mice. To this end, the CM was produced in the C3H10T1/2 murine MSC line. A bone defect was created in the calvaria, which was then covered with a gelatine scaffold containing alginate microspheres loaded with CM. These microspheres enabled the sustained

release of the CM, thereby facilitating bone regeneration. We tested both mCM-Ctrl and mCM-*Smurf1* in this setup with additional controls including empty microspheres (negative control) and microspheres releasing the pro-osteogenic molecule BMP2 (positive control).

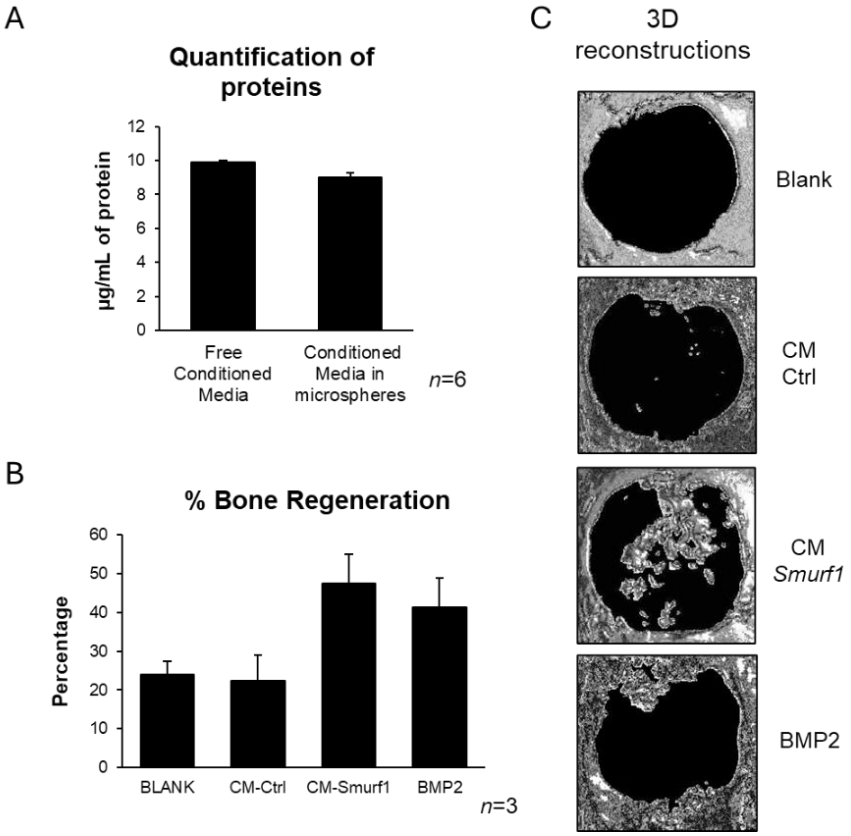

Figure 24. Analysis of the pro-osteogenic effect of the sustained release of Conditioned Media (CM) in the repair of a Calvaria bone defect in mice. (A) Efficiency of Conditioned Media encapsulation. Protein quantification in µg/mL of conditioned media pre- and post-encapsulation into PGLA microspheres. The data shown are the mean values of six independent measurements (n=6)**. (B)** Percentage of bone regeneration obtained in the bone calvaria defect model after 14 weeks of treatment with microspheres-loaded scaffolds containing polyvinyl acid (Blank), mCM-Ctrl, mCM-Smurf1 and BMP2. Bone regeneration levels were measured based on the size of the original. The data shown are the mean values of three independent scaffolds (n=3). Error bars show standard deviation of the mean values. **(C)** Representative images from the calvaria defects after the treatment with scaffolds sustainably releasing CM-Smurf1 quantified are shown.

Although the protocol for the encapsulation of compounds in microspheres had been well established by Dr Díaz-Rodríguez's group, it this was the first time that CM encapsulation had been performed. It was therefore important to measure the performance of this procedure. To this end, a direct methodology for quantifying the protein concentration present in the CM both pre- and post-encapsulation was employed. Protein concentration was measured before and after encapsulation, revealing an initial concentration of approximately 10 µg/mL

in the unencapsulated CM and around 9 µg/mL in the microspheres, resulting in an encapsulation yield of 91,17% (Figure 24A, left).

The results indicated a notable increase in bone formation, with over 25% more new bone in the mCM-*Smurf1* compared to the mCM-Ctrl group, however this increase did not reach statistical significance (p=0.06). Nonetheless, a clear trend was observed: Both mCM-*Smurf1* and BMP2 microspheres demonstrated higher regeneration values compared to the negative control and CM-Ctrl (Figure 24A, right), suggesting that treatments may positively influence resident MSCs located in the surrounding bone tissue (Figure 24B).

4.11. Analysis of the Pro-Osteogenic Effect of the mCM-*Smurf1* in an *In Vivo* Osteoporotic Mouse Model

To effectively translate the findings of this research to osteoporotic patients, it is necessary to establish an *in vivo* model that accurately mimics the characteristics of this condition. We employed an ovariectomized (OVX) murine model to replicate postmenopausal osteoporosis, aiming to evaluate the effect of CM derived from MSCs where *Smurf1* has been silenced on the prevention of bone loss inherent to osteoporotic disease. Healthy female mice underwent bilateral ovariectomy, and one week post-surgery, received a single intramedullary injection of CM into one femur. The study included three groups of OVX mice: one group received only NaCl (OVX), another group was received CM from murine MSCs transfected with a control GapmeR (mCM-Ctrl), and one last group received CM from C3H10T1/2 cells transfected with a GapmeR targeting *Smurf1* (mCM-*Smurf1*). An additional group that did not undergo ovariectomy or injection (Sham group) was included, serving as a positive control for the experiment. Both trabecular and cortical bone changes were assessed one month post-injection.

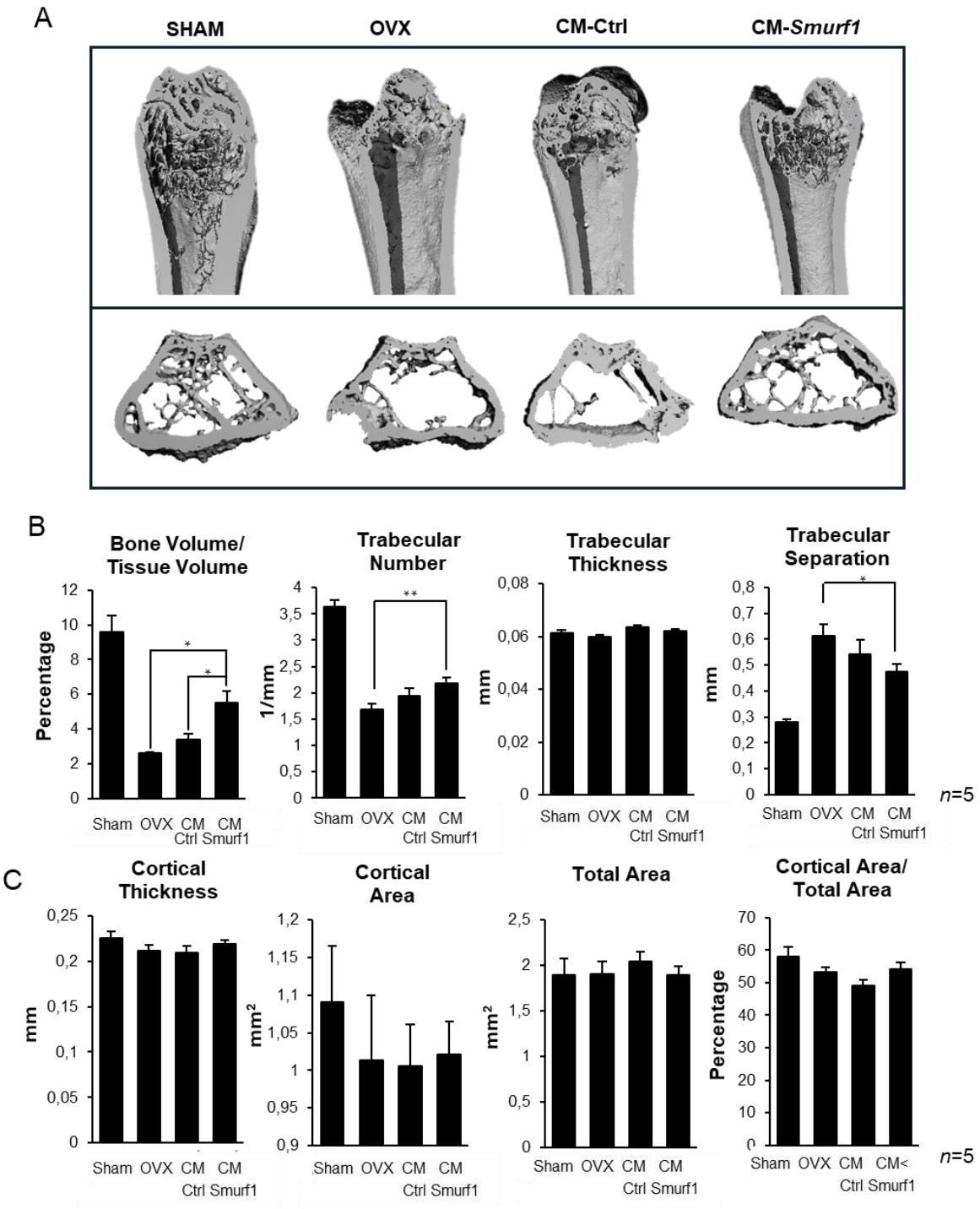

Figure 25. Trabecular and cortical microCT analysis of the effect of the local intraosseous administration of Conditioned Media (CM) in an ovariectomized (OVX) osteoporotic mouse model. (A) Representative micro-CT coronal and transaxial 3D reconstructions from the distal end of femurs from sham, untreated-OVX, OVX treated with CM-Ctrl and OVX treated with CM-*Smurf1* mice. **(B)** Bone volume/tissue volume (BV/TV), trabecular number (Tb.N), trabecular thickness (Tb.Th) and space between trabeculae (trabecular separation, Tb.sp) of femurs from each condition were analyzed by using micro-CT imaging system. **(C)** Cortical thickness (Ct.Th), Cortical Area (Ct.Ar), Total Area (Tt.Ar) and Cortical Area/Total Area (Ct.Ar/Tt.Ar) from the mid-point of femurs from each condition also were analised. The graphs display means of measures of 5 independent femurs (n=5). Error bars indicate the standard error of the mean value. (*: p-value < 0.05; **: p -value < 0.01).

Trabecular bone analysis at the distal femur showed a significant decrease in trabecular structures in the NaCl group compared to the Sham control with the NaCl group bones being almost depleted of trabecular structures compared to the Sham Control (no OVX mice). This confirmed successful induction of osteoporosis. Importantly, mice treated with the mCM-*Smurf1* exhibited a higher proportion of trabecular bone compared to both the OVX mice and mCM-Ctrl groups, suggesting a protective effect of mCM-*Smurf1* on trabecular bone preservation during osteoporotic conditions (Figure 25 A). Micro-CT analysis revealed a significant increase in the Bone Volume to Total Volume (BV/TV) ratio in the mCM-*Smurf1* group compared to the OVX and CM-Ctrl groups, indicating enhanced bone formation due to *Smurf1* silencing. The positive effect of mCM-*Smurf1* was also reflected in the trabecular number (Tb.N) and trabecular separation (Tb.sp) values, although no significant differences were observed at this level between the mCM-Ctrl and mCM-*Smurf1* groups. No significant changes in cortical bone parameters were detected among the different experimental groups (Figure 25C).

4.12. Isolation and Characterization of the Vesicular Fraction of MSC Conditioned Media

As outlined in the introduction, the secretome consists of both a soluble fraction and a vesicular fraction, also known as Extracellular Vesicles (EVs). To comprehensively analyse the secretome produced in the ASC52telo cells line, it is essential to separate and study these two components independently, which requires effective isolation of EVs from the secretome. For this purpose, we employed ultracentrifugation, a widely used technique for EV isolation. The resulting pellet contains the EVs, while the supernatant represents the soluble fraction.

Following isolation, EVs were characterized using Nanoparticle Tracking Analysis (NTA) to determine total particle count and mean size of the isolated EVs. The average particle diameter of EVs was stablished at 131.3 +/- 3.7 nm for the hCM-Ctrl and 114.3 +/- 6 nm for the hCM-*SMURF1* (Figure 26A). The prominent peaks observed within the 50-150 nm range suggest presence of exosomes, typically 30-150 nm in size. Transmission Electron Microscopy (TEM)

further confirmed the presence of EVs in both samples, displaying characteristic vesicular morphology (Figure 26B). To further characterize the isolated exosomes, an immunobead assay was performed using bead-bound capture antibodies and a fluorochrome-conjugated detection antibody. Flow cytometry analysis demonstrated the presence of specific exosome surface markers CD63 and CD9 in both hCM-Ctrl and hCM-*SMURF1* samples (Figure 26C).

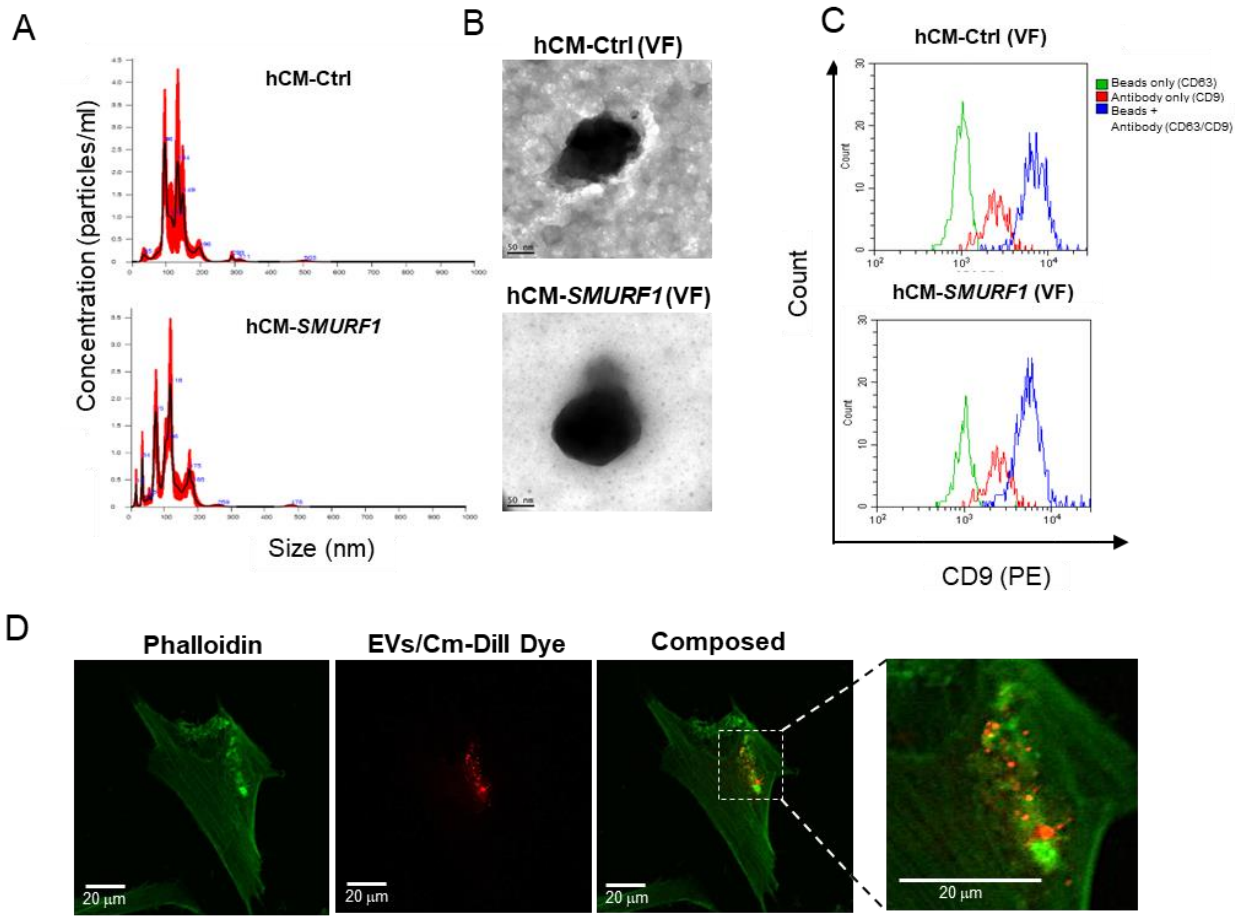

Figure 26. Characterization of the extracellular vesicles isolated from hCM-Ctrl and hCM-*SMURF1*. (A) Nanoparticle Tracking Analysis (NTA) displays total particle count and mean size of the isolated EVs. **(B)** Transmission Electronic Microscopy (TEM) image of EVs isolated from hCM-Ctrl and hCM-SMURF1. Typical vesicular morphology is displayed. Scale bar 50 nm. **(C)** Flow cytometry analysis using a bead-bound capture antibody system for the detection exosome markers CD63 and CD9. EVs from hCM-Ctrl and hCM-SMURF1 show CD63 marker, revealed through specific binding with autofluorescence beads, and CD9 marker due to the association with CD9-PE (phycoerythrin) antibody (blue). A control group using beads only (no EVs or CD9 antibody) was added to the analysis (green), showing lack of PE detection. Partial overlap in PE fluorescence is observed in the other control group, which consists of beads and CD9 antibody in absence of EVs (red). **(D)** Representative confocal microscopy images show EVs stained with Vybrant CM Dil (red) and MSCs stained with Phalloidin (green) after two hours of exposition of cells to the stained EVs.

To validate the functional capability of the isolated exosomes, we conducted internalization assays. Exosomes isolated from ASC52telo were stained utilizing Vybrant CM-DiI membrane dye (red dye) and incubated with ASC52telo cells in culture for 2 hours. Following this incubation, the cells were stained with phalloidin (green dye), allowing visualization of the cytoskeletal actin fibers. High-resolution three-dimensional images acquired from confocal microscopy confirmed the successful internalization of the isolated exosomes by MSCs within this 2-hour incubation period (Figure 26D).

4.13. Analysis of the Pro-Osteogenic Activity of the Soluble and Vesicular Fractions of hCM-*SMURF1*

After establishing the protocol for isolating soluble and vesicular fractions from hCM-Ctrl and hCM-*SMURF1*, we investigated their individual abilities to induce osteogenic differentiation. ASC52telo cells were incubated with either the soluble or vesicular fraction derived from hCM-Ctrl or hCM-*SMURF1* for 48 hours, prior to osteogenic induction. The media was then replaced, and osteogenic differentiation was induced according to standard procedures. Osteogenic markers, alkaline phosphatase activity and mineralization were analysed on day 16 post-induction.

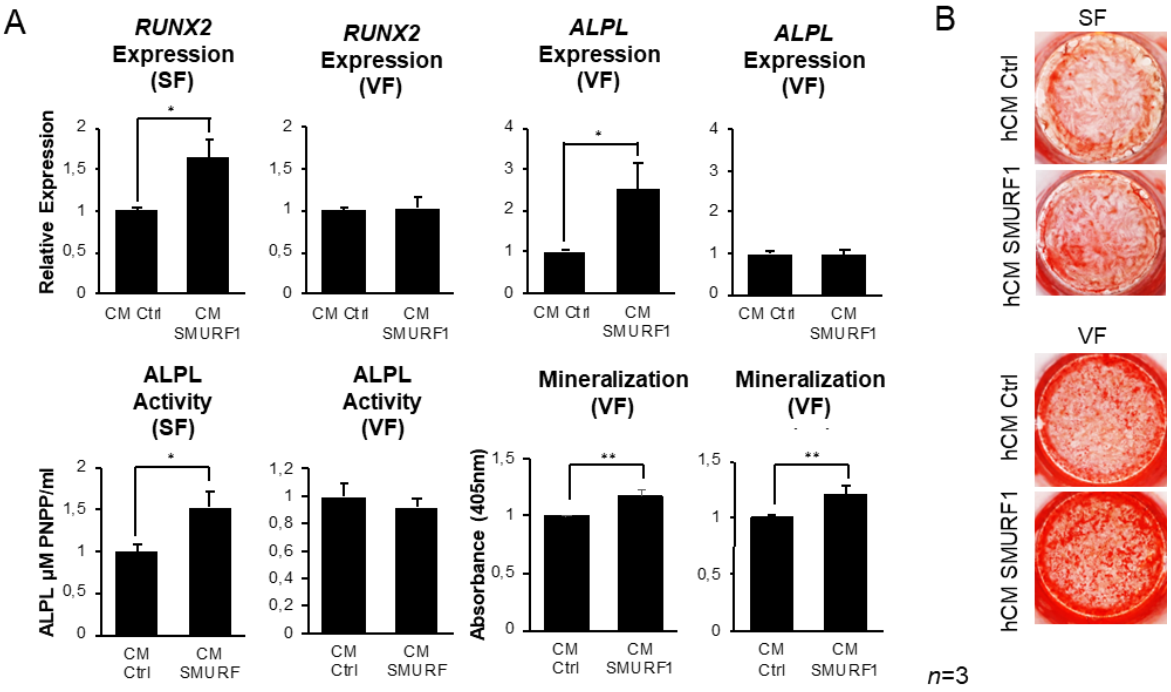

Figure 27. Assessment of pro-osteogenic activity of the soluble and vesicular fractions of hCM-*SMURF1*. (A) Expression of osteogenic markers, alkaline phosphatase activity and mineralization of ASC52telo cells at day 16 of osteogenic differentiation after 48 hours of induction of soluble (SF) or vesicular (VF) fraction of hCM. Top, left: *RUNX2* expression of cells exposed to SF and VF of hCM-Ctrl and hCM-*SMURF1*. Top, right: *ALPL* expression of cells exposed to SF and VF of hCM-Ctrl and hCM-SMURF1. Bottom, right: ALPL enzymatic activity of cells exposed to SF and VF of hCM-Ctrl and hCM-SMURF1. Bottom, right: Quantification of mineralization of cells exposed to SF and VF of hCM-Ctrl and hCM-SMURF1. Results are presented as means of 3 independent experiments (n=3). Error bars indicate the standard error of the mean value. p-value is represented with *. * is p-value <0.05 and ** is p-value <0.01. **(B)** Representative Alizarin Red Staining images showing the stimulation of mineralization seen in both fractions of hCM-*SMURF1*.

Analysis of osteogenic markers revealed a significant increase in the *RUNX2* expression in cells pre-treated with the soluble fraction (SF) of hCM-*SMURF1* compared to that of the hCM-Ctrl. This also applied to the expression levels of *ALPL*, which are mirrored by an enhanced alkaline phosphatase activity in cells treated with this SF (Figure 27A). Although no substantial changes were observed in these parameters between the vesicular fractions (VF) of hCM-Ctrl and hCM-*SMURF1*, both the SF and the VF of hCM-*SMURF1* showed significantly higher mineralization levels, as assessed by alizarin red staining, compared to hCM-Ctrl. This suggests that both the SF and VF of hCM-*SMURF1*, contribute to the mineralization process *in vitro* (Figure 27A and Figure 27B).

4.14. Evaluation of the Pro-Osteogenic Protein Content of Soluble and Vesicular Fractions of hCM-Ctrl and hCM-*SMURF1.*

Having established the pro-osteogenic effect of hCM-*SMURF1*, we demonstrated through the previous results that both the soluble and vesicular fractions contribute to this potential. Hence, our objective is to identify the specific components within each fraction that are responsible for this effect. We sought aimed to identify proteins that were differentially regulated in the soluble and vesicular fractions of hCM-Ctrl and hCM-*SMURF1*. For this purpose, we compared the proteomes of these fractions of hCM-Ctrl and hCM-*SMURF1* from four independent silencing experiments by mass spectrometry. The study identified a significant number of differentially expressed proteins. Proteins that were overexpressed by at least 2-fold (in blue) or under-expressed (in green) in hCM-*SMURF1* compared with hCM-Ctrl, with statistical significance are represented in a volcano plot (Figure 28A). Among these proteins, key regulators of bone formation: PREPL (Prolyl Endopeptidase Like) and FMOD (Fibromodulin) were overrepresented in the soluble fraction of hCM-*SMURF1*, while SPARC (Secreted Protein Acidic and Cysteine Rich) and CCN2 (Cellular Communication Network Factor 2) were overrepresented in the vesicular fraction of hCM-*SMURF1*. In all cases, qPCR validation of the results was consistent with the relative abundance of these proteins found in the mass spectrometry analysis (Figure 28B). The Heatmap show that the samples analysed show similar protein expression pattern, then reinforcing the reproducibility and reliability of the results (Figure 28C).

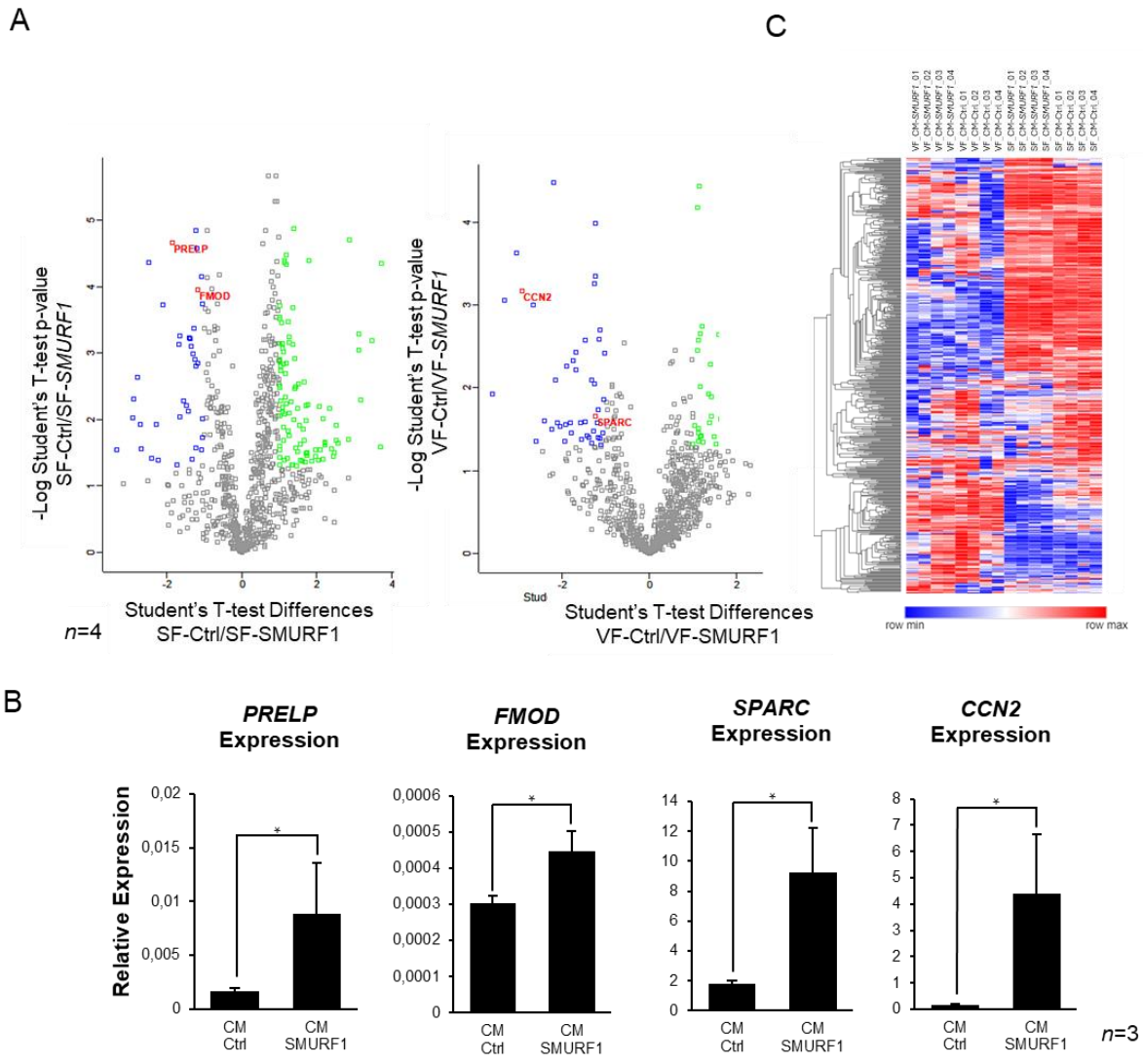

Figure 28. Determination of pro-osteogenic protein factors of the soluble and vesicular fractions of hCM-SMURF1. (A) Vulcano plot showing differently expressed proteins between hCM-Ctrl and hCM-SMURF1 for both soluble and vesicular fraction. Statistical significance was determined using an adjusted t-test against hCM-Ctrl, with a p-value threshold of 0.05 and a fold change of 2 or more. Proteins that are overexpressed by at least 2-fold in hCM-*SMURF1* compared with hCM-Ctrl are represented in blue. Proteins under-expressed in hCM-*SMURF1* compared with hCM-Ctrl are shown in green. 4 overexpressed proteins strongly related to prosteogenic activity are highlighted: SPARC, CTGF, PREPL and FMOD. Four independent samples of each conditioned media were tested (n=4) **(B)** Validation of relative expression by quantitative PCR of 2 proteins overexpressed in soluble fraction (SPARC and CTGF) and 2 proteins overexpressed in vesicular fraction (PREPL and FMOD) of CM-*SMURF1*. Results are presented as means of 3 independent genes measures (n=3). Error bars indicate the standard error of the mean value. *: p-value < 0.05. **(C)** The Heatmap of overexpressed and underexpressed proteins shows similar protein expression pattern between the 4 independent samples studied in this analysis (n=4).

To gain an overview of the principal biological processes associated with the proteins that were significantly different in the two sets of samples, we performed Gene Ontology (GO) analysis. Significantly enriched proteins from the

hCM-*SMURF1* vesicular fraction were associated with the GO biological processes “extracellular matrix organization” and “ossification” (Figure 29).

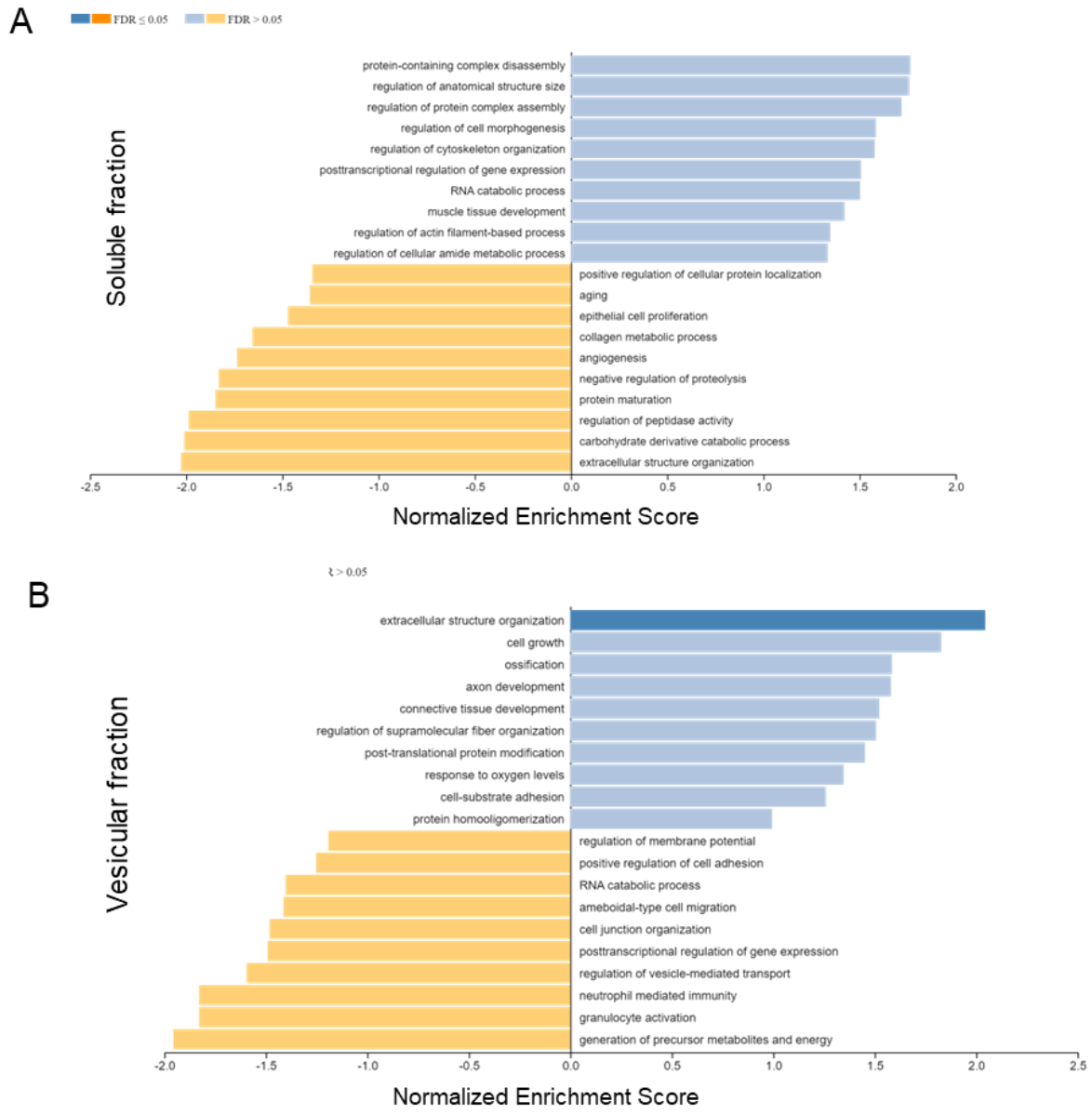

Figure 29. Gene Ontology (GO) analysis of proteins significantly enriched in soluble and vesicular fractions of hCM-*SMURF1*. Top ten GO terms differentially represented in the **(A)** soluble (SF) and **(B)** vesicular fraction (VF) protein content of hCM-Ctrl and hCM-*SMURF1*. Positive normalized enrichment score means GO terms overrepresented in hCM-*SMURF1* in comparison with CM-Ctrl (in blue). Negative normalized enrichment score means GO terms underrepresented in hCM-*SMURF1* in comparison with CM-Ctrl. Among GO biological processes enriched in SF of hCM-*SMURF1*, “Regulation of anatomical structure size” and “Regulation of morphogenesis” stand out. Importantly, GO biological processes of “Extracellular matrix organization” and “Ossification” are enriched in VF of hCM-*SMURF1*. FDR: False Discovery Rate.

4.15. Evaluation of the Effect Of CM-*Smurf1*/*SMURF1* on Other Cells of the Bone Microenvironment

The primary aim of this work is to develop a treatment for application to bone tissue. Consequently, it is anticipated that this intervention will not solely influence the resident MSCs but will also affect other cell types within the bone microenvironment, including osteocytes and osteoclasts. Analysing the impact of the modified MSCs' conditioned media on these cells is essential, given their interrelated roles in maintaining bone homeostasis, as outlined in the introductory section. Alterations affecting a specific cell type could potentially influence other cell types and determine the therapeutic efficacy or ineffectiveness of the proposed approach.

To this end, we conducted a study to assess the influence of mCM-Ctrl and mCM-*Smurf1* on osteocytes. Before we could perform the analysis, it was critical to ensure that they do not experience cytotoxicity upon exposure. We therefore conducted an initially cell viability assessment using the murine pre-osteocyte cell line Ocy454. These cells were exposed for 24 hours to standard culture medium, mCM-Ctrl, and mCM-*Smurf1*, at three distinct concentrations of CM (10%, 25%, and 50%) to ascertain whether any cytotoxic effects, if present, were dose-dependent. Following the 24-hour exposure period, both viable and non-viable cells were counted, revealing no significant increase in cell death in any of the conditions tested compared to the standard media, indicating that the CM does not induce cytotoxicity in Ocy454 cells (Figure 30A). Osteocytes function not only as structural elements but also as pivotal regulators of bone metabolism, capable of influencing osteoclastic and osteoblastic activities in response to external stimuli (12, 203); therefore, the effect of CM on these cells are relevant to all cellular types within the bone microenvironment. Accordingly, we performed a bone homeostasis marker study after the 24-hour exposure of Ocy454 cells to 50% mCM-Ctrl and mCM-*Smurf1*. Our findings indicate that mCM-*Smurf1* induces a statistically significant reduction in the *Rankl/Opg* ratio, suggesting a decrease in bone resorption and, consequently, a potential for bone preservation. Furthermore, Sclerostin (*Sost*), Dickkopf1 (*Dkk1*), and Macrophage Colony-Stimulating Factor (*M-csf*) also exhibit significant decreases (Figure 30B),

aligning with the observed results of the *Rankl/Opg* ratio, as *Sost* and *Dkk1* inhibit osteoblastic activity while *M-csf* facilitates osteoclast formation (13, 203).

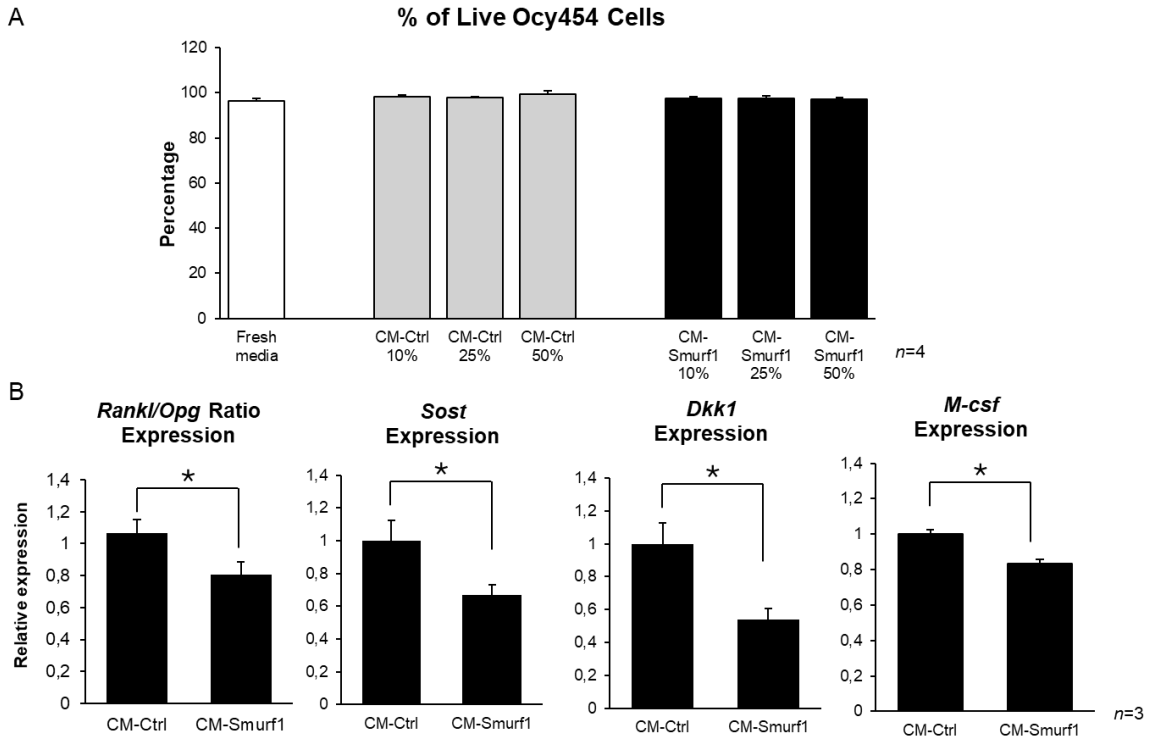

Figure 30. Effect of CM-*Smurf1* in murine Ocy454 preosteocytes-like cells. (A) Viability assay performed using trypan blue staining. Fresh standard media was used as a control, and a 24h-exposure of 10%, 25% and 50% of each conditioned media was tested. After that time, every condition was counted 4 times (n=4) **(B)** Relative expression of *Rankl/Opg*, *Sost*, *Dkk1* and *M-csf* genes by qPCR. The graphs present normalized values from 3 independent experiments (n=3). Error bars indicate the standard error of the mean value. *: p-value < 0.05.

Osteoclasts, on the other hand, are essential for bone homeostasis due to the role in bone resorption. Evaluating the effect of mCM-*Smurf1* on the activity of these cells can also provide significant insights into how bone tissue might respond to treatment in patients. For this purpose, we used the RAW 264.1 macrophage cells line. In this cellular model, osteoclastogenesis was induced by adding recombinant mouse RANKL protein to the culture medium. Additionally, a subset of the RAW 264.1 cells was subjected to treatment with mCM-Ctrl or mCM-*Smurf1* to assess whether the presence of the CM could either accelerate or inhibit osteoclast formation or activity. On day 6 of the experiment, nuclei counting, and tartrate-resistant acid phosphatase (TRAP) staining revealed that the number of multinucleated cells (≥3 nuclei) was significantly reduced in cells exposed to RANKL + mCM-*Smurf1* compared to the positive control, which received only RANKL, as well as to cells that were treated with RANKL + mCM-

Ctrl (Figure 31). This suggests that mCM-*Smurf1* could attenuate osteoclastogenesis and favour net bone mass gain.

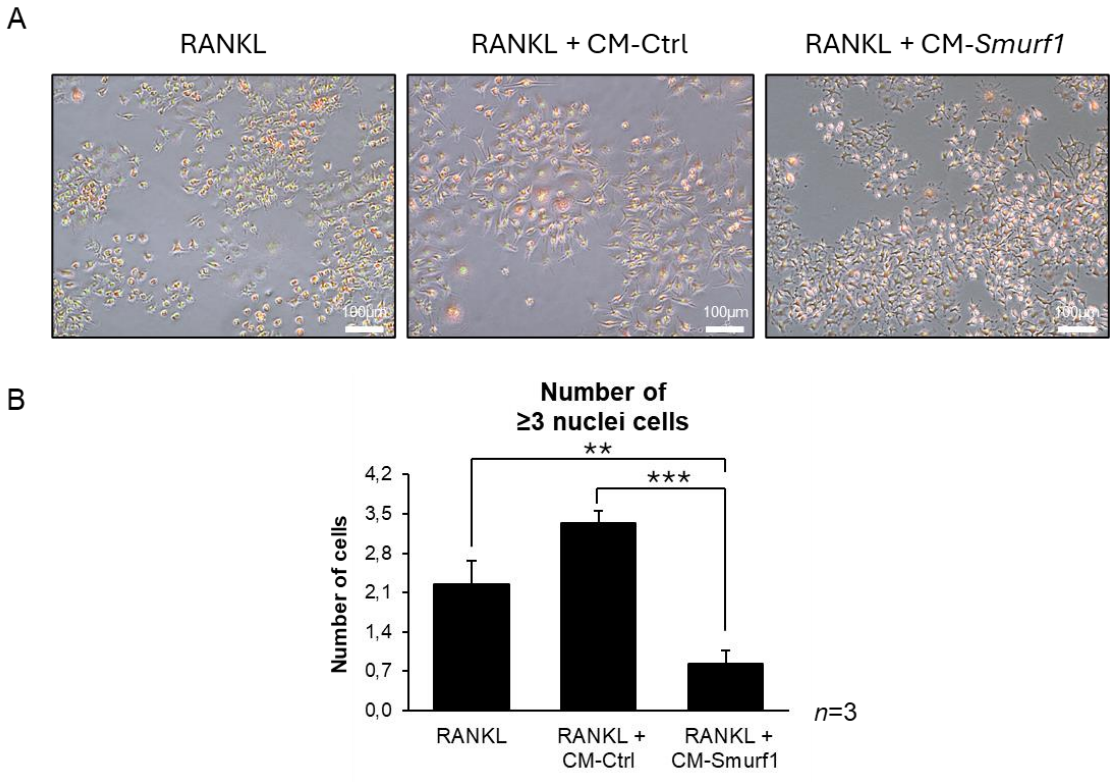

Figure 31. Effect of CM-*Smurf1* in RAW 264.1 macrophage cells line osteoclastogenesis. **(A)** Representative composite images showing nuclei and tartrate-resistant acid phosphatase (TRAP) activity after 6 days of osteoclastogenesis induction with recombinant mouse Rankl protein. Rankl is combined with CM-Ctrl or CM-Smurf1 to evaluate their impact during this process. **(B)** Number of cells counted containing 3 or more nuclei for each condition. The graphs present mean values of 4 measures from 3 independent experiments (n=3). Error bars indicate the standard error of the mean value. (**: p-value < 0.01, ***: p-value < 0.001).

DISCUSSION

5. DISCUSSION

5.1. Osteoporosis in the Present

Osteoporosis is the most prevalent chronic metabolic bone disorder, as noted by the World Health Organization (WHO). With an ageing population, osteoporosis cases are expected to double over the next two decades, affecting around 50% of women and 20% of men over 50 years old. Current treatments require personalised approaches, often involving complex therapeutic strategies to minimise long-term side effects such as atypical femoral fractures, osteonecrosis of the jaw, infections, and endocrine and cardiovascular complications. Therefore, there is an urgent need to optimise and improve therapeutic strategies to enhance clinical practice, treatment adherence, and the development of cost-effective interventions (45, 54). Our findings highlight the ongoing challenge of managing osteoporosis. The increase in cases, particularly among those over 50, calls for effective treatments that not only improve bone mineral density but also reduce the risk of fractures. This study shows potential in developing new therapeutic approaches that could better address these needs.

5.2. Mesenchymal Stem Cell Secretome as a Therapeutic Alternative

MSCs secretome therapies have gained interest due to their advantages, such as no need for engraftment, lower immunogenic risk, ease of production, safe storage, and flexibility. However, the natural secretome may not provide optimal regenerative effects, so bioengineering approaches like hypoxia, exposure to inflammatory factors, 3D culture systems, or genetic modification are being used to enhance its osteo-regenerative potential. These modifications aim to improve the therapeutic application of the MSC secretome by modulating key signalling pathways, including the bone morphogenetic proteins (BMPs) pathway (87, 204). Prior investigations conducted by our research explored this particular pathway to implement genetic alterations aimed at enhancing the osteogenic capacity of MSCs. Specifically, it was established that the transient silencing of *Smurf1*, a canonical inhibitor of the BMPs signalling pathway, in murine MSCs results in a notable augmentation of bone formation in osteoporotic subjects (69).

However, when *Smurf1* was silenced in murine MSCs *in vitro* prior to the induction of osteogenic differentiation, the pro-osteogenic effect was markedly diminished and did not correlate with the significant bone formation observed *in vivo* (205). This discrepancy between *in vivo* and *in vitro* effects suggests that paracrine signalling, rather than direct differentiation, is likely the primary mechanism behind the observed bone regeneration. Our research supports the idea that MSCs influence the bone microenvironment mainly through their secretome, enhancing the function of resident cells via the secretion of trophic factors and points to a crucial role of the paracrine mechanisms exerted by the *Smurf1*-silenced MSCs in the process of bone formation. These findings would corroborate earlier research that emphasizes that a substantial proportion of the regenerative effects attributed to MSCs arises from their capacity to enhance the functionality of tissue-resident cells via the secretion of trophic factors, rather than their intrinsic ability to differentiate into specific cell lineages (206-208).

5.3. Experimental Approaches

To further examine the osteogenic potential of the secretome or conditioned medium (CM) derived from MSCs with silenced *Smurf1*, various types of MSCs have been employed. Primary rat bone marrow MSCs (rMSCs), the murine bone marrow MSC cell line C3H10T1/2, and the human adipose-derived MSC cell line ASC52telo were used to generate CM for experiments involving rat, mouse, and human models, respectively. Despite the complexity of using different biological systems, obtaining results that point in the same direction across all these systems strengthens those findings and their biological significance, suggesting that the underlying molecular mechanisms are evolutionarily conserved.

Rat MSCs (rMSCs) were initially chosen for secretome experiments due to our group's prior expertise with these cells, while the ASC52telo cell line was specifically acquired for this project as our long-term aim is to develop a treatment intended for human application. The direct effect of *Smurf1* silencing in the C3H10T1/2 cell line was not investigated in this work since such study had previously been performed by our group (14). The decision to perform studies in the ACS52telo cell line was motivated not solely by the need to produce a human

secretome, but also by the additional advantages offered by the use of a cell line, such as easier manipulation, increased reproducibility of results and the elimination of the need to sacrifice animals for each experiment, and the potential for continuous CM production under suitable culture conditions, such as in a bioreactor (209). The characterization of ASC52telo cell line confirmed the findings reported by Wolbank et *al.* in 2009 (186). These cells meet the criteria established by the International Society for Cell and Gene Therapy (ISCT), as they adhere to plastic, can differentiate into bone, cartilage, and adipose tissue, and demonstrate positivity for the CD73, CD90, and CD105 surface markers and negative for CD34 and CD45.

After establishing the culture of rMSCs and the ASC52telo cell line and confirming the mesenchymal characteristics of the latter, we determined that the GapmeRs-mediated transient gene inhibition system was suitable for these models and effectively silenced the *Smurf1* gene. Cell morphology and viability were assessed post-inhibition, and the *Smurf1* expression levels in cells treated with specific GapmeRs were evaluated. The relative expression levels of the *Smurf1* gene were significantly lower in the murine and human cells treated with the *Smurf1*-specific GapmeR, showing over 80% silencing across both cellular types. The results showed high reproducibility, confirming the suitability of this system for generating CM from *Smurf1*-silenced MSCs. We investigated the osteogenic potential of the CM generated from MSCs, murine or human, where *Smurf1/SMURF1* gene had been silenced (rCM-*Smurf1* and hCM-*SMURF1* respectively). Various *in vitro* analyses were conducted where rMSCs and human ASC52telo cells were pre-treated with CM obtained from cells of the corresponding cell type before induction of osteogenic differentiation. Our findings clearly demonstrate that the CM from MSCs where *Smurf1*/*SMURF1* has been silenced promotes osteogenic differentiation *in vitro*, as evidenced by the significantly elevated alkaline phosphatase (Alpl) activity and mineralization in rMSCs, alongside the increased mineralization observed in the ASC52telo cells. However, except for the noted increase in *Alpl* expression in the murine model, none of the principal osteogenic markers exhibited statistically significant changes in their expression levels. One potential explanation to this effect is that the deposition of extracellular matrix components, such as collagen and

proteoglycans, could promote mineralization without directly influencing the expression of these key osteogenic markers. Extracellular matrix components like collagen and proteoglycans can enhance mineralization by altering tissue stiffness and interacting with specific receptors (210, 211). In fact, numerous studies have consistently indicated that mineralization assays, such as alizarin red staining, yield the most definitive evidence of functional osteogenesis (212, 213). Consequently, the increased mineral deposition observed after preconditioning human or murine MSCs with the corresponding CM indicates improved osteogenic differentiation in both experimental systems. The results obtained *in vivo* in the ectopic rat model reinforce the initial conclusions gathered from the *in vitro* models. The results from this experiment revealed that the new bone formation, assessed via Masson's trichrome staining, is markedly higher in rMSCs treated with rCM-*Smurf1* compared to rCM-Ctrl. The high degree of maturity of the bone formed is reflected by the presence of osteocyte in their lacunae in the scaffolds where cells pre-treated with the rCM-*Smurf1* had been seeded. The analysis of ALPL and osteocalcin (OCN) protein levels showed significant increases in rCM-*Smurf1*-treated cells, supporting the findings related to new bone formation, as these proteins serve as critical biomarkers for osteogenic activity. The results obtained with the additional controls included in this first *in vivo* experiment allowed us to verify that the ALPL and OCN expression levels were significantly higher in rCM-Ctrl condition compared to both controls, suggesting that the basic, not engineered, MSC secretome may have a baseline osteogenic effect, which could be enhanced by *Smurf1 downregulation* in these cells. This experimental setup provides a preliminary *in vivo* model to evaluate the impact of rCM-*Smurf1* in externally implanted MSCs in a controlled environment.

However, the controlled environment of the ectopic murine model differs from clinical settings, thus we needed to test the effect of the CM in a model that more closely approximates clinical application. To this end, we conducted, an experiment where primary human osteoporotic MSCs (hOP-MSCs) were subjected to treatment with hCM-*SMURF1* derived from ASC52telo cells. Although gene analyses did not reveal significant alterations in the gene expression levels of *RUNX2* or *ALPL*, the enzymatic activity of ALPL, along with

mineralization, which, as previously emphasized, constitutes the most critical parameter for osteogenic effect assessment, was significantly increased in hOP-MSCs. These results are highly important given the inherently diminished osteogenic potential of osteoporotic MSCs (185), highlighting the strong osteoinductive potential of hCM-*SMURF1*, even under pathological conditions. It is important to note that the osteogenic induction produced by hCM-*SMURF1* appears to be as effective as BMP2 in promoting bone regeneration in hOP-MSCs *in vitro*. While BMP2 is mainly used in surgical procedures for bone regeneration due to its osteoinductive properties, its ability to stimulate bone mineralization serves us as a benchmark for evaluating the functional capacity of hCM-*SMURF1* (214, 215). The results of this experiment are highly significant since it was conducted on a cohort of 23 independent female patients. This provides an in vitro model that closely mirrors clinical reality.

As previously mentioned, the use of ASC52telo in the production of the CM is critical for later translating these findings to an industrial setting. Another requirement to take this step forward is to verify the biosafety of this CM. To achieve this, hCM-*SMURF1* was subjected to further evaluations designed to clarify its effect on basic cellular functions in MSCs. Furthermore, these analyses are crucial because changes in MSCs' cell proliferation, migratory behaviour, or chemotactic potential of MSCs could significantly influence the therapy's effectiveness. The proliferation assay reveals no statistically significant variations in the proliferation of cells growing in the presence of the hCM-*SMURF1* over a nine-day exposure period. While increased cell proliferation can support tissue repair, excessive proliferation may be undesirable, as it could indicate a tendency towards tumorigenesis. In contrast, cells exposed to the CM for several days showed no discernible cytotoxic effects. Therefore, we substantiate the safety of employing hCM-*SMURF1* in therapeutic applications, potentially allowing the development of novel treatments without adverse effects on cellular health.

Additionally, migration analyses revealed that inhibiting *SMURF1* does not necessarily enhance the wound healing capacity of the CM, as no significant differences were observed compared to other CM groups. However, there is a notable and statistically significant improvement in the CM groups compared to the group that did not receive any CM. This suggests that hCM-*SMURF1* may

contribute to bone regeneration by inducing a reparative effect against mechanical impairments in MSCs.

Furthermore, the increased chemotactic responses observed in cells pre-treated with hCM-*SMURF1* indicated that this CM can attract MSCs, potentially facilitating bone regeneration at the site of administration. This ability to recruit adjacent MSCs may lead to better outcomes in *ex vivo* or *in vivo* settings compared to those achieved in the in vitro models.

In *ex vivo* models, the natural architecture of bone tissue is preserved, allowing bone cells to be studied within their microenvironment without the need for living organisms. This preservation is due to the spatial organization, extracellular matrix composition, and interactions among various cell types, such as osteoblasts, osteoclasts, and stromal cells, which more accurately replicate the *in vivo* environment compared to *in vitro* cultures of isolated bone marrow MSCs (191, 216). Our analysis of *ex vivo* human bone cultures revealed that incubation with hCM-*SMURF1* resulted in a significantly reduced *RANKL* expression, a key molecule essential for the differentiation and activation of osteoclasts. Meanwhile, the levels of osteoprotegerin (*OPG*), a decoy receptor that binds to *RANKL* and inhibits its interaction with its receptor, remained stable. This resulted in a decreased *RANKL*/*OPG* ratio, indicating diminished bone resorption, as an elevated OPG level relative to RANKL corresponds to reduced stimulation of osteoclast maturation and activity (217, 218). In this *ex vivo* system, the constant levels of *M-CSF*, an essential factor for the survival and proliferation of osteoclast precursors, suggest that the bioactive agents present in the hCM-*SMURF1* that influence *RANKL* do not disrupt the recruitment or survival of these precursors. Additionally, no substantial changes were observed in the expression levels of *BGLAP*, a marker indicative of osteoblast activity, implying that osteoblast activity remains unchanged within this model. Collectively, our findings would suggest that hCM-*SMURF1* selectively affects osteoclastogenesis without necessarily impacting other aspects of bone metabolism. These results underscore the potential of hCM-*SMURF1* as a targeted therapeutic agent for osteoporosis by inhibiting osteoclasts activity and, subsequent, bone resorption. The specificity and efficacy of hCM-*SMURF1* in diminishing *RANKL* levels

position it as a promising candidate for further *in vivo* investigations and clinical trials aimed at addressing disorders related to bone resorption.

Based on the migration and chemotaxis data suggesting that hCM-*SMURF1* may perform well *in vivo* by attracting MSCs to the sites of damage and promoting bone regeneration, we proceed to design an *in vivo* model using a calvaria bone defect. Initially, the data showed that the encapsulation system we used, which employs the double emulsion technique developed in Dr Díaz-Rodríguez's laboratory, is effective for encapsulating CM. The encapsulation efficiency exceeding 91 %, determined through direct quantification of the protein content within the CM and the microspheres, reflects a high level of success in the implementation of this methodology. Regarding therapeutic efficacy of this system, the regeneration achieved by mCM-*Smurf1* and the positive control (BMP2) showed an increasing trend compared to the negative control (Blank) and mCM-Ctrl. This enhanced bone regeneration is clearly visible in the images provided. However, although the data suggests a notable regenerative effect, the statistical analysis did not reach significance. This lack of significance could be due to the small sample size or variations in the scaffold’s composition, which are challenges associated with the manufacturing technique used.

While the bone defect model is highly useful for assessing bone regeneration, it does not accurately replicate the characteristics of osteoporotic disease. To effectively translate our findings to patients with osteoporosis, we employed an ovariectomized (OVX) murine model to simulate the pathophysiological features of osteoporosis in postmenopausal women. The in vivo evaluations, done through intraosseous injection in the femur, demonstrated that mCM-*Smurf1* significantly protects against trabecular bone loss induced by OVX. Specifically, the trabecular bone volume observed in the mCM-*Smurf1* group was significantly greater than in the non-treated and mCM-Ctrl-treated femurs, closely resembling the volume seen in the Sham group. This suggests that mCM-*Smurf1* has potential as a therapeutic intervention for osteoporosis. The importance of this experiment lies in our finding that a single administration of mCM-*Smurf1* is sufficient to prevent severe bone loss over a one-month period in mice, compared to untreated subjects and it also shows significant improvement over the CM-Ctrl group. Since the OVX model closely mimics

osteoporosis, these results suggests that the CM from MSCs where *Smurf1* has been silenced could be a viable therapy for the prevention of this disease.

Although we did not detected changes in cortical bone, this is consistent with our expectations due to the lower physiological activity of cortical bone compared to trabecular bone (219), and the short duration of the study. While our trabecular bone assessments validate the efficacy of ovariectomy, the cortical bone data did not show statistical significances between Sham and not treated groups. This suggests that an extended study might be necessary to detect changes in cortical bone density. Consequently, it is challenging to demonstrate potential positive effects of the treatment on cortical bone within the current study timeframe.

To investigate the secretome mechanisms underlying the osteogenic effects observed in various experimental models, we isolated the soluble and vesicular fractions of CM derived from ASC52telo cells in which *SMURF1* has been silenced, and subsequently examined the osteogenic effects of these fractions separately. Our findings indicate that the soluble fraction (SF) of hCM-*SMURF1* significantly increases the expression of *RUNX2*, a master regulatory gene (220), compared to the vesicular fraction (VF). Similarly, the expression of *ALPL*, encoding the alkaline phosphatase enzyme, is also significantly higher in cells treated with the SF treatment to those exposed to the VF. Despite these differences in the induction of osteogenic genes, both fractions produced comparable levels of *in vitro* mineralization. While the upregulation of osteogenic markers like *RUNX2* and *ALPL* is essential for the preliminary phases of osteoblast differentiation, mineralization encompasses a complex array of processes that necessitates not only gene expression but also the deposition of the extracellular matrix alongside subsequent mineral deposits. This process relies on the functional activities of various enzymes and matrix proteins. Consistent with current literature, extracellular vesicles (EVs) are involved in the enhancement of mineralization by providing essential components and signalling molecules that promote the deposition of mineral within the extracellular matrix, which represents a key step in bone formation (221). In summary, the VF likely promotes mineralization through mechanisms that would include the direct enhancement of mineral deposition, the provision of osteoinductive components,

and the modulation of the extracellular environment. These actions complement the early osteogenic gene expression driven by the soluble fraction, underscoring the synergistic effect of both fractions, and positioning the entire secretome as an optimal strategy for developing of osteogenic therapies.

To further understand the biological mechanisms and identify specific bioactive components responsible for the pro-osteogenic effects of the SF and VF, we conducted mass spectrometry analysis on both fractions, in the hCM-*SMURF1* compared to the hCM-Ctrl. Multiple factors were overrepresented in the SF and VF of the hCM-*SMURF1*, and the differential expression of some of them, crucial to the processes of bone formation, was confirmed by qPCR. PREPL (Prolyl Endopeptidase Like) predominantly binds collagen to basement membranes or cartilage as a matrix protein and is highly expressed in developing bones. PREPL can reduce bone loss in *in vivo* models of bone-related diseases linked to a high osteoclast activity by inhibiting osteoclastogenesis through nuclear factor-kappa β (NF-κB) signalling pathway (222, 223). FMOD (Fibromodulin) plays a significant role in fibrillogenesis and collagen cross-linking, which are essential for optimal bone formation and structural integrity. This protein is found abundantly in the extracellular matrix of mineralized tissues and has been identified in foetal chondrocytes and osteoblasts during both endochondral and intramembranous ossification (224). SPARC (Secreted Protein Acidic and Cysteine Rich) is essential for bone mineralization, as it modulates the deposition of minerals within the bone matrix. It interacts with extracellular matrix components and growth factors, enhancing the proliferation and differentiation of osteoblasts (225). Finally, CCN2 (Cellular Communication Network Factor 2) is vital for osteogenesis, since it facilitates osteoblasts differentiation and bone matrix production by engaging with pivotal signalling pathways such as TGF-β, BMPs, and Wnt. CCN2 binds to TGF-β and BMPs, amplifying their signalling and promoting bone matrix production. CCN2 is also involved in the complex signalling required for bone development (226-228). The presence of these osteogenesis-essential proteins in hCM-*SMURF1* aligns with the pro-osteogenic effects observed across multiple experimental models in this study. Additionally, the identification of these proteins in both SF and VF supports the results of the osteogenic induction experiment with the separated fractions, supporting the idea

that the development of a therapeutic approach should ideally incorporate the entire secretome rather than any of its isolated fractions. Consistent with the idea of using the complete secretome as a therapy, we conducted a gene ontology (GO) analysis of proteins that are differentially represented in the hCM-Ctrl and hCM-*SMURF1* samples. The analysis identified GO terms enriched in the hCM-*SMURF1* proteins related to regenerative processes, such as “regulation of cell morphogenesis” or “post-transcriptional regulation of gene expression” in the SF, and “extracellular matrix organization” or “ossification” in the VF. These findings further support our hypothesis regarding the efficacy of the whole secretome.

Given that the aim of this work was to develop a treatment targeting bone tissue, it was expected that this approach would not exclusively impact the resident MSCs but also elicit responses from various cellular components of the bone microenvironment. Due to the complex interactions among bone cells that are essential for maintaining homeostasis and regulating bone remodelling, it was crucial to evaluate the effects of CM-*Smurf1* on osteocytes and osteoclasts. Osteocytes represent approximately 95% of the bone tissue, so it was important to ensure that CM-*Smurf1* did not have cytotoxic effects on these cells. The results demonstrated not only the absence of cytotoxicity, but also suggested that mCM-*Smurf1* promotes an environment leading to the increase of bone mass. This was evidenced by a reduction in the *Rankl*/*Opg* ratio, indicating decreased osteoclastogenesis, as well as a decrease in the expression of other negative regulators of bone mass such as *Sost* and *Dkk1*, which inhibit osteoblast function, and *M-csf*, which induces osteoclastogenesis (12, 15).

Furthermore, the osteoclastogenesis induction experiment in RAW 264.7 cells supported these findings, showing a reduced formation of multinucleated cells when osteoclast induction occurred in the presence of mCM-*Smurf1*. Both sets of align, suggesting that at least part of the effect observed in the calvaria bone defect and intraosseous injection in osteoporotic models can be attributed to a decrease in osteoclast formation. This “collateral” effect of CM-*Smurf1* on cells within the bone microenvironment, complements the enhancement of bone formation induced on MSCs, as demonstrated in the *in vitro* experiments. Together, these effects result in a therapeutically comprehensive and safe approach from a biological perspective.

Overall, we conclude that the CM of MSCs where *Smurf1*/*SMURF1* has been silenced can enhance the osteogenic potential of MSCs, even when their osteogenic capacity is diminished, as seen in MSCs derived from patients with osteoporosis. Additionally, this CM promotes chemotactic and migratory responses in MSCs, thereby improving its regenerative efficacy. These effects on MSCs are further complemented by the induction of a pro-osteogenic profile in cells within the bone microenvironment, including osteocytes and osteoclasts, which collectively contribute to bone regeneration by reducing osteoclastogenesis. This dual mechanism makes this CM a highly promising therapeutic option for managing osteoporosis. Indeed, our findings show that a single administration of CM-*Smurf1* significantly alleviate the bone degeneration linked to a decrease in oestrogen levels. These effects are further supported by the enrichment of proteins essential for osteogenesis. The absence of cytotoxic effects observed throughout this study places the secretome of MSCs with silenced *SMURF1* expression as a viable alternative to existing pharmacological therapies for osteoporosis.

5.4. Future Perspectives and Limitations

5.4.1. Use of CM-*SMURF1* Clinical Practice

Current methodologies for addressing osteoporosis are complex, involving a wide range of pharmacological agents that come with various side effects. Some of these adverse effects, although infrequent, can be severe. Consequently, the administration of these medications requires stringent decision-making protocols and long-term patient follow-up to ensure that the therapeutic regimen maintains a favourable benefit-risk balance (229). Additionally, the lack of systematic screening protocols for osteoporosis results in the condition remaining undetected until a fracture occurs, at which point the patient's quality of life and/or physical self-dependence may be significantly compromised.

In contrast, the therapy we propose, based on the secretome of MSCs with silenced *SMURF1* gene expression, offers a potentially safer treatment. This therapy provides the benefits of a dual-action approach, similar to

Romosozumab, but, presumably, without the potential adverse effects on the endocrine and cardiovascular systems of this treatment (230). We suggest that, in clinical practice, the favourable safety profile of this therapeutic modality would make it suitable for use as a preventive intervention. Our experimental model for post-menopausal osteoporosis demonstrates that it effectively protects bone architecture under this pathological set up.

Implementing this therapy in clinical settings would require incorporating of bone turnover markers (BTMs), such as serum C-telopeptide cross-link type I collagen (CTX) or procollagen type I N-terminal pro-peptide (PINP), into the recommended monitoring of risk factors on all recent menopausal women, as stated by Asociación Española para el Estudio de la Menopausia (AEEM) (231). While the use of these biomarkers as predictors of bone mass is not generally recommended, empirical studies suggest their utility in the early identification of women who may exhibit a heightened rate of bone loss in the subsequent years following the onset of menopause (232-234). Additionally, elevated BTMs have been correlated with a higher risk of fractures (233), facilitating early intervention within the firsts 2-7 years post-menopause. The use of these markers should be complemented by other assessments, including additional biomarkers and bone mineral density (BMD) evaluation. One diagnostic approach for osteoporosis, prior to the occurrence of a fracture, involves the utilization of the T-score, which compares a patient's BMD to that of a young, healthy reference population. A T-score below -2.5 is classified as osteoporotic, while a T-score ranging from -1 to -2.5 indicates that the patient is osteopenic. Women in this latter category specially those with increased BTMs and other risk factors, may be suitable candidates for this novel therapeutic intervention, thereby reducing the probability of reaching more reduced T-scores or even fractures.

While we do not rule out the potential for this treatment to repair osteoporotic bones, i.e. serving as an osteosynthesis treatment, this hypothesis requires further experimental validation. To explore this possibility, an intraosseous injection model similar to our current design would need to be implemented, where CM is administered one month post-ovariectomy, once the pathological state is well established.

5.4.2. Feasibility of Developing the Treatment

The development of new therapies based on artificial or engineered tissues, cells or their derivatives has been in the spotlight in recent years. These therapies are classified as Advanced Therapy Medicinal Products (ATMPs) and are considerably more complex than conventional medicines. As a result, production and regulatory approval processes by authorities such as the European Medicines Agency (EMA) are considerably more challenging, often resulting in higher costs. The feasibility of making our therapy accessible to the broader population depends on the economically viable production of the secretome. To achieve this, we propose the utilization of immortalized mesenchymal stem cell (iMSCs) lines which can facilitate prolonged culture periods without undergoing senescence. These iMSCs, with permanent inhibition of the *SMURF1* gene, would be cultivated in bioreactors designed for the continuous collection of conditioned medium while providing the necessary oxygen and nutrients to maintain cell viability and productivity. Notably, this year, García et al. (209) published findings indicating the feasibility of this approach. They successfully isolated conditioned medium from iMSCs for a duration of up to four weeks without compromising cellular phenotype, and additionally developed a system for the specific isolation of extracellular vesicles. Therefore, the latest advancements in bioreactor technology, standardization protocols, and modifications in regulatory frameworks will facilitate the economical large-scale production of the secretome-based therapies.

Furthermore, the recent authorization granted to the Basque company Histocell Regenerative Medicine, specialised in the development, scale-up and Good Manufacturing Practice (GMP) manufacturing of products based on MSCs, by the Agencia Española de Medicamentos y Productos Sanitarios (AEMPS) to produce MSC secretomes and exosomes products underscores the significant role of MSC secretome in developing innovative therapies (235).

The optimization and subsequent cost-reduction associated with secretome production are also correlated with potential savings for the healthcare system In Spain alone, the healthcare system allocated €4.2 billion to osteoporotic patients in 2017, with projections indicating an increase of over 30%

within 15 years. These estimates do not account for indirect costs such as work absenteeism and caregivers burdens due to patients' reduced mobility and daily activity limitations (47). Thus, preventive treatments using our therapeutic approach would present a financially advantageous alternative.

5.4.3. Administration Method

In the preliminary *in vivo* osteoporotic model performed in this work, we assayed a local injection of the secretome. The reason was trying to diminish any possible cytotoxic effects that may arise in systemic administration, as well as enhance the concentration of secretome factors within bone tissue. This administration method showed effectiveness and no apparent adverse effects. However, in pursuit a refinement in the application of this therapy, we propose that a targeted delivery of the secretome could be employed in order to achieve active osteotropism, with higher concentrations in bone tissue, prolonged localized release, and reduced minimal effective doses.

While designing targeted therapies for bone tissue is more challenging than other tissues due to limited vascularization, and complex remodelling and homeostatic regulation mechanism, our group had previous expertise implementing such approaches. In a work recently published (236), we encapsulated GapmeRs specifically designed to inhibit the gene encoding Secreted Frizzled-related Protein 1 (*Sfrp1*), an inhibitor of the osteogenic Wnt/β-catenin signalling pathway, in nanoparticles that were targeted to MSCs using specific aptamers. The systemic administration of the GapmeR-nanoparticle-aptamer complex yielded a four-fold enhancement in the accumulation of released GapmeR in bone tissue, while concurrently decreasing hepatic accumulation by ten-fold. The outcomes of the study indicated an increase in trabecular and cortical bone thickness in ovariectomized mice, without presenting any toxic effects.

In the study of the calvaria bone defect model, we have shown that it is possible to encapsulate the conditioned media within nanoparticles, which could similarly be targeted to bone tissue. Given that, based on our results, the secretome would exert beneficial effects on MSCs as well as osteocytes and osteoclasts, the therapy will not be restricted to a specific cell type, but rather

directed towards the bone matrix, thereby influencing the whole microenvironment. There are molecules such as bisphosphonates (and their analogues), phytic acid, tetracycline, acidic oligopeptides (consisting of aspartic acid or glutamic acid) or aspartate-serine-serine (DSS) peptides that can recognize and bind specifically to hydroxiapatite crystals, the major inorganic component in bone matrix (237). In principle, any of these molecules can be used as ligands for the design of targeted therapies, as it has been demonstrated in numerous preclinical studies. The selection of one molecule over another would depend on which of them provides better characteristic for secretome-based therapies in terms of drug release, bone distribution, binding rate, strength, circulation time, long term side effects or excretion. Regardless, there are reasons to consider that the development of a safe and cost-effective *SMURF1*-silenced MSC secretome-based therapy for osteoporosis could be achieved.

CONCLUSIONS

6. CONCLUSIONS

1. The use of specific GapmeRs for *Smurf1/SMURF1* BMP signalling pathway inhibitor significantly reduces the expression of this gene.
2. The transient silencing of *Smurf1/SMURF1* in mesenchymal stem cells (MSCs) induces the synthesis of a collection of factors, referred to as secretome or conditioned medium (CM-*Smurf1*/CM-*SMURF1*), which enhances the osteogenic potential of both healthy murine and human MSCs *in vitro*.
3. hCM-*SMURF1* increases the osteogenic capacity of MSCs from osteoporotic patients *in vitro*, reaching osteogenic values similar to those obtained with the pro-osteogenic molecule BMP2.
4. While hCM-*SMURF1* does not compromise the viability or proliferative ability of MSCs, it does promote their migratory capacity and exerts a chemotactic influence on these cells.
5. In a murine *in vivo* context, rCM-*Smurf1* similarly enhances the osteogenic potential of MSCs as it was evidenced *in vitro*.
6. mCM-*Smurf1* shows efficacy in diminishing trabecular bone loss associated with ovariectomy in murine models.
7. Both the soluble and vesicular fractions of hCM-*SMURF1* contribute synergistically to the augmentation of the osteogenic potential of MSCs *in vitro*.
8. In both the soluble and vesicular fractions of hCM-*SMURF1*, we observed a significant enrichment of proteins that are notably implicated in osteogenic activity.
9. The study of the impact of CM-*Smurf1*/CM-*SMURF1* on cells within the bone microenvironment, conducted through both *ex vivo* bone experiments and directly with osteocytes and osteoclasts *in vitro*, reveals that it promotes a pro-osteogenic profile by inhibiting osteoclastogenesis.

REFERENCES

7. REFERENCES

1. Le BQ, Nurcombe V, Cool SM, van Blitterswijk CA, de Boer J, LaPointe VLS. The Components of Bone and What They Can Teach Us about Regeneration. Materials (Basel). 2017;11(1).
2. Walker J. Skeletal system 1: the anatomy and physiology of bones. Nursing Times. 2020;116(2):38-42.
3. Boskey AL. Mineralization of Bones and Teeth. Elements. 2007;3(6):385-91.
4. Brett E, Flacco J, Blackshear C, Longaker MT, Wan DC. Biomimetics of Bone Implants: The Regenerative Road. Biores Open Access. 2017;6(1):1-6.
5. Bartl R, Bartl C. Structure and Architecture of Bone. Bone Disorders 2017. p. 11-20.
6. Burr DB. Bone Morphology and Organization. Basic and Applied Bone Biology 2019. p. 3-26.
7. Gasser JA, Kneissel M. Bone Physiology and Biology. Bone Toxicology. Molecular and Integrative Toxicology. 2017. p. 27-94.
8. Canelon SP, Wallace JM. beta-Aminopropionitrile-Induced Reduction in Enzymatic Crosslinking Causes In Vitro Changes in Collagen Morphology and Molecular Composition. PLoS One. 2016;11(11):e0166392.
9. Nahian A, Chauhan PR. Histology, Periosteum And Endosteum. StatPearls Publising. 2023;Online.
10. Guillerman RP. Marrow: red, yellow and bad. Pediatr Radiol. 2013;43 Suppl 1:S181-92.
11. Gurevitch O, Slavin S, Resnick I, Khitrin S, Feldman A. Mesenchymal Progenitor Cells in Red and Yellow Bone Marrow. Folia Biologica. 2009;55:27-34.
12. Bellido T, Plotkin LI, Bruzzaniti A. Bone Cells. Basic and Applied Bone Biology 2019. p. 37-55.
13. Raggatt LJ, Partridge NC. Cellular and Molecular Mechanisms of Bone Remodeling. Journal of Biological Chemistry. 2010;285(33):25103-8.
14. García-Sánchez D. Specific gampers system assay with osteogenic effect as a therapy for the treatment of osteoporosis. Santander: Universidad de Cantabria; 2023.
15. Delgado-Calle J, Bellido T. The osteocyte as a signaling cell. Physiol Rev. 2022;102(1):379-410.
16. Plotkin LI, Aguilar-Pérez A, Bivi N. Local Regulation of Bone Cell Function. Basic and Applied Bone Biology2019. p. 57-84.
17. Ikebuchi Y, Aoki S, Honma M, Hayashi M, Sugamori Y, Khan M, et al. Coupling of bone resorption and formation by RANKL reverse signalling. Nature. 2018;561(7722):195-200.
18. Kim JM, Lin C, Stavre Z, Greenblatt MB, Shim JH. Osteoblast-Osteoclast Communication and Bone Homeostasis. Cells. 2020;9(9).
19. Allen MR, Burr DB. Bone Growth, Modeling, and Remodeling. Basic and Applied Bone Biology2019. p. 85-100.
20. Ding DC, Shyu WC, Lin SZ. Mesenchymal stem cells. Cell Transplant. 2011;20(1):5-14.
21. Caplan AI. Mesenchymal stem cells. J Orthop Res. 1991;9(5):641-50.
22. Dominici M, Le Blanc K, Mueller I, Slaper-Cortenbach I, Marini F, Krause D, et al. Minimal criteria for defining multipotent mesenchymal stromal cells. The International Society for Cellular Therapy position statement. Cytotherapy. 2006;8(4):315-7.
23. Han Y, Li X, Zhang Y, Han Y, Chang F, Ding J. Mesenchymal Stem Cells for Regenerative Medicine. Cells. 2019;8(8).
24. Naji A, Eitoku M, Favier B, Deschaseaux F, Rouas-Freiss N, Suganuma N. Biological functions of mesenchymal stem cells and clinical implications. Cell Mol Life Sci. 2019;76(17):3323-48.

25. Samsonraj RM, Raghunath M, Nurcombe V, Hui JH, van Wijnen AJ, Cool SM. Concise Review: Multifaceted Characterization of Human Mesenchymal Stem Cells for Use in Regenerative Medicine. Stem Cells Transl Med. 2017;6(12):2173-85.
26. PubMed [Internet]. [cited 2024].
27. Oishi T, Koizumi S, Kurozumi K. Mesenchymal stem cells as therapeutic vehicles for glioma. Cancer Gene Ther. 2024.
28. Hu BY, Xin M, Chen M, Yu P, Zeng LZ. Mesenchymal stem cells for repairing glaucomatous optic nerve. Int J Ophthalmol. 2024;17(4):748-60.
29. Li C SY, Xu W, Chang F, Wang Y, Ding J. Mesenchymal Stem Cells-Involved Strategies for Rheumatoid Arthritis Therapy. Adv Sci (Weinh). 2024.
30. Zheng Z, Liu H, Liu S, Luo E, Liu X. Mesenchymal stem cells in craniofacial reconstruction: a comprehensive review. Front Mol Biosci. 2024;11:1362338.
31. Nejabati HR NS, Roshangar L. Therapeutic Potential of Mesenchymal Stem Cells in PCOS. Curr Stem Cell Res Ther. 2024;19(2):134-44.
32. Cui M, Chen F, Shao L, Wei C, Zhang W, Sun W, et al. Mesenchymal stem cells and ferroptosis: Clinical opportunities and challenges. Heliyon. 2024;10(3):e25251.
33. Xu H, Wang B, Li A, Wen J, Su H, Qin D. Mesenchymal Stem Cells-based Cell-free Therapy Targeting Neuroinflammation. Aging Dis. 2024;15(3):965-76.
34. Hou XY, Danzeng LM, Wu YL, Ma QH, Yu Z, Li MY, et al. Mesenchymal stem cells and their derived exosomes for the treatment of COVID-19. World J Stem Cells. 2024;16(4):353-74.
35. Yang Z PY, Yuan J, Xia H, Luo L, Wu X. Mesenchymal Stem Cells: A Promising Treatment for Thymic Involution. Adv Exp Med Biol. 2024;1450:29-38.
36. Ma C CM, Wu Y, Xu X. The Role of Mesenchymal Stem Cells in Hair Regeneration and Hair Cycle. Stem Cells Dev. 2024;33(1-2):1-10.
37. Pratiwi DIN, Alhajlah S, Alawadi A, Hjazi A, Alawsi T, Almalki SG, et al. Mesenchymal stem cells and their extracellular vesicles as emerging therapeutic tools in the treatment of ischemic stroke. Tissue Cell. 2024;87:102320.
38. ClinicalTrials.gov [Internet]. 2024.
39. Maldonado VV, Patel NH, Smith EE, Barnes CL, Gustafson MP, Rao RR, et al. Clinical utility of mesenchymal stem/stromal cells in regenerative medicine and cellular therapy. J Biol Eng. 2023;17(1):44.
40. Friedenstein AJ, Chailakhyan RK, Latsinik NV, Panasyuk AF, Keiliss-Borok IV. Stromal cell responsible for transferring the microenvironment of the hemopoietic tissues. Transplantation. 1974;17(4):331-40.
41. Owen M, Friendenstein A. Stromal stem cells: marrow-derived osteogenic precursors. Cell and molecular biology of vertebrate hard tissues. 1988;136:42-60.
42. Shu DY, Lovicu FJ. Insights into Bone Morphogenetic Protein-(BMP-) Signaling in Ocular Lens Biology and Pathology. Cells. 2021;10(10).
43. Chen G, Deng C, Li YP. TGF-beta and BMP signaling in osteoblast differentiation and bone formation. Int J Biol Sci. 2012;8(2):272-88.
44. Coughlan T, Dockery F. Osteoporosis and fracture risk in older people. Clinical Medicine. 2014;14(2):187-91.
45. Sozen T, Ozisik L, Basaran NC. An overview and management of osteoporosis. Eur J Rheumatol. 2017;4(1):46-56.
46. Etxebarria-Foronda I, Caeiro-Rey JR, Larrainzar-Garijo R, Vaquero-Cervino E, Roca-Ruiz L, Mesa-Ramos M, et al. [SECOT-GEIOS guidelines in osteoporosis and fragility fracture. An update]. Rev Esp Cir Ortop Traumatol. 2015;59(6):373-93.
47. International Osteoporosis Foundation https://www.osteoporosis.foundation/ 2024 [
48. van der Eerden BC, Teti A, Zambuzzi WF. Bone, a dynamic and integrating tissue. Arch Biochem Biophys. 2014;561:1-2.
49. Langdahl BL. Overview of treatment approaches to osteoporosis. Br J Pharmacol. 2021;178(9):1891-906.

50. Appelman-Dijkstra NM, Papapoulos SE. Modulating Bone Resorption and Bone Formation in Opposite Directions in the Treatment of Postmenopausal Osteoporosis. Drugs. 2015;75(10):1049-58.
51. Noh JY, Yang Y, Jung H. Molecular Mechanisms and Emerging Therapeutics for Osteoporosis. Int J Mol Sci. 2020;21(20).
52. Paspaliaris V, Kolios G. Stem cells in Osteoporosis: From Biology to New Therapeutic Approaches. Stem Cells Int. 2019;2019:1730978.
53. Hu L, Yin C, Zhao F, Ali A, Ma J, Qian A. Mesenchymal Stem Cells: Cell Fate Decision to Osteoblast or Adipocyte and Application in Osteoporosis Treatment. Int J Mol Sci. 2018;19(2).
54. Compston JE, McClung MR, Leslie WD. Osteoporosis. Lancet. 2019;393(10169):364-76.
55. Singh S, Dutta S, Khasbage S, Kumar T, Sachin J, Sharma J, et al. A systematic review and meta-analysis of efficacy and safety of Romosozumab in postmenopausal osteoporosis. Osteoporos Int. 2022;33(1):1-12.
56. Lim SY, Bolster MB. Profile of romosozumab and its potential in the management of osteoporosis. Drug Des Devel Ther. 2017;11:1221-31.
57. Wang Z, James Goh, De SD, Ge Z, Ouyang H, Chong JSW, et al. Efficacy of Bone Marrow–Derived Stem Cells in Strengthening Osteoporotic Bone in a Rabbit Model. Tissue Engineering. 2006;12(7):1753-61.
58. Ichioka N, Inaba M, Kushida T, Esumi T, Takahara K, Inaba K, et al. Prevention of Senile Osteoporosis in SAMP6 Mice by Intrabone Marrow Injection of Allogeneic Bone Marrow Cells. Stem Cells. 2002;20:542-51.
59. Ocarino Nde M, Boeloni JN, Jorgetti V, Gomes DA, Goes AM, Serakides R. Intra-bone marrow injection of mesenchymal stem cells improves the femur bone mass of osteoporotic female rats. Connect Tissue Res. 2010;51(6):426-33.
60. Sui B, Hu C, Zhang X, Zhao P, He T, Zhou C, et al. Allogeneic Mesenchymal Stem Cell Therapy Promotes Osteoblastogenesis and Prevents Glucocorticoid-Induced Osteoporosis. Stem Cells Transl Med. 2016;5(9):1238-46.
61. Kiernan J, Hu S, Grynpas MD, Davies JE, Stanford WL. Systemic Mesenchymal Stromal Cell Transplantation Prevents Functional Bone Loss in a Mouse Model of Age-Related Osteoporosis. Stem Cells Transl Med. 2016;5(5):683-93.
62. Cho SW, Sun HJ, Yang JY, Jung JY, Choi HJ, An JH, et al. Human adipose tissue-derived stromal cell therapy prevents bone loss in ovariectomized nude mouse. Tissue Eng Part A. 2012;18(9-10):1067-78.
63. Mirsaidi A, Genelin K, Vetsch JR, Stanger S, Theiss F, Lindtner RA, et al. Therapeutic potential of adipose-derived stromal cells in age-related osteoporosis. Biomaterials. 2014;35(26):7326-35.
64. Aggarwal R, Pompili VJ, Das H. Generation of osteoporosis in immune-compromised mice for stem cell therapy. Methods Mol Biol. 2014;1213:209-14.
65. Lien CY, Chih-Yuan Ho K, Lee OK, Blunn GW, Su Y. Restoration of bone mass and strength in glucocorticoid-treated mice by systemic transplantation of CXCR4 and cbfa-1 co-expressing mesenchymal stem cells. J Bone Miner Res. 2009;24(5):837-48.
66. You L, Pan L, Chen L, Chen JY, Zhang X, Lv Z, et al. Suppression of zinc finger protein 467 alleviates osteoporosis through promoting differentiation of adipose derived stem cells to osteoblasts. J Transl Med. 2012;10:11.
67. Stamnitz S, Klimczak A. Mesenchymal Stem Cells, Bioactive Factors, and Scaffolds in Bone Repair: From Research Perspectives to Clinical Practice. Cells. 2021;10(8).
68. Jiang Y, Zhang P, Zhang X, Lv L, Zhou Y. Advances in mesenchymal stem cell transplantation for the treatment of osteoporosis. Cell Prolif. 2021;54(1):e12956.
69. Garcia-Garcia P, Ruiz M, Reyes R, Delgado A, Evora C, Riancho JA, et al. *Smurf1* Silencing Using a LNA-ASOs/Lipid Nanoparticle System to Promote Bone Regeneration. Stem Cells Transl Med. 2019;8(12):1306-17.

70. Centro de Información de la Agencia Española de Medicamentos y Productos Sanitarios. Ministerio de Sanidad. Gobierno de España https://cima.aemps.es/ 2024 [
71. Saxer F, Scherberich A, Todorov A, Studer P, Miot S, Schreiner S, et al. Implantation of Stromal Vascular Fraction Progenitors at Bone Fracture Sites: From a Rat Model to a First-in-Man Study. Stem Cells. 2016;34(12):2956-66.
72. Baglio SR, Pegtel DM, Baldini N. Mesenchymal stem cell secreted vesicles provide novel opportunities in (stem) cell-free therapy. Front Physiol. 2012;3:359.
73. Barkholt L, Flory E, Jekerle V, Lucas-Samuel S, Ahnert P, Bisset L, et al. Risk of tumorigenicity in mesenchymal stromal cell-based therapies--bridging scientific observations and regulatory viewpoints. Cytotherapy. 2013;15(7):753-9.
74. Russo FP, Alison MR, Bigger BW, Amofah E, Florou A, Amin F, et al. The bone marrow functionally contributes to liver fibrosis. Gastroenterology. 2006;130(6):1807-21.
75. Fischer UM, Harting MT, Jimenez F, Monzon-Posadas WO, Xue H, Savitz SI, et al. Pulmonary passage is a major obstacle for intravenous stem cell delivery: the pulmonary first-pass effect. Stem Cells Dev. 2009;18(5):683-92.
76. Chang C, Yan J, Yao Z, Zhang C, Li X, Mao HQ. Effects of Mesenchymal Stem Cell-Derived Paracrine Signals and Their Delivery Strategies. Adv Healthc Mater. 2021;10(7):e2001689.
77. Gonzalez-Gonzalez A, Garcia-Sanchez D, Dotta M, Rodriguez-Rey JC, Perez-Campo FM. Mesenchymal stem cells secretome: The cornerstone of cell-free regenerative medicine. World J Stem Cells. 2020;12(12):1529-52.
78. Vizoso FJ, Eiro N, Cid S, Schneider J, Perez-Fernandez R. Mesenchymal Stem Cell Secretome: Toward Cell-Free Therapeutic Strategies in Regenerative Medicine. Int J Mol Sci. 2017;18(9).
79. Gnecchi M, He H, Liang OD, Melo LG, Morello F, Mu H, et al. Paracrine action accounts for marked protection of ischemic heart by Akt-modified mesenchymal stem cells. Nature Medicina. 2005;11(4):367-8.
80. Psaltis PJ, Zannettino AC, Worthley SG, Gronthos S. Concise review: mesenchymal stromal cells: potential for cardiovascular repair. Stem Cells. 2008;26(9):2201-10.
81. Zhao Q, Ren H, Zhu D, Han Z. Stem/progenitor cells in liver injury repair and regeneration. Biol Cell. 2009;101(10):557-71.
82. Bussolati B, Tetta C, Camussi G. Contribution of stem cells to kidney repair. Am J Nephrol. 2008;28(5):813-22.
83. Oh JY, Kim MK, Shin MS, Lee HJ, Ko JH, Wee WR, et al. The anti-inflammatory and anti-angiogenic role of mesenchymal stem cells in corneal wound healing following chemical injury. Stem Cells. 2008;26(4):1047-55.
84. Chimenti I, Smith RR, Li TS, Gerstenblith G, Messina E, Giacomello A, et al. Relative roles of direct regeneration versus paracrine effects of human cardiosphere-derived cells transplanted into infarcted mice. Circ Res. 2010;106(5):971-80.
85. Teixeira FG, Salgado AJ. Mesenchymal stem cells secretome: current trends and future challenges. Neural Regen Res. 2020;15(1):75-7.
86. Fuentes P, Torres MJ, Arancibia R, Aulestia F, Vergara M, Carrion F, et al. Dynamic Culture of Mesenchymal Stromal/Stem Cell Spheroids and Secretion of Paracrine Factors. Front Bioeng Biotechnol. 2022;10:916229.
87. González-González A, García-Sánchez D, Alfonso-Fernández A, Haider KH, Rodríguez-Rey JC, Pérez-Campo FM. Regenerative Medicine Applied to the Treatment of Musculoskeletal Pathologies. Handbook of Stem Cell Therapy2022. p. 1-36.
88. L. PK, Kandoi S, Misra R, S V, K.c R, Verma RS. The mesenchymal stem cell secretome: A new paradigm towards cell-free therapeutic mode in regenerative medicine. Cytokine Growth Factor Rev. 2019;46:1-9.
89. Gao F, Chiu SM, Motan DA, Zhang Z, Chen L, Ji HL, et al. Mesenchymal stem cells and immunomodulation: current status and future prospects. Cell Death Dis. 2016;7(1):e2062.

90. Li W, Zhang Q, Wang M, Wu H, Mao F, Zhang B, et al. Macrophages are involved in the protective role of human umbilical cord-derived stromal cells in renal ischemia-reperfusion injury. Stem Cell Res. 2013;10(3):405-16.
91. Xu G, Zhang Y, Zhang L, Ren G, Shi Y. The role of IL-6 in inhibition of lymphocyte apoptosis by mesenchymal stem cells. Biochem Biophys Res Commun. 2007;361(3):745-50.
92. Zhang ZH, Zhu W, Ren HZ, Zhao X, Wang S, Ma HC, et al. Mesenchymal stem cells increase expression of heme oxygenase-1 leading to anti-inflammatory activity in treatment of acute liver failure. Stem Cell Res Ther. 2017;8(1):70.
93. Osugi M, Katagiri W, Yoshimi R, Inukai T, Hibi H, Ueda M. Conditioned media from mesenchymal stem cells enhanced bone regeneration in rat calvarial bone defects. Tissue Eng Part A. 2012;18(13-14):1479-89.
94. Ogata K, Matsumura M, Moriyama M, Katagiri W, Hibi H, Nakamura S. Cytokine Mixtures Mimicking Secretomes From Mesenchymal Stem Cells Improve Medication-Related Osteonecrosis of the Jaw in a Rat Model. JBMR Plus. 2018;2(2):69-80.
95. Welsh JA, Goberdhan DCI, O'Driscoll L, Buzas EI, Blenkiron C, Bussolati B, et al. Minimal information for studies of extracellular vesicles (MISEV2023): From basic to advanced approaches. J Extracell Vesicles. 2024;13(2):e12404.
96. Crescitelli R, Lasser C, Szabo TG, Kittel A, Eldh M, Dianzani I, et al. Distinct RNA profiles in subpopulations of extracellular vesicles: apoptotic bodies, microvesicles and exosomes. J Extracell Vesicles. 2013;2.
97. Thery C, Witwer KW, Aikawa E, Alcaraz MJ, Anderson JD, Andriantsitohaina R, et al. Minimal information for studies of extracellular vesicles 2018 (MISEV2018): a position statement of the International Society for Extracellular Vesicles and update of the MISEV2014 guidelines. J Extracell Vesicles. 2018;7(1):1535750.
98. Lai RC, Arslan F, Lee MM, Sze NS, Choo A, Chen TS, et al. Exosome secreted by MSC reduces myocardial ischemia/reperfusion injury. Stem Cell Res. 2010;4(3):214-22.
99. ExoCarta. exocarta.org 2024.
100. Munshi A, Mehic J, Creskey M, Gobin J, Gao J, Rigg E, et al. A comprehensive proteomics profiling identifies NRP1 as a novel identity marker of human bone marrow mesenchymal stromal cell-derived small extracellular vesicles. Stem Cell Res Ther. 2019;10(1):401.
101. Katagiri W, Kawai T, Osugi M, Sugimura-Wakayama Y, Sakaguchi K, Kojima T, et al. Angiogenesis in newly regenerated bone by secretomes of human mesenchymal stem cells. Maxillofac Plast Reconstr Surg. 2017;39(1):8.
102. UniProt. uniprot.org: National Institutes of Health EMBL-EBI; 2024.
103. Hade MD, Suire CN, Suo Z. Mesenchymal Stem Cell-Derived Exosomes: Applications in Regenerative Medicine. Cells. 2021;10(8).
104. Yang Z, Zhang W, Ren X, Tu C, Li Z. Exosomes: A Friend or Foe for Osteoporotic Fracture? Front Endocrinol (Lausanne). 2021;12:679914.
105. Lu TX, Rothenberg ME. MicroRNA. J Allergy Clin Immunol. 2018;141(4):1202-7.
106. Ando Y, Matsubara K, Ishikawa J, Fujio M, Shohara R, Hibi H, et al. Stem cell-conditioned medium accelerates distraction osteogenesis through multiple regenerative mechanisms. Bone. 2014;61:82-90.
107. Liu X, Zhou C, Li Y, Ji Y, Xu G, Wang X, et al. SDF-1 promotes endochondral bone repair during fracture healing at the traumatic brain injury condition. PLoS One. 2013;8(1):e54077.
108. Sfeir C, Ho L, Doll BA, Azari K, Hollinger JO. Fracture repair. In: Inc. HP, editor. Bone regeneration and repair: Biology and clinical applications. Totowa, NJ2007.
109. Mori S, Hatori N, Kawaguchi N, Hamada Y, Shih TC, Wu CY, et al. The integrin-binding defective FGF2 mutants potently suppress FGF2 signalling and angiogenesis. Biosci Rep. 2017;37(2).

110. Song R, Wang D, Zeng R, Wang J. Synergistic effects of fibroblast growth factor-2 and bone morphogenetic protein-2 on bone induction. Mol Med Rep. 2017;16(4):4483-92.
111. Haumer A, Bourgine PE, Occhetta P, Born G, Tasso R, Martin I. Delivery of cellular factors to regulate bone healing. Adv Drug Deliv Rev. 2018;129:285-94.
112. Takeuchi R, Katagiri W, Endo S, Kobayashi T. Exosomes from conditioned media of bone marrow-derived mesenchymal stem cells promote bone regeneration by enhancing angiogenesis. PLoS One. 2019;14(11):e0225472.
113. Katagiri W, Watanabe J, Toyama N, Osugi M, Sakaguchi K, Hibi H. Clinical Study of Bone Regeneration by Conditioned Medium From Mesenchymal Stem Cells After Maxillary Sinus Floor Elevation. Implant Dent. 2017;26(4):607-12.
114. Li J, Dong J, Zhang ZH, Zhang DC, You XY, Zhong Y, et al. miR-10a restores human mesenchymal stem cell differentiation by repressing KLF4. J Cell Physiol. 2013;228(12):2324-36.
115. Zhang F, Jing S, Ren T, Lin J. MicroRNA-10b promotes the migration of mouse bone marrow-derived mesenchymal stem cells and downregulates the expression of E-cadherin. Mol Med Rep. 2013;8(4):1084-8.
116. Wang J, Liu S, Li J, Zhao S, Yi Z. Roles for miRNAs in osteogenic differentiation of bone marrow mesenchymal stem cells. Stem Cell Res Ther. 2019;10(1):197.
117. Hassan MQ, Maeda Y, Taipaleenmaki H, Zhang W, Jafferji M, Gordon JA, et al. miR-218 directs a Wnt signaling circuit to promote differentiation of osteoblasts and osteomimicry of metastatic cancer cells. J Biol Chem. 2012;287(50):42084-92.
118. Kang H, Chen H, Huang P, Qi J, Qian N, Deng L, et al. Glucocorticoids impair bone formation of bone marrow stromal stem cells by reciprocally regulating microRNA-34a-5p. Osteoporos Int. 2016;27(4):1493-505.
119. Chen S, Zheng Y, Zhang S, Jia L, Zhou Y. Promotion Effects of miR-375 on the Osteogenic Differentiation of Human Adipose-Derived Mesenchymal Stem Cells. Stem Cell Reports. 2017;8(3):773-86.
120. Li H, Li T, Fan J, Li T, Fan L, Wang S, et al. miR-216a rescues dexamethasone suppression of osteogenesis, promotes osteoblast differentiation and enhances bone formation, by regulating c-Cbl-mediated PI3K/AKT pathway. Cell Death Differ. 2015;22(12):1935-45.
121. Huang S, Wang S, Bian C, Yang Z, Zhou H, Zeng Y, et al. Upregulation of miR-22 promotes osteogenic differentiation and inhibits adipogenic differentiation of human adipose tissue-derived mesenchymal stem cells by repressing HDAC6 protein expression. Stem Cells Dev. 2012;21(13):2531-40.
122. Qin Y, Wang L, Gao Z, Chen G, Zhang C. Bone marrow stromal/stem cell-derived extracellular vesicles regulate osteoblast activity and differentiation in vitro and promote bone regeneration in vivo. Sci Rep. 2016;6:21961.
123. Liao YH, Chang YH, Sung LY, Li KC, Yeh CL, Yen TC, et al. Osteogenic differentiation of adipose-derived stem cells and calvarial defect repair using baculovirus-mediated co-expression of BMP-2 and miR-148b. Biomaterials. 2014;35(18):4901-10.
124. Nakamura Y, Miyaki S, Ishitobi H, Matsuyama S, Nakasa T, Kamei N, et al. Mesenchymal-stem-cell-derived exosomes accelerate skeletal muscle regeneration. FEBS Lett. 2015;589(11):1257-65.
125. Qin Y, Sun R, Wu C, Wang L, Zhang C. Exosome: A Novel Approach to Stimulate Bone Regeneration through Regulation of Osteogenesis and Angiogenesis. Int J Mol Sci. 2016;17(5).
126. Ferguson SW, Wang J, Lee CJ, Liu M, Neelamegham S, Canty JM, et al. The microRNA regulatory landscape of MSC-derived exosomes: a systems view. Sci Rep. 2018;8(1):1419.
127. Kuehbacher A, Urbich C, Zeiher AM, Dimmeler S. Role of Dicer and Drosha for endothelial microRNA expression and angiogenesis. Circ Res. 2007;101(1):59-68.

128. Umezu T, Tadokoro H, Azuma K, Yoshizawa S, Ohyashiki K, Ohyashiki JH. Exosomal miR-135b shed from hypoxic multiple myeloma cells enhances angiogenesis by targeting factor-inhibiting HIF-1. Blood. 2014;124(25):3748-57.
129. Yamada N, Tsujimura N, Kumazaki M, Shinohara H, Taniguchi K, Nakagawa Y, et al. Colorectal cancer cell-derived microvesicles containing microRNA-1246 promote angiogenesis by activating Smad 1/5/8 signaling elicited by PML down-regulation in endothelial cells. Biochim Biophys Acta. 2014;1839(11):1256-72.
130. Bao L, You B, Shi S, Shan Y, Zhang Q, Yue H, et al. Metastasis-associated miR-23a from nasopharyngeal carcinoma-derived exosomes mediates angiogenesis by repressing a novel target gene TSGA10. Oncogene. 2018;37(21):2873-89.
131. Ghosh G, Subramanian IV, Adhikari N, Zhang X, Joshi HP, Basi D, et al. Hypoxia-induced microRNA-424 expression in human endothelial cells regulates HIF-alpha isoforms and promotes angiogenesis. J Clin Invest. 2010;120(11):4141-54.
132. van Balkom BW, de Jong OG, Smits M, Brummelman J, den Ouden K, de Bree PM, et al. Endothelial cells require miR-214 to secrete exosomes that suppress senescence and induce angiogenesis in human and mouse endothelial cells. Blood. 2013;121(19):3997-4006, S1-15.
133. Zhao C, Sun W, Zhang P, Ling S, Li Y, Zhao D, et al. miR-214 promotes osteoclastogenesis by targeting Pten/PI3k/Akt pathway. RNA Biol. 2015;12(3):343-53.
134. Li Z, Hassan MQ, Jafferji M, Aqeilan RI, Garzon R, Croce CM, et al. Biological functions of miR-29b contribute to positive regulation of osteoblast differentiation. J Biol Chem. 2009;284(23):15676-84.
135. Bhushan R, Grunhagen J, Becker J, Robinson PN, Ott CE, Knaus P. miR-181a promotes osteoblastic differentiation through repression of TGF-beta signaling molecules. Int J Biochem Cell Biol. 2013;45(3):696-705.
136. Kang IH, Jeong BC, Hur SW, Choi H, Choi SH, Ryu JH, et al. MicroRNA-302a stimulates osteoblastic differentiation by repressing COUP-TFII expression. J Cell Physiol. 2015;230(4):911-21.
137. Lv C, Hao Y, Han Y, Zhang W, Cong L, Shi Y, et al. Role and mechanism of microRNA-21 in H2O2-induced apoptosis in bone marrow mesenchymal stem cells. J Clin Neurosci. 2016;27:154-60.
138. Hu Y, Rao SS, Wang ZX, Cao J, Tan YJ, Luo J, et al. Exosomes from human umbilical cord blood accelerate cutaneous wound healing through miR-21-3p-mediated promotion of angiogenesis and fibroblast function. Theranostics. 2018;8(1):169-84.
139. Yang N, Wang G, Hu C, Shi Y, Liao L, Shi S, et al. Tumor necrosis factor alpha suppresses the mesenchymal stem cell osteogenesis promoter miR-21 in estrogen deficiency-induced osteoporosis. J Bone Miner Res. 2013;28(3):559-73.
140. Yang C, Liu X, Zhao K, Zhu Y, Hu B, Zhou Y, et al. miRNA-21 promotes osteogenesis via the PTEN/PI3K/Akt/HIF-1alpha pathway and enhances bone regeneration in critical size defects. Stem Cell Res Ther. 2019;10(1):65.
141. Furuta T, Miyaki S, Ishitobi H, Ogura T, Kato Y, Kamei N, et al. Mesenchymal Stem Cell-Derived Exosomes Promote Fracture Healing in a Mouse Model. Stem Cells Transl Med. 2016;5(12):1620-30.
142. Xu J, Wang B, Sun Y, Wu T, Liu Y, Zhang J, et al. Human fetal mesenchymal stem cell secretome enhances bone consolidation in distraction osteogenesis. Stem Cell Res Ther. 2016;7(1):134.
143. Ogata K, Katagiri W, Osugi M, Kawai T, Sugimura Y, Hibi H, et al. Evaluation of the therapeutic effects of conditioned media from mesenchymal stem cells in a rat bisphosphonate-related osteonecrosis of the jaw-like model. Bone. 2015;74:95-105.
144. Shanbhag S, Al-Sharabi N, Kampleitner C, Mohamed-Ahmed S, Kristoffersen EK, Tangl S, et al. The use of mesenchymal stromal cell secretome to enhance guided bone regeneration in comparison with leukocyte and platelet-rich fibrin. Clin Oral Implants Res. 2024;35(2):141-54.

145. Tang J, Wang X, Lin X, Wu C. Mesenchymal stem cell-derived extracellular vesicles: a regulator and carrier for targeting bone-related diseases. Cell Death Discov. 2024;10(1):212.
146. Tan SHS, Wong JRY, Sim SJY, Tjio CKE, Wong KL, Chew JRJ, et al. Mesenchymal stem cell exosomes in bone regenerative strategies-a systematic review of preclinical studies. Mater Today Bio. 2020;7:100067.
147. Liu F, Sun T, An Y, Ming L, Li Y, Zhou Z, et al. The potential therapeutic role of extracellular vesicles in critical-size bone defects: Spring of cell-free regenerative medicine is coming. Front Bioeng Biotechnol. 2023;11:1050916.
148. Qi X, Zhang J, Yuan H, Xu Z, Li Q, Niu X, et al. Exosomes Secreted by Human-Induced Pluripotent Stem Cell-Derived Mesenchymal Stem Cells Repair Critical-Sized Bone Defects through Enhanced Angiogenesis and Osteogenesis in Osteoporotic Rats. Int J Biol Sci. 2016;12(7):836-49.
149. Qayoom I, Teotia AK, Kumar A. Nanohydroxyapatite Based Ceramic Carrier Promotes Bone Formation in a Femoral Neck Canal Defect in Osteoporotic Rats. Biomacromolecules. 2020;21(2):328-37.
150. Qiu M, Zhai S, Fu Q, Liu D. Bone Marrow Mesenchymal Stem Cells-Derived Exosomal MicroRNA-150-3p Promotes Osteoblast Proliferation and Differentiation in Osteoporosis. Hum Gene Ther. 2021;32(13-14):717-29.
151. Katagiri W, Osugi M, Kawai T, Hibi H. First-in-human study and clinical case reports of the alveolar bone regeneration with the secretome from human mesenchymal stem cells. Head Face Med. 2016;12:5.
152. Ferreira JR, Teixeira GQ, Santos SG, Barbosa MA, Almeida-Porada G, Goncalves RM. Mesenchymal Stromal Cell Secretome: Influencing Therapeutic Potential by Cellular Pre-conditioning. Front Immunol. 2018;9:2837.
153. Liu Y, Ren L, Li M, Zheng B, Liu Y. The Effects of Hypoxia-Preconditioned Dental Stem Cell-Derived Secretome on Tissue Regeneration. Tissue Eng Part B Rev. 2024.
154. Zhuang Y, Cheng M, Li M, Cui J, Huang J, Zhang C, et al. Small extracellular vesicles derived from hypoxic mesenchymal stem cells promote vascularized bone regeneration through the miR-210-3p/EFNA3/PI3K pathway. Acta Biomater. 2022;150:413-26.
155. Liu P, Qin L, Liu C, Mi J, Zhang Q, Wang S, et al. Exosomes Derived From Hypoxia-Conditioned Stem Cells of Human Deciduous Exfoliated Teeth Enhance Angiogenesis via the Transfer of let-7f-5p and miR-210-3p. Front Cell Dev Biol. 2022;10:879877.
156. Liu W, Li L, Rong Y, Qian D, Chen J, Zhou Z, et al. Hypoxic mesenchymal stem cell-derived exosomes promote bone fracture healing by the transfer of miR-126. Acta Biomater. 2020;103:196-212.
157. Bogatcheva NV, Coleman ME. Conditioned Medium of Mesenchymal Stromal Cells: A New Class of Therapeutics. Biochemistry (Mosc). 2019;84(11):1375-89.
158. Miceli V, Bulati M, Iannolo G, Zito G, Gallo A, Conaldi PG. Therapeutic Properties of Mesenchymal Stromal/Stem Cells: The Need of Cell Priming for Cell-Free Therapies in Regenerative Medicine. Int J Mol Sci. 2021;22(2).
159. Kang M, Huang CC, Gajendrareddy P, Lu Y, Shirazi S, Ravindran S, et al. Extracellular Vesicles From TNFalpha Preconditioned MSCs: Effects on Immunomodulation and Bone Regeneration. Front Immunol. 2022;13:878194.
160. Lu Z, Chen Y, Dunstan C, Roohani-Esfahani S, Zreiqat H. Priming Adipose Stem Cells with Tumor Necrosis Factor-Alpha Preconditioning Potentiates Their Exosome Efficacy for Bone Regeneration. Tissue Eng Part A. 2017;23(21-22):1212-20.
161. Torrecillas-Baena B, Pulido-Escribano V, Dorado G, Galvez-Moreno MA, Camacho-Cardenosa M, Casado-Diaz A. Clinical Potential of Mesenchymal Stem Cell-Derived Exosomes in Bone Regeneration. J Clin Med. 2023;12(13).
162. Torres Crigna A, Uhlig S, Elvers-Hornung S, Kluter H, Bieback K. Human Adipose Tissue-Derived Stromal Cells Suppress Human, but Not Murine Lymphocyte Proliferation, via Indoleamine 2,3-Dioxygenase Activity. Cells. 2020;9(11).

163. Tasso R, Gaetani M, Molino E, Cattaneo A, Monticone M, Bachi A, et al. The role of bFGF on the ability of MSC to activate endogenous regenerative mechanisms in an ectopic bone formation model. Biomaterials. 2012;33(7):2086-96.
164. Stamnitz S, Krawczenko A, Szalaj U, Gorecka Z, Antonczyk A, Kielbowicz Z, et al. Osteogenic Potential of Sheep Mesenchymal Stem Cells Preconditioned with BMP-2 and FGF-2 and Seeded on an nHAP-Coated PCL/HAP/beta-TCP Scaffold. Cells. 2022;11(21).
165. Man K, Brunet MY, Fernandez-Rhodes M, Williams S, Heaney LM, Gethings LA, et al. Epigenetic reprogramming enhances the therapeutic efficacy of osteoblast-derived extracellular vesicles to promote human bone marrow stem cell osteogenic differentiation. J Extracell Vesicles. 2021;10(9):e12118.
166. Cha KY, Cho W, Park S, Ahn J, Park H, Baek I, et al. Generation of bioactive MSC-EVs for bone tissue regeneration by tauroursodeoxycholic acid treatment. J Control Release. 2023;354:45-56.
167. Liu D, Song G, Ma Z, Geng X, Dai Y, Yang T, et al. Resveratrol improves the therapeutic efficacy of bone marrow-derived mesenchymal stem cells in rats with severe acute pancreatitis. Int Immunopharmacol. 2020;80:106128.
168. Sung DK, Chang YS, Sung SI, Ahn SY, Park WS. Thrombin Preconditioning of Extracellular Vesicles Derived from Mesenchymal Stem Cells Accelerates Cutaneous Wound Healing by Boosting Their Biogenesis and Enriching Cargo Content. J Clin Med. 2019;8(4).
169. Cabezas J, Rojas D, Wong Y, Telleria F, Manriquez J, Mancanares ACF, et al. In vitro preconditioning of equine adipose mesenchymal stem cells with prostaglandin E(2), substance P and their combination changes the cellular protein secretomics and improves their immunomodulatory competence without compromising stemness. Vet Immunol Immunopathol. 2020;228:110100.
170. Heo JS, Lim JY, Yoon DW, Pyo S, Kim J. Exosome and Melatonin Additively Attenuates Inflammation by Transferring miR-34a, miR-124, and miR-135b. Biomed Res Int. 2020;2020:1621394.
171. Kim M, Yun HW, Park DY, Choi BH, Min BH. Three-Dimensional Spheroid Culture Increases Exosome Secretion from Mesenchymal Stem Cells. Tissue Eng Regen Med. 2018;15(4):427-36.
172. Cesarz Z, Tamama K. Spheroid Culture of Mesenchymal Stem Cells. Stem Cells Int. 2016;2016:9176357.
173. Imamura A, Kajiya H, Fujisaki S, Maeshiba M, Yanagi T, Kojima H, et al. Three-dimensional spheroids of mesenchymal stem/stromal cells promote osteogenesis by activating stemness and Wnt/beta-catenin. Biochem Biophys Res Commun. 2020;523(2):458-64.
174. Hodge JG, Robinson JL, Mellott AJ. Tailoring the secretome composition of mesenchymal stem cells to augment specific functions of epidermal regeneration: an in vitro diabetic model. Front Med Technol. 2023;5:1194314.
175. Su N, Gao PL, Wang K, Wang JY, Zhong Y, Luo Y. Fibrous scaffolds potentiate the paracrine function of mesenchymal stem cells: A new dimension in cell-material interaction. Biomaterials. 2017;141:74-85.
176. Carter K, Lee HJ, Na KS, Fernandes-Cunha GM, Blanco IJ, Djalilian A, et al. Characterizing the impact of 2D and 3D culture conditions on the therapeutic effects of human mesenchymal stem cell secretome on corneal wound healing in vitro and ex vivo. Acta Biomater. 2019;99:247-57.
177. Cesarz Z, Funnell JL, Guan J, Tamama K. Soft Elasticity-Associated Signaling and Bone Morphogenic Protein 2 Are Key Regulators of Mesenchymal Stem Cell Spheroidal Aggregates. Stem Cells Dev. 2016;25(8):622-35.
178. Martins M, Ribeiro D, Martins A, Reis RL, Neves NM. Extracellular Vesicles Derived from Osteogenically Induced Human Bone Marrow Mesenchymal Stem Cells Can Modulate Lineage Commitment. Stem Cell Reports. 2016;6(3):284-91.

179. Huang CC, Kang M, Lu Y, Shirazi S, Diaz JI, Cooper LF, et al. Functionally engineered extracellular vesicles improve bone regeneration. Acta Biomater. 2020;109:182-94.
180. Li H, Zuo S, He Z, Yang Y, Pasha Z, Wang Y, et al. Paracrine factors released by GATA-4 overexpressed mesenchymal stem cells increase angiogenesis and cell survival. Am J Physiol Heart Circ Physiol. 2010;299(6):H1772-81.
181. Li H, Liu D, Li C, Zhou S, Tian D, Xiao D, et al. Exosomes secreted from mutant-HIF-1alpha-modified bone-marrow-derived mesenchymal stem cells attenuate early steroid-induced avascular necrosis of femoral head in rabbit. Cell Biol Int. 2017;41(12):1379-90.
182. Ying C, Wang R, Wang Z, Tao J, Yin W, Zhang J, et al. BMSC-Exosomes Carry Mutant HIF-1alpha for Improving Angiogenesis and Osteogenesis in Critical-Sized Calvarial Defects. Front Bioeng Biotechnol. 2020;8:565561.
183. Garcia-Sanchez D, Gonzalez-Gonzalez A, Alvarez-Iglesias I, Dujo-Gutierrez MD, Bolado-Carrancio A, Certo M, et al. Engineering a Pro-Osteogenic Secretome through the Transient Silencing of the Gene Encoding Secreted Frizzled Related Protein 1. Int J Mol Sci. 2023;24(15).
184. Fafian-Labora J, Fernandez-Pernas P, Fuentes I, De Toro J, Oreiro N, Sangiao-Alvarellos S, et al. Influence of age on rat bone-marrow mesenchymal stem cells potential. Sci Rep. 2015;5:16765.
185. Del Real A, Perez-Campo FM, Fernandez AF, Sanudo C, Ibarbia CG, Perez-Nunez MI, et al. Differential analysis of genome-wide methylation and gene expression in mesenchymal stem cells of patients with fractures and osteoarthritis. Epigenetics. 2017;12(2):113-22.
186. Wolbank S, Stadler G, Peterbauer A, Gillich A, Karbiener M, Streubel B, et al. Telomerase immortalized human amnion- and adipose-derived mesenchymal stem cells: maintenance of differentiation and immunomodulatory characteristics. Tissue Eng Part A. 2009;15(7):1843-54.
187. Gregory CA, Gunn WG, Peister A, Prockop DJ. An Alizarin red-based assay of mineralization by adherent cells in culture: comparison with cetylpyridinium chloride extraction. Anal Biochem. 2004;329(1):77-84.
188. Livak KJ, Schmittgen TD. Analysis of relative gene expression data using real-time quantitative PCR and the 2(-Delta Delta C(T)) Method. Methods. 2001;25(4):402-8.
189. Delgado-Calle J, Sanudo C, Sanchez-Verde L, Garcia-Renedo RJ, Arozamena J, Riancho JA. Epigenetic regulation of alkaline phosphatase in human cells of the osteoblastic lineage. Bone. 2011;49(4):830-8.
190. SPINREACT. Quantitative determination of alkaline phosphatase (ALP). Spinreact.com; 2015.
191. Bellido T, Delgado-Calle J. Ex Vivo Organ Cultures as Models to Study Bone Biology. JBMR Plus. 2020;4(3).
192. Garmilla-Ezquerra P, Sanudo C, Delgado-Calle J, Perez-Nunez MI, Sumillera M, Riancho JA. Analysis of the bone microRNome in osteoporotic fractures. Calcif Tissue Int. 2015;96(1):30-7.
193. Rodriguez-Evora M, Garcia-Pizarro E, del Rosario C, Perez-Lopez J, Reyes R, Delgado A, et al. *Smurf1* knocked-down, mesenchymal stem cells and BMP-2 in an electrospun system for bone regeneration. Biomacromolecules. 2014;15(4):1311-22.
194. IHC WORD. Masson's Trichrome Staining Protocol for Collagen Fibers. https://ihcworld.com/2024/01/26/massons-trichrome-staining-protocol-for-collagen-fibers/#:~:text=Description%3A%20This%20method%20is%20used%20for%20the%20detection,stained%20black%20and%20the%20background%20is%20stained%20red2024 [
195. Souza VR, Mendes E, Casaro M, Antiorio A, Oliveira FA, Ferreira CM. Description of Ovariectomy Protocol in Mice. Methods Mol Biol. 2019;1916:303-9.

196. Turriziani B, Garcia-Munoz A, Pilkington R, Raso C, Kolch W, von Kriegsheim A. On-beads digestion in conjunction with data-dependent mass spectrometry: a shortcut to quantitative and dynamic interaction proteomics. Biology (Basel). 2014;3(2):320-32.
197. Demichev V, Messner CB, Vernardis SI, Lilley KS, Ralser M. DIA-NN: neural networks and interference correction enable deep proteome coverage in high throughput. Nat Methods. 2020;17(1):41-4.
198. Tyanova S, Temu T, Sinitcyn P, Carlson A, Hein MY, Geiger T, et al. The Perseus computational platform for comprehensive analysis of (prote)omics data. Nat Methods. 2016;13(9):731-40.
199. Spatz JM, Wein MN, Gooi JH, Qu Y, Garr JL, Liu S, et al. The Wnt Inhibitor Sclerostin Is Up-regulated by Mechanical Unloading in Osteocytes in Vitro. J Biol Chem. 2015;290(27):16744-58.
200. Zia S, Cavallo C, Vigliotta I, Parisi V, Grigolo B, Buda R, et al. Effective Label-Free Sorting of Multipotent Mesenchymal Stem Cells from Clinical Bone Marrow Samples. Bioengineering (Basel). 2022;9(2).
201. Guan M, Xu Y, Wang W, Lin S. Differentiation into neurons of rat bone marrow-derived mesenchymal stem cells. Eur Cytokine Netw. 2014;25(3):58-63.
202. Harichandan A, Buhring HJ. Prospective isolation of human MSC. Best Pract Res Clin Haematol. 2011;24(1):25-36.
203. Bellido T. Osteocyte-driven bone remodeling. Calcif Tissue Int. 2014;94(1):25-34.
204. Lin GL, Hankenson KD. Integration of BMP, Wnt, and notch signaling pathways in osteoblast differentiation. J Cell Biochem. 2011;112(12):3491-501.
205. Garcia-Sanchez D, Gonzalez-Gonzalez A, Garcia-Garcia P, Reyes R, Perez-Nunez MI, Riancho JA, et al. Effective Osteogenic Priming of Mesenchymal Stem Cells through LNA-ASOs-Mediated Sfrp1 Gene Silencing. Pharmaceutics. 2021;13(8).
206. Marques CR, Marote A, Mendes-Pinheiro B, Teixeira FG, Salgado AJ. Cell secretome based approaches in Parkinson's disease regenerative medicine. Expert Opin Biol Ther. 2018;18(12):1235-45.
207. Miranda JP, Camoes SP, Gaspar MM, Rodrigues JS, Carvalheiro M, Barcia RN, et al. The Secretome Derived From 3D-Cultured Umbilical Cord Tissue MSCs Counteracts Manifestations Typifying Rheumatoid Arthritis. Front Immunol. 2019;10:18.
208. Noronha NC, Mizukami A, Caliari-Oliveira C, Cominal JG, Rocha JLM, Covas DT, et al. Priming approaches to improve the efficacy of mesenchymal stromal cell-based therapies. Stem Cell Res Ther. 2019;10(1):131.
209. Garcia SG, Sanroque-Muñoz M, Clos-Sansalvador M, Font-Morón M, Monguió-Tortajada M, Borràs FE, et al. Hollow fiber bioreactor allows sustained production of immortalized mesenchymal stromal cell-derived extracellular vesicles. Extracellular Vesicles and Circulating Nucleic Acids. 2024;5(2):201-20.
210. Long KR, Newland B, Florio M, Kalebic N, Langen B, Kolterer A, et al. Extracellular Matrix Components HAPLN1, Lumican, and Collagen I Cause Hyaluronic Acid-Dependent Folding of the Developing Human Neocortex. Neuron. 2018;99(4):702-19 e6.
211. Deng M, Tan J, Dai Q, Luo F, Xu J. Macrophage-Mediated Bone Formation in Scaffolds Modified With MSC-Derived Extracellular Matrix Is Dependent on the Migration Inhibitory Factor Signaling Pathway. Front Cell Dev Biol. 2021;9:714011.
212. Serguienko A, Wang MY, Myklebost O. Real-Time Vital Mineralization Detection and Quantification during In Vitro Osteoblast Differentiation. Biol Proced Online. 2018;20:14.
213. Moester MJ, Schoeman MA, Oudshoorn IB, van Beusekom MM, Mol IM, Kaijzel EL, et al. Validation of a simple and fast method to quantify in vitro mineralization with fluorescent probes used in molecular imaging of bone. Biochem Biophys Res Commun. 2014;443(1):80-5.
214. Bez M, Pelled G, Gazit D. BMP gene delivery for skeletal tissue regeneration. Bone. 2020;137:115449.

215. Scarfi S. Use of bone morphogenetic proteins in mesenchymal stem cell stimulation of cartilage and bone repair. World J Stem Cells. 2016;8(1):1-12.
216. Cramer EEA, Ito K, Hofmann S. Ex vivo Bone Models and Their Potential in Preclinical Evaluation. Curr Osteoporos Rep. 2021;19(1):75-87.
217. Theoleyre S, Wittrant Y, Tat SK, Fortun Y, Redini F, Heymann D. The molecular triad OPG/RANK/RANKL: involvement in the orchestration of pathophysiological bone remodeling. Cytokine Growth Factor Rev. 2004;15(6):457-75.
218. Wright HL, McCarthy HS, Middleton J, Marshall MJ. RANK, RANKL and osteoprotegerin in bone biology and disease. Curr Rev Musculoskelet Med. 2009;2(1):56-64.
219. Oftadeh R, Perez-Viloria M, Villa-Camacho JC, Vaziri A, Nazarian A. Biomechanics and mechanobiology of trabecular bone: a review. J Biomech Eng. 2015;137(1):0108021-01080215.
220. Komori T. Regulation of osteoblast differentiation by Runx2. Adv Exp Med Biol. 2010;658:43-9.
221. Anderson C. Matrix Vesicle and Calcification. Current Rheumatology Reports. 2003;5:222-6.
222. Zhang D, Du J, Yu M, Suo L. Ginsenoside Rb1 prevents osteoporosis via the AHR/PRELP/NF-kappaB signaling axis. Phytomedicine. 2022;104:154205.
223. Li H, Cui Y, Luan J, Zhang X, Li C, Zhou X, et al. PRELP (proline/arginine-rich end leucine-rich repeat protein) promotes osteoblastic differentiation of preosteoblastic MC3T3-E1 cells by regulating the beta-catenin pathway. Biochem Biophys Res Commun. 2016;470(3):558-62.
224. Tevlin R, Griffin M, Chen K, Januszyk M, Guardino N, Spielman A, et al. Denervation during mandibular distraction osteogenesis results in impaired bone formation. Sci Rep. 2023;13(1):2097.
225. Rosset EM, Bradshaw AD. SPARC/osteonectin in mineralized tissue. Matrix Biol. 2016;52-54:78-87.
226. Kubota S, Takigawa M. Role of CCN2/CTGF/Hcs24 in bone growth. Int Rev Cytol. 2007;257:1-41.
227. Abreu JG, Ketpura NI, Reversade B, De Robertis EM. Connective-tissue growth factor (CTGF) modulates cell signalling by BMP and TGF-beta. Nat Cell Biol. 2002;4(8):599-604.
228. Leask A, Abraham DJ. All in the CCN family: essential matricellular signaling modulators emerge from the bunker. J Cell Sci. 2006;119(Pt 23):4803-10.
229. Riancho J, Peris P, González-Macías J, Pérez-Castrillón J. Resumen Ejecutivo de las Guías de práctica clínica en la osteoporosis postmenopausica, glucorticoidea y del varón. Revista de Osteoporosis y Metabolismo Mineral. 2022;14:5-12.
230. Cosman F, Crittenden DB, Adachi JD, Binkley N, Czerwinski E, Ferrari S, et al. Romosozumab Treatment in Postmenopausal Women with Osteoporosis. The New England journal of medicine. 2016;375(16):1532-43.
231. Asociación Española para el Estudio de la Menopausia. Menoguía: Osteoporosis. 2013(https://aeem.es/menoguias-para-profesionales/).
232. Romero Barco CM, Manrique Arija S, Rodriguez Perez M. Biochemical markers in osteoporosis: usefulness in clinical practice. Reumatol Clin. 2012;8(3):149-52.
233. Eastell R, Szulc P. Use of bone turnover markers in postmenopausal osteoporosis. Lancet Diabetes Endocrinol. 2017;5(11):908-23.
234. Ross P, Knowlton W. Rapid Bone Loss Is Associated with Increased Levels of Biochemical Markers. Journal of Bone and Mineral Research. 1998;13:297-302.
235. Histocell Regenerative Medicine https://histocell.com/2024 [
236. Garcia-Garcia P, Reyes R, Garcia-Sanchez D, Perez-Campo FM, Rodriguez-Rey JC, Evora C, et al. Nanoparticle-mediated selective Sfrp-1 silencing enhances bone density in osteoporotic mice. J Nanobiotechnology. 2022;20(1):462.

237. Xu H, Wang W, Liu X, Huang W, Zhu C, Xu Y, et al. Targeting strategies for bone diseases: signaling pathways and clinical studies. Signal Transduct Target Ther. 2023;8(1):202.